FINAL REPORT for APN PROJECT

Project Reference Number: ARCP2011-05CMY-Bae

"Climate Change Impact Assessment on the Asia-Pacific Water Resources under AWCI/GEOSS"

The following collaborators worked on this project:

Deg-Hyo Bae, Sejong University, Korea, dhbae@sejong.ac.kr

Md. Mafizur Rahman, Bangladesh University, Bangladesh, mafizur@gmail.com

Toshio Koike, University of Tokyo, Japan, tkoike@hydra.t.u-tokyo.ac.jp

Bashir Ahmad, Pakistan Agricultural Research Council, Pakistan, bashirad@hotmail.com

“Climate Change Impact Assessment on the Asia-Pacific Water Resources under AWCI/GEOSS”

Project Reference Number: ARCP2011-05CMY-Bae
Final Report submitted to APN

PAGE LEFT INTENTIONALLY BLANK

OVERVIEW OF PROJECT WORK AND OUTCOMES

Non-technical summary

This project was started under the GEOSS/Asian Water Cycle Initiative (AWCI) framework to analyze historical climate and hydrology trend with future climate change impact assessment. The analysis was conducted over Asia including AWCI 18 basins. The temperature was observed to increase over most regions in Asia during past 30 years but the precipitation and runoff was observed to decrease. To analyze future climate change impact, three GCMs (CGCM2_3_2, CGCM3_T47, and CM4) were selected according to the results of the probabilistic uncertainty analysis, correlation coefficient, and RMSE. The temperature was expected to increase in all regions. The precipitation and runoff was projected to increase for all seasons over most regions in Asia except central Asia. The water balance over selected 18 basins showed increasing trend toward future periods. This study enabled us to better understand the past and future trends of climate and hydrology over Asia. The results analyzed in this study will be useful in establishing future climate adaptation measure over Asia.

Objectives

The main objectives of the project were:

1. Historical trend analysis of climate and hydrology over Asia including AWCI 18 countries using the Mann-Kendall test.
2. Selection of suitable GCMs, scenario, and hydrology model to analyze the future climate and hydrology impact assessment.
3. Future climate and hydrology impact assessment over Asia including AWCI 18 countries.

Amount received and number years supported

The Grant awarded to this project was:
US$ 42,000 for Year 1: 2010/2011
US$ 42,000 for Year 2: 2011/2012

Activity undertaken

Meeting event: The project included two AWCI meetings: (i) the AWCI training course for the Climate Change Assessment and Adaptation Study was held in Seoul, October 2011. Regarding the main objectives, aside from the usual review of the AWCI and its working group activities, the International Coordination Group (ICG) meeting focused on preparation for planning of the next step of the Initiative. With its strong collaborative framework and data integration principles developed, AWCI is now eligible as one of the pillars of the newly proposed GEOSS Water Cycle Integrator (WCI), targeting enhanced coordination in the water cycle arena on the global level. (ii) the 9th AWCI ICG meeting and the workshop in Tokyo, October 2012 on Climate Change Adaptation organized by APWF was held. Main objective was to synthesize the provided country inputs into a complex implementation plan that will be in line with the GEOSS WCI goals.

Results

The analysis of historical climate and hydrology trend with future climate change impact was conducted over Asia region covering 18 designated basins of AWCI. The Mann-Kendall test was

employed for historical trend analysis using observed gridded climate data from APHRODITE and hydrology data from VIC model at horizontal grid resolution of 0.5° x 0.5° for period of 1977 to 2006. The trend analysis showed increase in temperature over Asia region except some parts of Southeast Asia. The precipitation was observed to decrease about 100~200mm during past 30 years over Asian region. Similarly, the decreasing trend was observed for runoff. The runoff was observed to decrease approximately 70～80mm over Asia region. The seasonal trend analysis showed increasing trend of temperature for all the seasons. The seasonal precipitation showed decreasing trend over Asia with increase in some parts. The seasonal runoff was also appeared to decrease like precipitation. The spatial features of runoff were similar to that of precipitation. The hydrological components over AWCI 18 basins were calculated using VIC model which revealed various distinct regional features at each basin.

To analyze future climate change impact, the optimum GCMs were selected using probabilistic uncertainty analysis, correlation coefficient, and RMSE methods. Selected GCMs include CGCM3_T47, CGCM2_3_2, and CM4. The uncertainty of selected GCMs was also evaluated. The results showed increased uncertainty of GCMs toward future periods. For future climate and hydrology impact, the ensemble mean value of selected GCMs was used. The temperature was expected to increase in all regions. The precipitation was projected to increase during all seasons in most regions except central Asia. The future change in runoff was expected similar with that of precipitation. The latitudinal features showed high increase in temperature change with increasing latitudes. The latitudinal precipitation change was estimated high at high latitudes and low at low latitudes. The change rate of latitudinal runoff was high at mid latitude regions. The water balance for precipitation, runoff, evapotranspiration and soil moisture was evaluated over 18 selected basins. The results showed increasing tendency of water balance for the future periods.

Relevance to the APN Goals, Science Agenda and to Policy Processes

This project focused on historical trend analysis of climate and hydrology over Asia with future climate impact assessment. We were able to understand the historical trend of climate and hydrology over Asia region. Also, we found future climate change and hydrology impact. The results analyzed in this study will be useful in establishing the water resources management and future climate adaptation measures over Asia.

Self evaluation

We believe this project has accomplished its objectives as given above. At first, the historical climate and hydrology trend was analyzed over Asia including AWCI 18 countries. The appropriate GCMs were selected to analyze future climate change impact. The future climate change impact was assessed over Asia using the multi GCMs and A2 scenario.

Potential for further work

The historical climate and hydrology trend with future climate change impact over Asia was evaluated. The observed gridded data of 0.5° x 0.5° resolution, A2 scenario, and VIC mode was used. For more detailed analysis of climate and hydrology features over Asia, high-resolution observation data will be used. The multi GCM, hydrology model, and climate scenario will be used to evaluate future climate change impact details. Furthermore, we used IPCC AR4 output in this study; we will be able to obtain more useful results using Representative Concentration Pathway of IPCC AR5.

Publications

Son, K.H., Lee, M.H. and Bae, D.H. (2012) Runoff Analysis and Assessment Using Land Surface Model on East Asia, Journal of Korean Water Resources Association, 45(2), pp. 165-178. (in Korean)

Shin, S.H. and Bae, D.H. (2013) Future Projections of Koppen Climate Shifts in the Asia Regions Using A2 Scenario, Journal of Korean Water Resources Association, 46(3), pp. 253-265. (in Korean)

Le, T. and Bae, D.H. (2013) Evaluating the Utility of IPCC AR4 GCMs for Hydrological Application in South Korea, Water Resources Management, 27(9), pp. 3227-3246.

Son, K.H. and Bae, D.H. (2012) Validity of Land Surface Model for Drought Analysis in the East Asia Region, IAHR-APD 2012, Jeju-island, Korea, August 2012

Lee, M.H. and Bae, D.H. (2012) Uncertainty Assessment of Bias Correction methods for Climate Change Impact Assessment on Water resources, IAHR-APD 2012, Jeju-island, Korea, August 2012.

References

Acknowledgments

We would like to thank the APN which made this project possible. Also, we would like to thank for their continued collaboration AWCI.

TECHNICAL REPORT

Preface

The historical climate and hydrology trend with future climate change impact over Asia including AWCI 18 countries was analyzed. The temperature was observed to increase over most regions in Asia during past 30 years but the precipitation and runoff was observed to decrease. To analyze future climate change impact, three GCMs were selected. In future, the temperature was expected to increase in all regions. The precipitation and runoff was projected to increase for all seasons over most regions in Asia except central Asia.

Table of Contents

1.0 Introduction

The human-induced climate change is caused by the emissions of carbon dioxide and other greenhouse gases (GHGs) that have accumulated in the atmosphere mainly over the past 100 years. The scientific evidence that climate change is a serious and urgent issue is now compelling. It warrants strong action to reduce greenhouse gas emissions around the world to reduce the risk of very damaging and potentially irreversible impacts on ecosystems, societies and economies. With good policies the costs of action need not be prohibitive and would be much smaller than the damage averted. Reversing the trend to higher global temperatures requires an urgent, world-wide shift towards a low-carbon economy. Delay makes the problem much more difficult and action to deal with it much more costly. Managing that transition effectively and efficiently poses ethical and economic challenges. The current level or stock of greenhouse gases in the atmosphere is equivalent to around 430 parts per million (ppm) CO_2, compared with only 280ppm before the Industrial Revolution. These concentrations have already caused the world to warm by more than half a degree Celsius and will lead to at least a further half degree warming over the next few decades, because of the inertia in the climate system.

To evaluate and resolve the impact of climate change, the General Circulation Model (GCM) is used. A GCM is a mathematical model of the general circulation of a planetary atmosphere or ocean and based on the Navier–Stokes equations on a rotating sphere with thermodynamic terms for various energy sources (radiation, latent heat). These equations are the basis for complex computer programs commonly used for simulating the atmosphere or ocean of the Earth. Atmospheric and oceanic GCMs (AGCM and OGCM) are key components of global climate models along with sea ice and land-surface components. GCMs and global climate models are widely applied for weather forecasting, understanding the climate, and projecting climate change. Versions designed for decade to century time scale climate applications were originally created by Syukuro Manabe and Kirk Bryan at the Geophysical Fluid Dynamics Laboratory in Princeton, New Jersey.[1] These computationally intensive numerical models are based on the integration of a variety of fluid dynamical, chemical, and sometimes biological equations.

The Intergovernmental Panel on Climate Change (IPCC) used output of GCMs. According to 4th assessment report of the Intergovernmental Panel on Climate Change (IPCC, 2007), the temperatures during recent five decades have double-increased (approximately 0.13℃/decade), compared to temperature increasing (approximately 0.07℃/decade) trend of past hundred years (1906~2005). These 12 years (1998, 2005, 2003, 2002, 2004, 2006, 2001, 1997, 1995, 1999, 1990, and 2000) of the record-breaking high temperatures after 1850's have occurred after 1990, there are ongoing events even now (IPCC, 2007). This climate change has been recently getting an attention from human being since the changes on ecosystem and frequent extreme events have started through global warming. Global warming has already produced significant impacts on many parts (IPCC, 2007).

In the Asia/Pacific region there is evidence of prominent increases in the intensity and/or frequency of many extreme events such as heat waves, tropical cyclones, prolonged dry spells, intense rainfall, tornadoes, snow avalanches, thunderstorms, and severe dust storms in the region. Furthermore, the region is highly subject to natural hazards, such as the 2004 Indian Ocean tsunami, the 2005 Pakistan

earthquake, and the 2006 landslides in the Philippines. Such impacts pose additional risks for already vulnerable communities striving to combat poverty and achieve sustainable development. The Asia/Pacific region accounted for 91% of the world's total death and 49% of the world's total damage due to natural disasters in the last century. Therefore, climate change poses a serious and additional threat to poor farmers and rural communities in the region who live in remote, marginal areas such as mountains, drylands and deserts; areas with limited natural resources, communication and transportation networks and weak institutions. In particular, climate models indicate temperature increases in the Asia/Pacific region on the order of 0.5-2.0°C by 2030 and 1.0-7.0°C by 2070. Temperatures are expected to increase more rapidly in the arid areas of northern Pakistan and India, and western China. Additionally, GCM indicate rising rainfall concentration throughout much of the region, including greater rainfall during the summer monsoon. Furthermore, winter rainfall is likely to decline in South and Southeast Asia, suggesting increased aridity from the winter monsoon. The region will be affected by an increase in global sea level of approximately 3-16cm by 2030 and 7-50cm by 2070 in conjunction with regional sea level variability. Other scientific studies have also indicated the potential for more intense tropical cyclones and changes in important modes of climate variability such as the El Niño-Southern Oscillation.

Also, the Asia monsoon plays an important role on global water circulation and provides substantial precipitations and water resources to the peoples living within the domain. It provides several benefits such as power generation and transportation facilities, but also causes serious flood and drought problems. Of course, there are various reasons for these water-related disasters, but the current climate change makes them much more complicated and difficult to manage. Besides, at this moment, management decisions in the water sector are often made with uncertain information regarding the future state of climate and the available water resources. Thus, the prediction of future climate trend could be the key point affecting further development of Asian region.

In this study, the historical climate and hydrology trend, and future climate change impact over Asia including AWCI 18 countries were analyzed. For historical trend analysis, the gridded climatology and hydrology datasets (0.5^{o} x 0.5^{o}) were obtained from APHRODTIE and VIC model datasets respectively. To analyze the future climate change and its impact on water resources the A2 climate scenario with best three GCMs were used. This study demonstrated the past and future climate and hydrology trends over Asia region with detailed analysis at 18 selected basins.

2.0 Methodology

The methodology adopted to analyze the historical and future trend of climate and hydrology over Asia including 18 AWCI basins is presented in Figure 2.1. Primarily, the past climatology (precipitation, max/min/mean temperature, wind speed) data at horizontal grid resolution of 0.5 degree was collected from APHRODITE and VIC model dataset, respectively. The VIC model was employed for analysis of historical hydrology data. The Mann-Kendall test was used for trend analysis from collected data and hydrology model output. To analyze future trend, three best GCMs were selected based on methods of probabilistic uncertainty analysis, correlation coefficient, and RMSE. The future scenarios (A2) of three selected GCMs were disaggregated to daily time scale using delta method. Finally, the hydrology model was run using scenarios data to analyze future hydrology features.

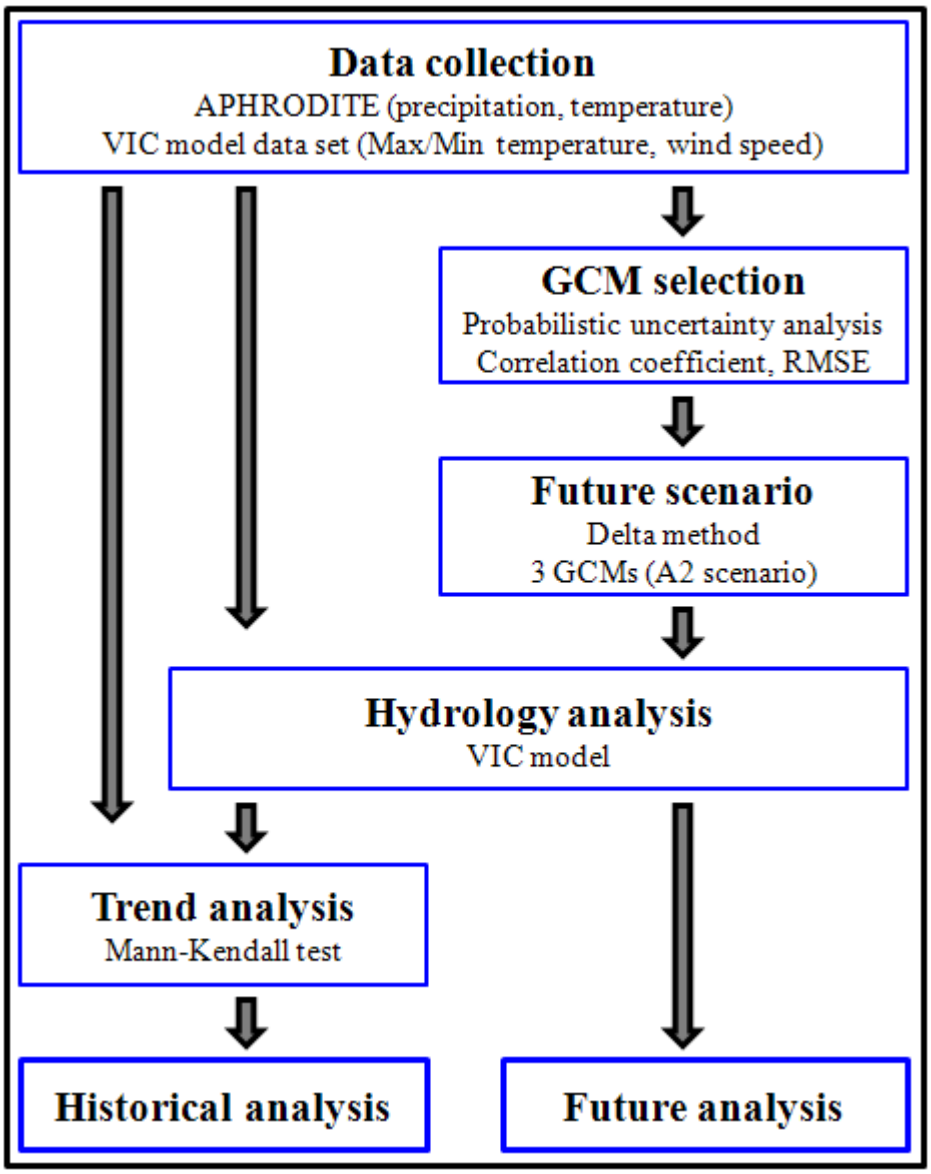

Figure 2.1: Overall procedure of this study.

2.1 Study area

In this study, Asia monsoon region including Asian Water Cycle Initiative (AWCI) 18 countries was selected to analyze the historical and future trend of climate and hydrology (Figure 2.2). The study area covered North, East, Southeast, Central, and South Asia which includes Bangladesh, Cambodia, India, Indonesia, Japan, Laos, Malaysia, Mongolia, Nepal, Pakistan, Philippines, South Korea, Sri Lanka, Thailand, Uzbekistan, Bhutan, Myanmar, and Vietnam. Moreover, the 18 demonstration basins one from each country were selected for basin scale analysis. The demonstration basins were selected based on the following criteria.

· Importance of the basin from the viewpoint of the socio-economic benefit area and hydrological sciences

· Minimum requirement of data availability:

a) Data type: Precipitation, maximum and minimum temperature, stream flow, wind speed.
b) Spatial density of observation stations: according to the WMO standards but local specifics are to be considered.
c) Watershed characteristics information

· Highly expected data:

a) Upper air observation is highly recommended.
b) Near-real time data availability is highly recommended.
c) Ground water and water quality data availability are essential for the river basins where those problems should be addressed.

· Size of the watershed: 100 km^2 - 1,000,000 km^2

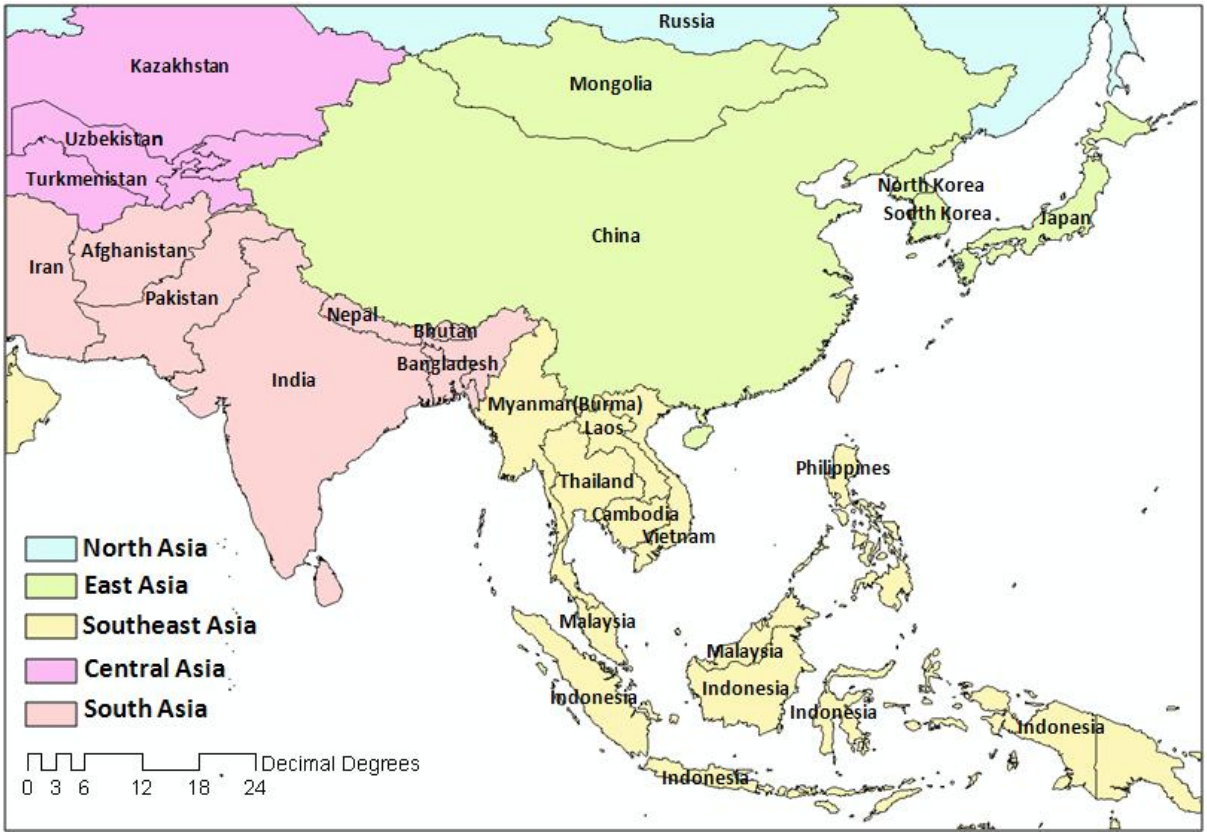

Figure 2.2: Study area with AWCI 18 countries in this study

Table 2.1 presents the selected demonstration basins of 18 countries. The basins were located from tropical to high latitude regions. Most regions were in close proximity of coastal areas. Also, some areas were located in Southern Hemisphere. The climate regime of the most basins was humid and semi-arid. The area of basins was different ranging from 303~61,021Km^2. The detailed description of individual basins is provided in the following sections.

Table 2.1: General description of demonstration basins of AWCI 18 countries

No.	Country	Basin name	Area (Km^2)	Climate regime
1	Bangladesh	Meghna	61,021	Humid
2	Bhutan	Punatsangchhu	13,263	Temperate

3	Cambodia	Sangker	2,961	Very Humid
4	India	Seonath	30,760	Humid
5	Indonesia	Mamberamo	78,992	Humid
6	Japan	Tone	3,300	Humid
7	Korea	Upper Chungju-dam	6,662	Temperate
8	Lao PDR	Sebangfai	8,560	Very Humid
9	Malaysia	Langat	2,350	Very Humid
10	Mongolia	Selbe	303	Semi-arid
11	Myanmar	Shwegyin	1,747	Very Humid
12	Nepal	Bagmati	3,700	Humid
13	Pakistan	Gilgit	12,800	Humid
14	Philippines	Pampanga	10,540	Humid
15	Sri Lanka	Kalu Ganga	2,720	Very Humid
16	Thailand	Mae Wang	600	Humid
17	Uzbekistan	Chirchik-Okhangaran	20,160	Humid
18	Vietnam	Huong	2,830	Very Humid

Bangladesh

The Meghna basin was selected from Bangladesh. Natural disasters like flood and drought occurs almost every year in Bangladesh. In recent years (2004 and 2007), the occurrence of flood in Meghna basin hampered the development of the country. Moreover, there is a shortage of observational data that hampers proper monitoring of flood situation and utilization of forecasting techniques. The inundation areas are widely extended throughout the country. Targets to be addressed through demonstration are to set-up a hydrological and flood inundation model with use of satellite data and downscaling techniques.

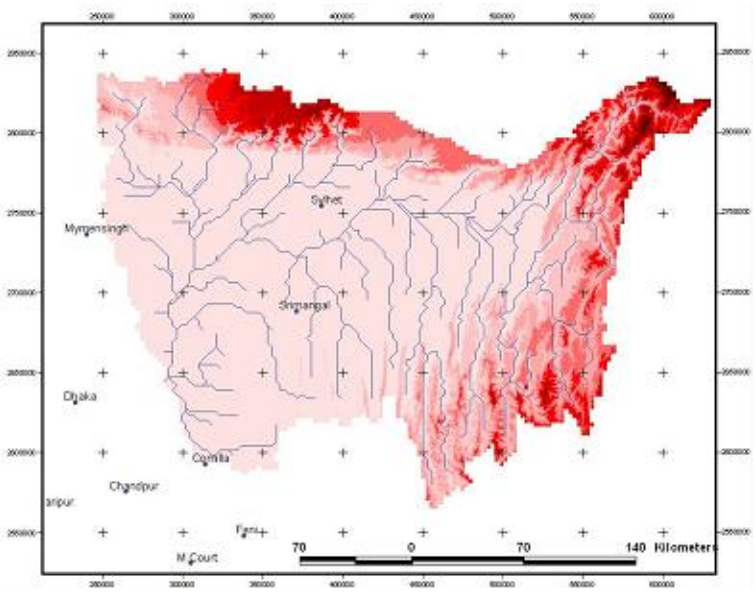

Figure 2.3: Location of the Meghna basin in Bangladesh.

Bhutan

The Punatsangchhu river basin was selected from Bhuttan which is the second largest basin in Bhutan and very important from an economic point of view. Punatsangchhu River is located in Punakha-Wangdue which is one of the most fertile valley. In addition, the biggest hydropower plants are also planned in this basin. On the other hand, the frequent glacier melt increases the risk of Glacial Lake Outburst Floods (GLOF) and then decreasing flow in the rivers afterwards. Targets to be addressed through demonstration are flood forecast, impacts on the hydropower generation, and a sediment transport study.

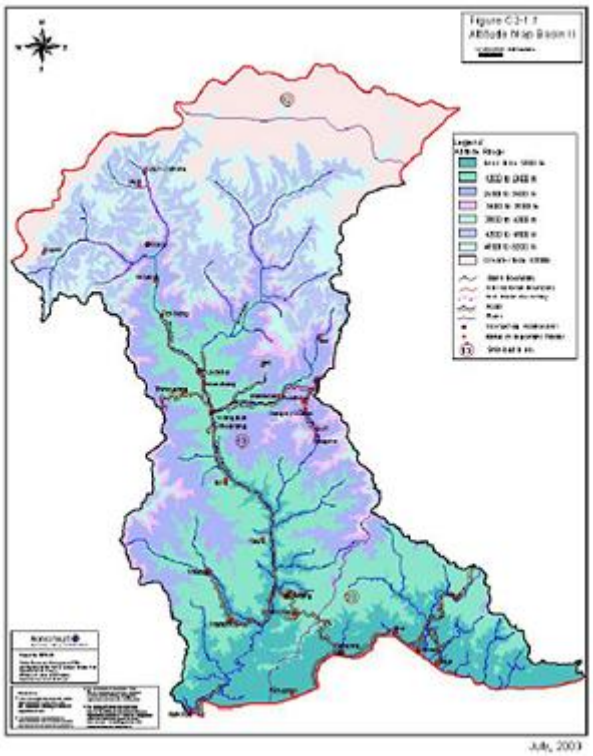

Figure 2.4: Location of the Punatangchhu basin in Bhutan.

Cambodia

Sangker river basin was selected from Cambodia which is one of the tributaries of Tonle Sap Lake, located in Battambang province at southwest of Cambodia. Two hydropower stations are being planned at its upper basin. The middle basin is covered with mixed agriculture and urban area, and suffers from flash flood. The downstream region is inundated for 6-months in a year by the flood from Tonle Sap Lake. Targets to be addressed through demonstration are impact of changes in the demands of water intake and dams (basin simulation model), Impact of changes in climate, water resources, land cover (hydrological model) and impact of changes in the canal level, sediment, flooding, and river works (hydrodynamic model).

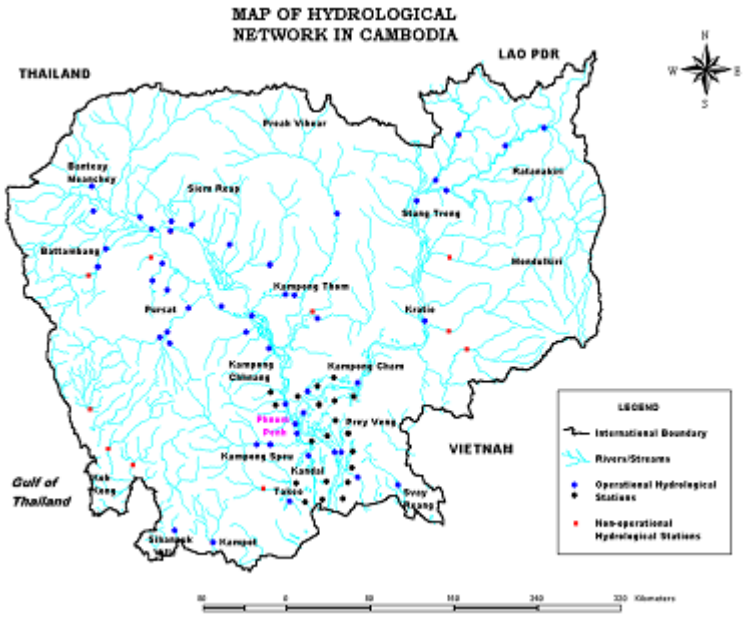

Figure 2.5: Location of the Sangker river basin and Tonle Sap Lake in Cambodia.

India

Seonath basins was selected from India. Seonath is the largest tributary of Mahanadi basin. It rises in the Chandrapur district of Maharashtra at an elevation of about 532m and meets Mahanadi River after traversing a distance of about 383 km.

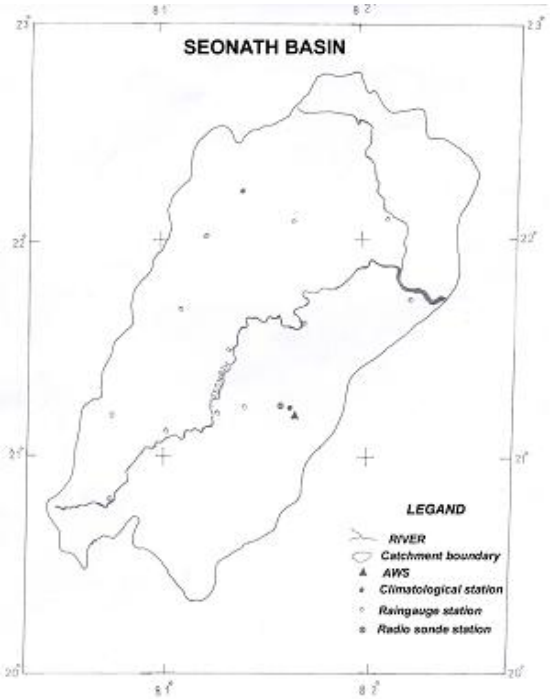

Figure 2.6: Location of the Seonath basin in India.

Indonesia

The Citarum river basin was selected from Indonesia. Indonesia is located in monsoon climate zone. The flooding occurs in Indonesia during rainy season and nowadays also during drought season. Targets to be addressed through demonstration are to take advantage of GIS database system and to support floods decision-makers.

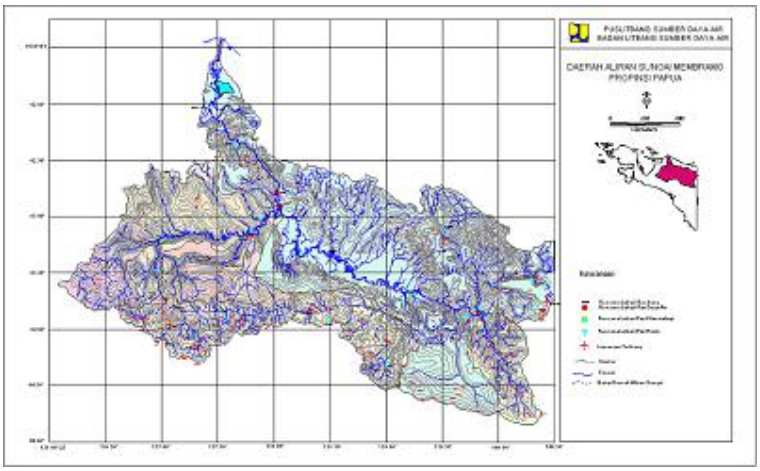

Figure 2.7: Location of the Citarum river basin in Indonesia.

Japan

The Tone river basin was selected from Japan. The Tone River is a very important source of water supply, irrigation and power generation for the Tokyo area. Therefore its management is crucial for the region. According to Japan Meteorological Agency (JMA), the trend of frequency and intensity of heavy rainfall in this region has been increasing on average from 1961-2001. Targets to be addressed through demonstration: A system capable to reduce flood peaks at downstream and replenish water levels in reservoirs after a flood event by using quantitative precipitation forecast will be developed. The error forecast will be also considered by the best means.

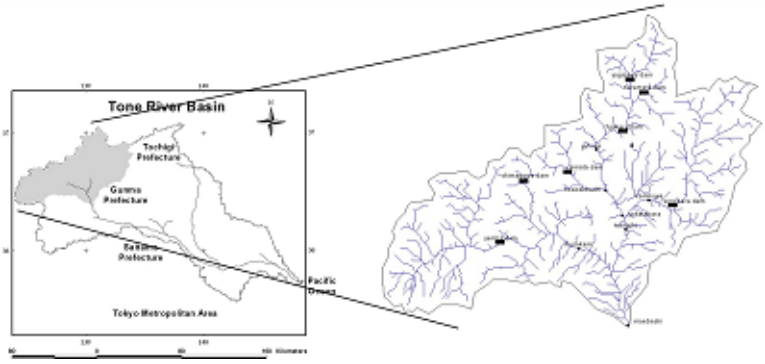

Figure 2.8: Location of the Tone river basin in Japan.

Korea

The Chungju-dam basin was selected from Korea. The basin is located at the middle-east of Korean Peninsula. It is an upper part of South Han River and the outlet is at Chungju-dam, which is the largest multi-purpose dam in South Han River basin. There have been significant damages from

floods and flash floods in Korea. In addition to flood control works, some other non-structural countermeasures are needed to be considered. Targets to be addressed through demonstration: (i) The use of satellite data for flood and drought monitoring and prediction for enhancement of the existing system (ii) Utilization of an integrated hydrological and meteorological forecast system for the optimal dam operation and flood risk reduction.

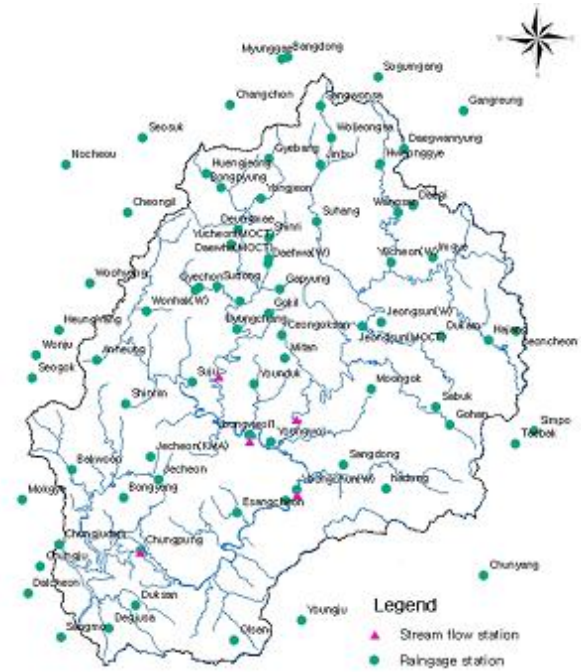

Figure 2.9: Location of the upper Chungju-dam basin in Korea.

Laos

The Sebangfai river basin was selected from Laos which is located in Khammouane province. At the source, the river flows from the Vietnam border in the southeast-northwest direction to Boualapha District and changes direction to the west to Mahaxay District and then turns from the northeast-southwest into the Mekong. With an annual increase of 2.6% since 1990, the total population in the basin was estimated to reach 192,200 in 1998. Targets to be addressed through demonstration: (i) Capacity building of the staffs of Department of Meteorology and Hydrology in making a more accurate flood forecast and analysis (ii) Assessment of the current conditions of hydro-meteorological stations (iii) Discussion on how to improve the current data transmission system and the operation and maintenance of these stations.

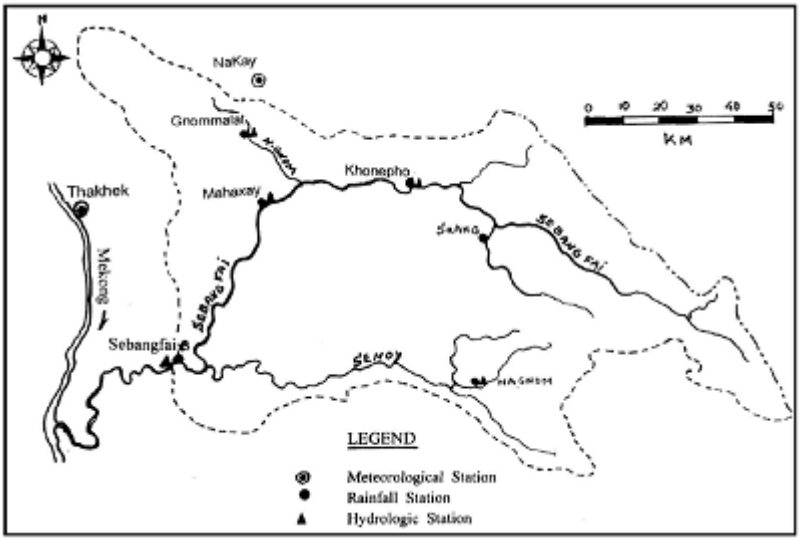

Figure 2.10: Location of the Sebangfai river basin in the Mekong river basin in Laos.

Malaysia

The Langat river basin was selected from Malaysia which is one of the four major basins in Selangor State. Langat Dam is the major source of domestic water supply for Kuala Lumpur, Putrajaya and areas adjoining to it. Groundwater extraction for industrial use is the minor water source of the basin. The Malaysian Government Administrative Centre Putrajaya is located at the centre of the basin. Targets to be addressed through demonstration: (i) Impact of climate change and land use change on hydrology, water resources and socio-economic activities (Hydro Climate Model) (ii) Impact of changes in the demands of water intake and dam (Basin Simulation Model), and (iii) Impact of changes in the sediment, river level, flooding, and river networks (Hydrodynamic Model).

Figure 2.11: Location of the Langat river basin in Malaysia.

Mongolia

The selected Selbe river basin is located in center of Mongolia, in the north of Ulaanbaatar. It is the upper basin of the Tuul Stream basin (6,300 km^2). From mid of 1990s, settling area and population have been rapidly increasing. Following the human activities, individual house building, paved areas, groundwater wells and livestock pasture are increasing. Also, forest cut and cultivation took place in some extent. Targets to be addressed through demonstration: (i) Environmental degradation i.e. vegetation, soil degradation, deforestation and rapid urbanization impacting on surface and ground water regime and interaction mechanism, ground water contamination, water scarcity and flood control (ii) Surface and ground water monitoring and modelling to assist better management in light of anthropogenic influences and climate change impact and flood control, and (iii) Assistance in the development of information systems for promoting the implementation of Integrated Water Resources Management (IWRM) in the Selbe and Tuul Stream Basins.

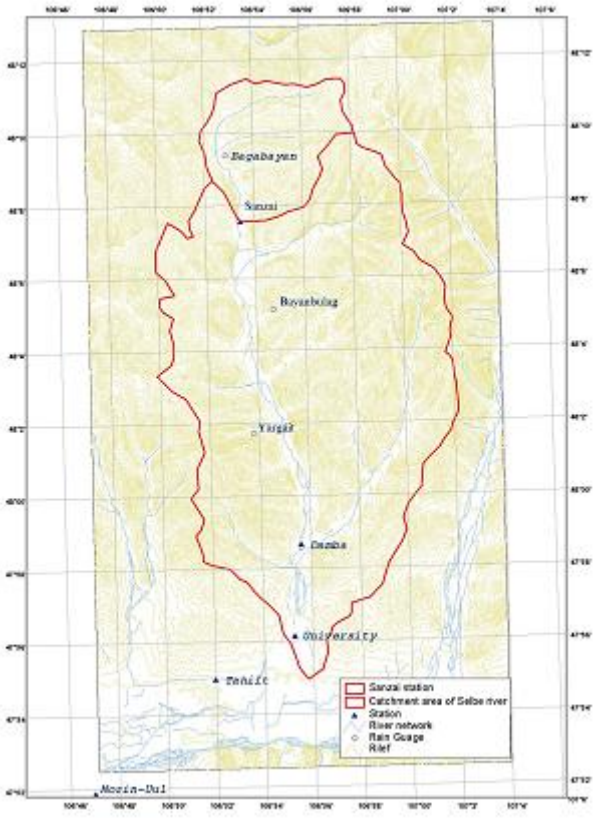

Figure 2.12: Location of the Selbe river basin in Mongolia.

Myanmar

The Shwegyin basin was selected from Myanmar. The Shwegyin town is situated on the mouth of Shwegyin river and composed of 8 wards and 26 villages. It is about 42 miles from north to south and 19 miles from east to west. The high mountains are formed in northern and eastern part, and plain areas are in the western and southern part of the basin. There are 5 rivers flowing through the township including Shwegyin river. Targets to be addressed through demonstration: (i) To install two telemeter stations and a receiving station in Shwegyin basin (ii) To develop forecasting technique for

flash flood and (iii) To develop accurate flood inundation maps using all available data including GIS data sources.

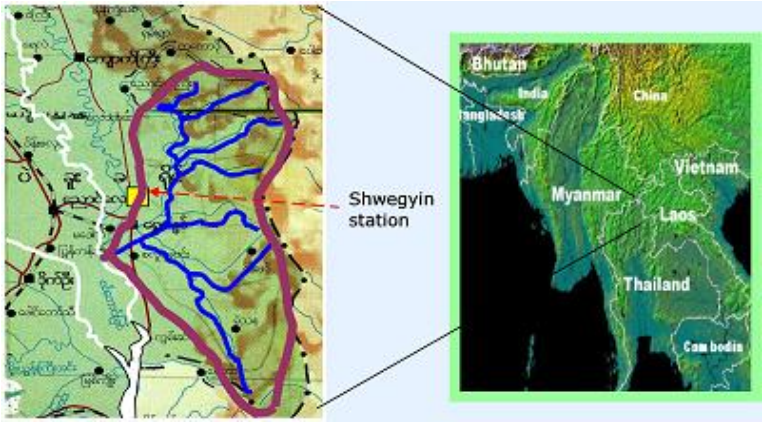

Figure 2.13: Location of the Shwegyin Basin in Myanmar.

Nepal

The Bagmati river basin was selected from Nepal. The Bagmati River originates from the southern slopes of Shivapuri Lekh at Vagdhara, north of Kathmandu. It flows towards south west from its origin and turns to west in Kathmandu city and emerges out of Kathmandu Valley at Chovar. The observed maximum flood discharge is about 11,000 m^3/s. Targets to be addressed through demonstration: (i) Reduce flood damages, bank erosion and inundation (ii) Reduce landslides and debris flows by means of landslides hazard mapping and (iii) Water pollution is crucial since it is used to meet the irrigation demand.

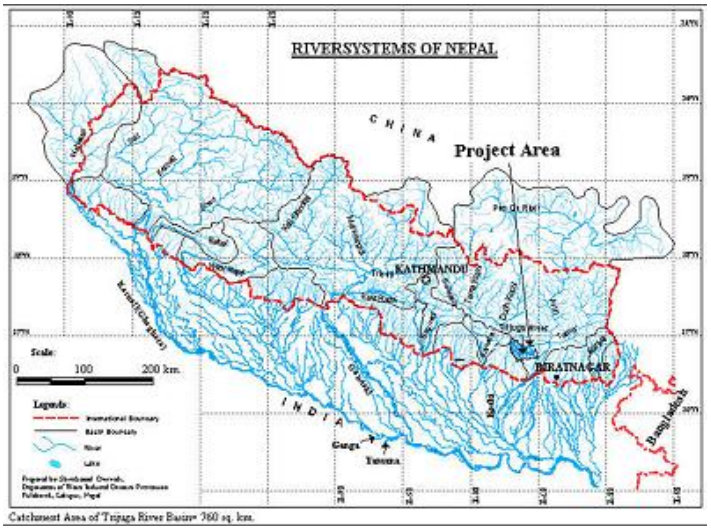

Figure 2.14: Location of the river basin in Nepal.

Pakistan

The Gilgit basin consisting of two main rivers, Gilgit and Hunza, located in the upper Indus river basin was selected for the Hunza basin also for the Climate Change Assessment and Adaptation (CCAA). These basins are located in the Karakoram mountain region with steep slopes and large extent covered with glaciers and snow. The upper part of the whole Indus basin represents about 20% of its

extent but contributes about 80% of all discharge of the Indus River. Majority of the flow is produced by snow and glacier melting during the summer season. Accordingly, the main focus of the CCAA was on snow and glacier processes, in particular better ability to simulate and predict discharge for flood forecasting and warning, including GLOF and to assess possible impacts of climate change on glacier and snow water reservoirs in the area (APN, 2011).

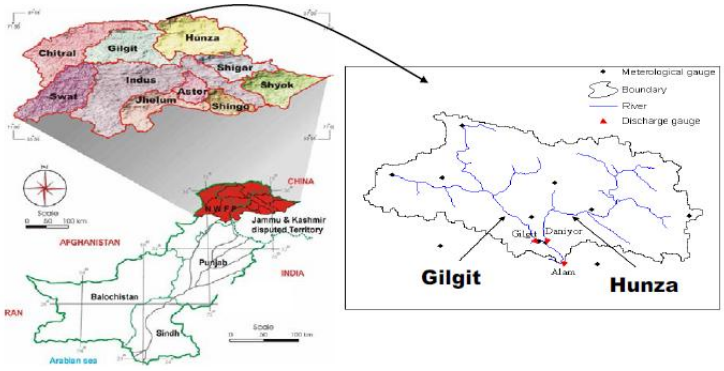

Figure 2.15: Location of the Gilgit river basin in Pakistan.

Philippines

The selected Pampanga river basin is the fourth largest basin in the Philippines. The total length of the main river is about 260 km. The basin is drained through the Pampanga River and via the Labangan Channel into the Manila Bay. The main river is supported by several tributaries. It has a relatively low-gradient channel at the middle and lower sections. There are two dams within the river basin. Targets to be addressed through demonstration: (i) Downscaling and (ii) optimal multi-purpose reservoir operation.

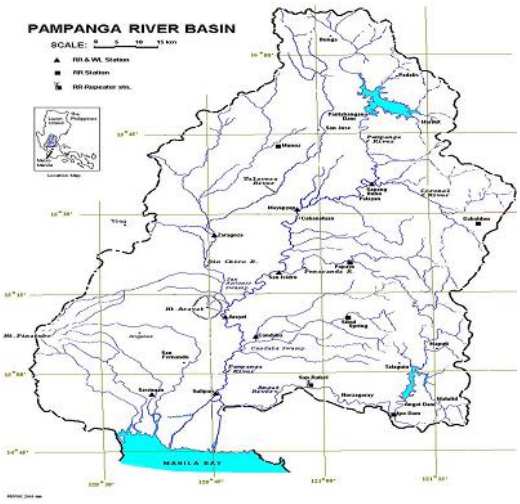

Figure 2.16: Location of the Pampanga river basin in Philippines.

Sri lanka

The Kaluganga River basin is located at the South-Western part of Sri Lanka. It is about 130 km long and discharges into the Indian Ocean. The flood disasters continue in the basin due to climatic, hydrologic, topographic and land use characteristics in the basin. There is a hydropower reservoir at one of the upper reaches. Population density in Kalutara and Ratnapura districts are 677 and 314 person/km^2. Targets to be addressed through demonstration: (i) Flood risk reduction (ii) Identification of inundation levels and (iii) Implementation of early warning systems based on real time flood forecasting.

Figure 2.17: Location of the Kaluganga river basin in Sri Lanka.

Thailand

Mae Wang basin is one of the sub-basins of the Mae Ping Basin in Northern Thailand. Most of the basin is mountain area declining from west to east that consists of the mixed unit of steep slope highland soil series. Targets to be addressed through demonstration: (i) To install telemetering station for observation and collection of Hydro-meteorological data (ii) Developing a flood warning model and effective water management

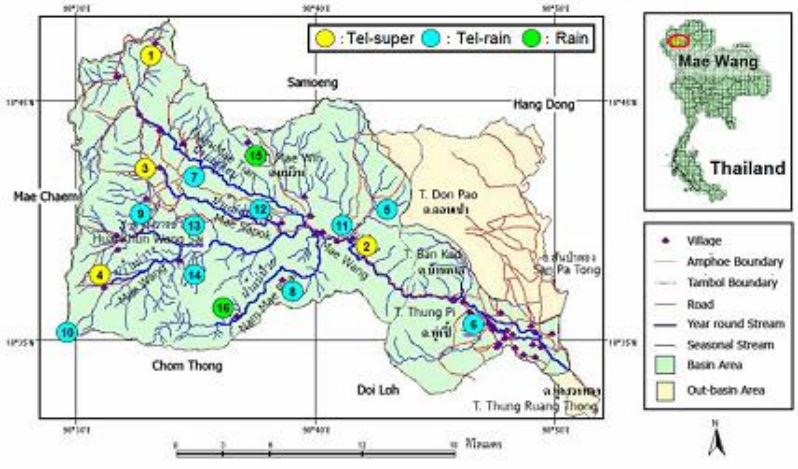

Figure 2.18: Location of the Mae Wang basin in North Thailand.

Uzbekistan

The selected Chirchik-Okhangaran basin is located in northeastern part of Uzbekistan. Snowmelt induced runoff of rivers of the Chirchik – Okhangaran basin comprised 60-90% of the total stream flow. The Chirchik - Okhangaran river basins have 19 hydropower stations. There are two rivers – Chirchik (161 km) and Okhangaron (223 km). River basin has 67 lakes with different genesis type. This basin has 2,385 thousand people. Targets to be addressed through demonstration: (i) Sediment transport (ii) impacts of hydrological processes and on hydropower generation and (iii) to monitor the flow regimes in the rivers due to climate change.

Figure 2.19: Location of the Chirchik-Akhangaran basin in Uzbekistan.

Vietnam

The Huong river basin belongs to the Thua Thien Hue province in coastal area of the Central Vietnam. The Huong river system contains 3 main rivers: Ta Trach, Huu Trach and Bo River. The Huong River is short and steep which runs from mountain to the low plain area. Time of concentration is short and river basin has low storage capacity. Floods and inundation often occur very quickly and severely. Targets to be addressed through demonstration: To improve accuracy of the forecast, effective natural disaster preparedness, prevention measures and reducing the losses.

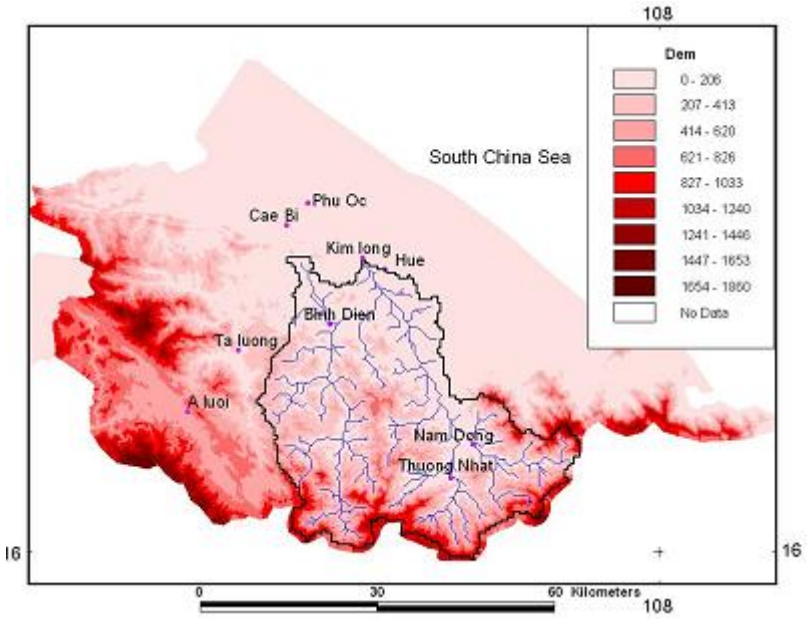

Figure 2.20: Location of the Huong river basin basin in Veitnam.

2.2 Data

2.2.1 Observed meteorological data

To analyze climate and hydrology trend over Asia, the precipitation and temperature data at 0.5° horizontal grid resolution was obtained from APHRODITE (Asian Precipitation-Highly-Resolved Observational Data Integration towards Evaluation of Water Resources). The APHRODITE project develops state-of-the-art daily precipitation and temperature with high-resolution grids for Asia. The data set is created primarily with data obtained from a rain-gauge-observation network (Yasutomi et al., 2011 and Yatagai et al., 2012). Also, to analyze hydrology trend over Asia, we used maximum temperature, minimum temperature, and wind speed from the dataset of Variable Infiltration Capacity (VIC) Macroscale Hydrologic Model. This dataset provides 0.5° resolution input data to run VIC model. This Gridded data is generated using monthly precipitation from the University of Delaware (UDel) Willmott and Matsuura (2007) gridded observation. Gauge precipitation adjusted for gauge undercatch as described by Adam and Lettenmaier (2003) and for orographic effects as described by Adam et al. (2006). Monthly gridded minimum and maximum temperatures were obtained from the Climate Research Unit (CRU) of the University of Eastern Anglia (Mitchell et al., 2004). Wind speed data was obtained from NCEP-NCAR reanalysis (Kalnay et al. 1996). The daily variability of NCEP/NCAR is used to create daily precipitation and temperatures data using monthly CRU (for temperatures) and UDel (for Precipitation) data as a control. We used all datasets from January 1977 to December 2006.

2.2.2 Geophysical data (DEM, Soil, Land use)

The Digital Elevation Model (DEM) is basic elevation data to apply VIC model. The selection of coordinates, resolution, grid points and extraction of elevation is conducted using the DEM analysis. Also, spatial resolution of land use and soil map is determined from spatial resolution of the DEM. In

this study, 30 x 30 seconds DEM from USGS (http://eros.usgs.gov/) was obtained. The collected DEM data was converted to 0.5 x 0.5 degree DEM to comply with other datasets of 0.5 degree used in this study. Further, the elevation data at each grid point was extracted from DEM.

The soil map is also needed to build VIC model. To build soil data over Asia, 5 x 5 minutes resolution data from the Food Agriculture Organization (FAO, 1998) was used. In the FAO system, approximately 50 attributes of soil are included. The FAO soil database has global coverage. Table 2.2 shows the coordinate and kind of target area provided from FAO-soil. The target area in the FAO system is divided into 15 regions.

Table 2.2: Coordinate and kind of target area provided from FAO-soil.

File	Land Area	Cols	Rows	NW-Corner		SE-Corner	
AfSoil	Africa	876	912	38°00'N	19°00'W	38°00'S	54°00'E
AusSoil	Australia	504	408	10°00'S	112°00'E	44°00'S	154°00'E
CAmSoil	CentralAmerica	708	312	33°00'N	118°00'W	7°00'N	59°00'W
CntASoil	CentralAsia	504	252	56°00'N	46°00'E	35°00'N	88°00'E
EurSoil	Europe	1128	468	73°00'N	25°00'W	34°00'N	69°00'E
FEsSoil	FarEast	1044	588	54°00'N	60°00'E	5°00'N	147°00'E
NESoil	Near East	516	336	40°00'N	32°00'E	12°00'N	75°00'E
NewNAm	North America + Greenland	2016	792	84°00'N	180°00'W	18°00'N	12°00'W
NZEast	New Zealand	168	168	34°00'S	166°00'E	48°00'S	180°00'E
NZWest	New Zealand (part)	47	47	38°05'S	180°00'W	42°00'S	176°05'W
SAmSoil	South America	696	834	130°00'N	92°00'W	56°30'S	34°00'W
SEAEast	South East Asia (upto 180)	1056	624	29°00'N	92°00'E	23°00'S	180°00'E
SEAWest	South East Asia (west side)	120	156	10°00'S	180°00'W	23°00'S	170°00'W
Sib180	Siberia	1536	456	80°00'N	52°00'E	42°00'N	180°00'E
World	World	4320	1686	84°00'N	180°00'W	56°30'S	180°00'E

The land use data was obtained from UMD (University of Maryland). The collected land use data was converted to 0.5 degree to comply with resolution of other datasets used in the study. Table 2.3 shows the global land use classification and area ratio. The land use data is divided into 14 elements.

Table 2.3: Global land use classification and area ratio.

No.	Land use classification	Area ratio (%)
1	Water	0.15
2	Evergreen Needleleaf Forest	4.18
3	Evergreen Broadleaf Forest	6.00

4	Deciduous Needleleaf Forest	0.67
5	Deciduous Broadleaf Forest	1.30
6	Mixed Cover	3.06
7	Woodland	10.24
8	Wooded Grassland	13.84
9	Closed Shrubland	2.48
10	Open Shrubland	17.31
11	Grassland	17.76
12	Cropland	13.25
13	Bare Ground	9.60
14	Urban and Built-Up	0.17

2.3 Climate change scenario

2.3.1 Emission scenario

The GCMs used in this study were driven by A2, A1B and B1 scenarios which have an important role for climate projection and water resource management in the future. Generally, IPCC DDC provides the data from 24 GCMs and there are 16 GCMs which have all A2, A1B and B1 scenarios. However, in this study we only tested 10 GCMs due to the availability of data.

By 2100, the world will have changed in ways that are difficult to imagine as difficult as it would have been at the end of the 19th century to imagine the changes of the 100 years since. Each storyline assumes a distinctly different direction for future developments, such that the four storylines differ in increasingly irreversible ways. Together they describe divergent futures that encompass a significant portion of the underlying uncertainties in the main driving forces. They cover a wide range of key “future” characteristics such as demographic change, economic development, and technological change. For this reason, their plausibility or feasibility should not be considered solely on the basis of an extrapolation of current economic, technological, and social trends.

The A1 storyline and scenario family describes a future world of very rapid economic growth, global population that peaks in mid-century and declines thereafter, and the rapid introduction of new and more efficient technologies. Major underlying themes are convergence among regions, capacity building, and increased cultural and social interactions, with a substantial reduction in regional differences in per capita income. The A1 scenario family develops into three groups that describe alternative directions of technological change in the energy system. The three A1 groups are distinguished by their technological emphasis: fossil intensive (A1FI), non-fossil energy sources (A1T), or a balance across all sources (A1B).

The A2 storyline and scenario family describes a very heterogeneous world. The underlying theme is self-reliance and preservation of local identities. Fertility patterns across regions converge very slowly, which results in continuously increasing global population. Economic development is primarily regionally oriented and per capita economic growth and technological change is more fragmented

and slower than in other storylines.

The B1 storyline and scenario family describes a convergent world with the same global population that peaks in midcentury and declines thereafter, as in the A1 storyline, but with rapid changes in economic structures toward a service and information economy, with reductions in material intensity, and the introduction of clean and resource-efficient technologies. The emphasis is on global solutions to economic, social, and environmental sustainability, including improved equity, but without additional climate initiatives.

The B2 storyline and scenario family describes a world in which the emphasis is on local solutions to economic, social, and environmental sustainability. It is a world with continuously increasing global population at a rate lower than A2, intermediate levels of economic development, and less rapid and more diverse technological change than in the B1 and A1 storylines. While the scenario is also oriented toward environmental protection and social equity, it focuses on local and regional levels.

Fig. 2.21 shows total global annual CO2 emissions from all sources (energy, industry, and land-use change) from 1990 to 2100 (in gigatonnes of carbon (GtC/yr)) for the families and six scenario groups. Each colored emission band shows the range of harmonized and non-harmonized scenarios within each group.

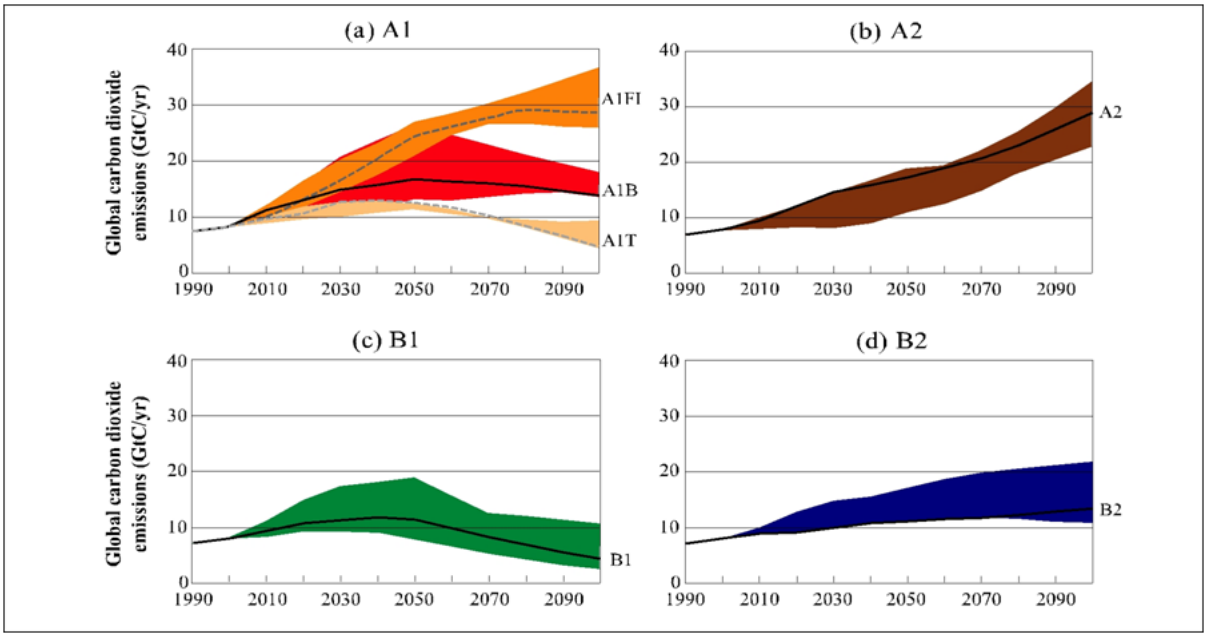

Figure 2.21: Total global annual CO_2 emission from all sources (energy, industry, and land-use change) from 1990 to 2100 (in gigatonnes of carbon (GtC/yr)) for the families and six scenario groups

2.3.2 Selection of GCMs

The objective of this section is to compare the effectiveness of each GCM for their future application in Asian region. The GCMs data was collected from the IPCC Data Distribution Center (DDC, http://www.ipcc-data.org/index.html). The information of each GCM is shown in Table 2.4. The

simulated data for the study at hand consist of the surface nodal precipitation and temperature estimates from 9 atmospheric global circulation models. The comparison of GCMs was based on several statistical measures i.e. the probabilistic uncertainty analysis, correlation coefficient, and RMSE. Firstly, we considered the effectiveness of each GCM using the score index of each test. We then established the overall effectiveness of each GCM based on the results of all three tests. Finally, we selected the best GCMs with high overall effectiveness score for future application in Asian region.

Table 2.4: List of model name, version, and simplified abbreviation for each model.

No.	Model (agency: version)	Abb.	Country	Resolution (km x km)	Number of scenarios	Number of ensemble
1	MPIM: ECHAM5	ECHAM5	Germany	187.5 x187.5	8	3
2	CSIRO: MK3.0	MK3.0	Australia	187.5 x187.5	7	3
3	GFDL: CM2_1	CM2_1	USA	250 x 200	8	3
4	CNRM: CM3	CM3	France	281.25 x 281.25	8	1
5	MRI: CGCM2_3_2	CGCM2_3_2	Japan	281.25 x 281.25	8	3
6	UKMO: HADCM3	HADCM3	UK	375 x 250	7	2
7	IPSL: CM4	CM4	France	375 x 250	8	2
8	CCCMA: CGCM3_T47	CGCM3_T47	Canada	375 x 375	8	3
9	CONS: ECHO-G	ECHO-G	Germany/Korea	375 x 375	8	3

Fig. 2.22 illustrates the general methodology adopted in this study which has two main approaches. Firstly, we used probabilistic screening methodology to examine the capability of GCMs in discriminating the extreme events. After that, statistical tests of correlation coefficient and root mean squared error were used to analyze the general capability of GCMs. We then quantified the effectiveness of GCMs by using the score index. It should be noted that, in this study we provided several approaches to examine the quality of GCMs and our method was generally more accurate than previous studies. The statistical methods used for GCMs selection are explained in the following sections.

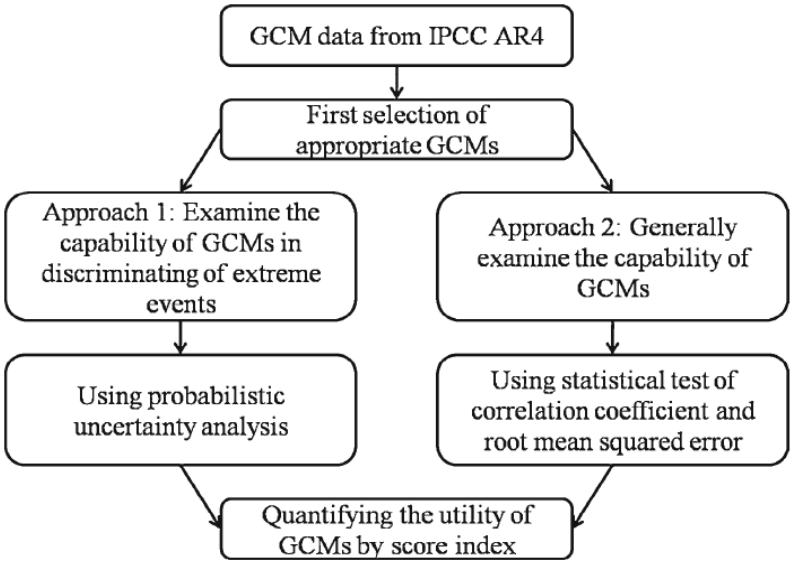

Figure 2. Procedure for evaluating the utility of IPCC AR4 GCMs

Probabilistic screening methodology

The probabilistic screening methodology (Georgakakos, 2003) is based on the premise that times of extremes in climate model nodal values (climate model scale) should correspond to times of extremes of the target variable (watershed scale) for climate model simulations/predictions of a certain indicator variable (e.g., nodal precipitation) to be useful for water resources applications that involve regional surface target variables (e.g., watershed mean areal precipitation). If there is no such ''signal'' in the climate nodal values it is unlikely that they will be useful for applications that involve the mentioned target variable (Bae et al., 2007). The theory accounts for potential shifts in climate model output in space and time, and allows for ensemble simulation/predictions. It implicitly involves downscaling climate model simulations to watershed scales. It may also be generalized for vector indicator and target variables given adequate record lengths (Georgakakos, 2003).

Consider a watershed of interest and a region centered on it that contains several nodes of a climate model. The end goal of this analysis is to determine if the climate simulations/predictions associated with nodes in the region have information that may be used for identifying and discriminating watershed hydroclimatic extreme events. Fig. 2.23 exemplifies the geometrical configuration for one of the Korean watersheds and its analysis window. In Fig. 2.23, (x_n, y_n) are the longitude and latitude coordinates of the n^{th} node of the climate model under consideration, e_x and e_y are the inter-nodal distances in the longitude and latitude directions, (x_0, y_0) are the coordinates of the centroids of the study watershed, and d_x and d_y are the longitude and latitude distances of the watershed centroid from the boundaries of the window of analysis that contains all the climate model nodes used in the analysis. The distances d_x and d_y are multiples of the inter-nodal distances e_x and e_y, respectively, with factor λ specified by the user. The larger the value of λ, the larger the number of climate model nodes used in the analysis.

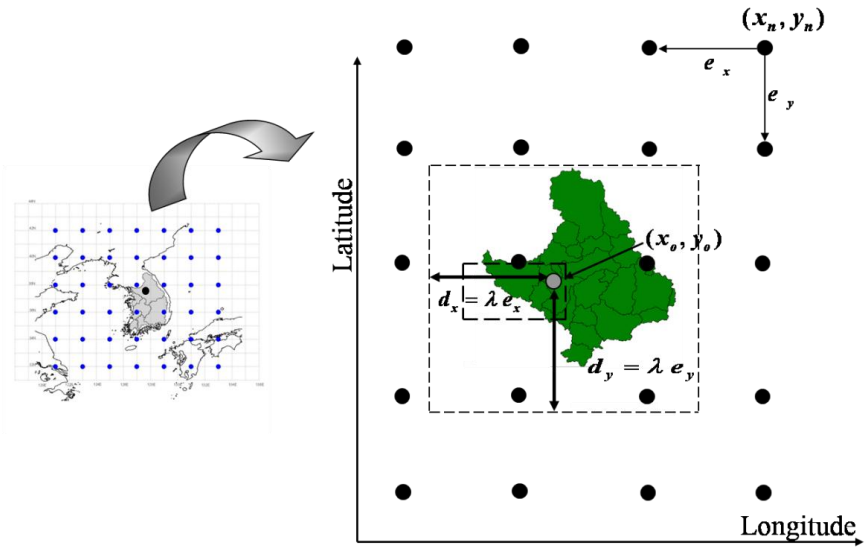

Figure 2.23: Specific application basin and analysis window with climate model nodes (Han river basin and CM2 climate model).

In this work, we used the formulation for the utility index, E_p, which is based on simple averaging of nodal and ensemble simulations/predictions in the vicinity of the application watershed:

$$E_p = \frac{1}{N_\lambda K} \sum_{n=1}^{N_\lambda} \sum_{k=1}^{K} P_{KS}(D > D_{n,k}) \quad (1)$$

where K is the number of climate model ensembles, N_k is the number of climate-model nodes within the window of analysis specified by λ, and $P_{KS}(D > D_{n,k})$ is (for each node and ensemble) the exceeding probability of the maximum difference in cumulative probabilities: (A) the cumulative probability of the watershed target variable values that are concurrent with climate-model nodal values that fall in a specified upper quantile of their distribution, and (B) the cumulative probability of the watershed target variable values that are concurrent with climate-model nodal values that fall in the corresponding lower quantile of their distribution. In particular, the nomenclature is such that the probability, $P_{KS}(D > D_{n,k})$, refers to the event that an observed $D_{n,k}$ is exceeded by an arbitrary value D (Bae et al., 2007).

The theory uses the formula of the Kolmogorov–Smirnov test to determine the utility index E_p. In this study, we used the tercile for discriminating high and low extremes for the watershed target variable.

In applications of the formulated utility index E_p to data, lower values of the index are more significant in general than higher values. The question arises as to what values of this index are statistically significant and what values are likely to be obtained by chance in any given application. For an individual watershed and using a tercile for high and low values, Monte Carlo simulation indicates that the theoretical upper threshold of the index E_p for a significance level of 10% is approximately equal to 1⁄3. In case, the index E_p of original run is smaller than the index E_p of threshold, it is defined as a significant result for given GCM and basin. The interested reader is referred to Georgakakos (2003) for more information on the formulation and significance tests of the utility index (Bae et al., 2007).

Statistical tests for examining the general capability of GCMs

The correlation coefficient and root mean square error are commonly used methods for model evaluations. The correlation coefficient test has been known as a powerful and easy to use goodness-of-fit test. Correlation coefficient is a measure of linear dependency between a pair of random variables. For the problem discussed herein, the variables are GCM data and observed data of both precipitation and temperature.
Let (x, y) denote a pair of climate model data and observed data (precipitation or temperature). The correlation coefficient of x and y can be defined as:

$$r_{xy} = \frac{\sum_{i=1}^{n} (x_i - \bar{x})(y_i - \bar{y})}{n S_x S_y} \quad (2)$$

where $\bar{x}$ and $\bar{y}$ are sample mean of x and y; S_x and S_y are sample standard deviation of x and y; n is number of data. The window of analysis is similar as presented in the previous section of probabilistic uncertainty analysis with fixed parameter λ of 1.05.

The root mean square error (RMSE) shows the fitting between the GCM predicted data and observed target data. The index ranges from zero to infinity, with zero corresponding to the ideal.

Let x denotes GCM data, y denotes observed data. The RMSE of GCM data compared with observed data is then defined as:

$$RMSE = \sqrt{\frac{1}{n}\sum_{i=1}^{n}(x_i - y_i)^2} \quad (3)$$

It is noted that, the analysis window used for RMSE test is similar to that of probabilistic uncertainty test. However, the parameter λ is fixed with the value of 1.05. The final purpose of RMSE test is to examine the error in simulation of a GCM in root mean squared sense.

Quantifying the overall effectiveness of GCMs by score index

It is noted that, to evaluate the utility of a GCM for general application using both simulation of precipitation and temperature we need an overall score for each GCM. Therefore, in this section we suggest a score index for each GCM, based on its results of both precipitation and temperature using each statistical test.

- **Probabilistic uncertainty test**

The overall score index of probabilistic uncertainty test is defined as:

$$S_{P,total} = \sum_{i=1}^{n_b}\sum_{j=1}^{n_d}\sum_{k=1}^{4} S_{i,j,k} + \sum_{i=1}^{n_b}\sum_{j=1}^{n_d}\sum_{l=1}^{12} S_{i,j,l} \quad (4)$$

where $S_{i,j,k}$ denotes component score of a GCM for given basin i (with n_b is total number of basins) with type of data used j (with n_d is number of type of data used) in the season k(k=1,2,3,4). $S_{i,j,l}$ denotes the component score of a GCM for certain basin i with type of data used j in the month l(l=1,2,…,12). $S_{i,j,k}$ and $S_{i,j,l}$ are defined as follows: For a given GCM, if there is a significant result at basin i of season k or month l with type of data used j, then $S_{i,j,k}$ and $S_{i,j,l}$ are defined as 1, otherwise these are defined as 0 (the significant result is defined in the section of Methodology).

- **Statistical tests of correlation coefficient and root mean squared error**

The overall score index of correlation coefficient test (or RMSE test) is defined as:

$$S_{r,total}(S_{RMSE,total}) = \sum_{i=1}^{n_b}\sum_{j=1}^{n_d}\sum_{k=1}^{4} S_{i,j,k} + \sum_{i=1}^{n_b}\sum_{j=1}^{n_d}\sum_{l=1}^{12} S_{i,j,l} \quad (5)$$

where $S_{i,j,k}$ denotes component score of a GCM for given basin i with type of data used j in the season k (k=1,2,3,4) where n_b is total number of basins and n_d is number of type of data used. $S_{i,j,l}$ denotes the component score of a GCM for certain basin i with type of data used j in the month l (l=1,2,…,12). For correlation coefficient test, $S_{i,j,k}$ or $S_{i,j,l}$ are defined as follows: for a given GCM m, if the correlation coefficient ($r_{i,j,k,m}$ or $r_{i,j,l,m}$) at basin i for season k (or month l) with type of data used j, is greater than the average correlation coefficient ($r_{i,j,k,average}$ or $r_{i,j,l,average}$) of all 10 GCMs at similar basin, season (or month) , then $S_{i,j,k}$ (or $S_{i,j,l}$) is defined as 1, otherwise as 0. Similarly, if the RMSE of a given GCM m is smaller than the average RMSE of all GCMs then $S_{i,j,k}$ (or $S_{i,j,l}$) is defined as 1 otherwise as 0.

The variety of approaches allows us to examine and compare the effectiveness of all GCMs for fitting between predicted data and observed data. From the component score index of each approach, we may then build the overall utility of each GCM and select the best GCMs among them. The score index system applied for correlation coefficient and RMSE test is very effective because it evaluates the effectiveness of each GCM by directly comparing the value of correlation coefficient and root mean squared error at given basin and season or month.

- **Establishing the overall score**

The overall score index of each GCM is computed based on their scores in the probabilistic uncertainty test and statistical tests. Our goal is to build the overall score with equal contribution from scores of these 3 tests. However, each test produces its own score with difference in magnitude. In order to remove this difference, we firstly normalize the total score of each test. The normalized scores of probabilistic uncertainty test, correlation coefficient test and RMSE test for given GCM(m) are given by:

$$S_{t,normalized,m} = \frac{S_{t,total,m} - S_{t,total,min}}{S_{t,total,max} - S_{t,total,min}} \quad (6)$$

where the index t denotes the type of tests i.e. probabilistic uncertainty test, correlation coefficient test or RMSE test; $S_{t,normalized,m}$ is normalized score of GCM m in the test t; $S_{t,total,m}$ is the total score of GCM m in the test t; $S_{t,total,min}$ and $S_{t,total,max}$ are the minimum and maximum score of all GCMs in the test t, respectively.

We then define the overall normalized score of given GCM m by:

$$S_{overall,normalized,m} = S_{P,normalized,m} + 0.5(S_{r,normalized,m} + S_{RMSE,normalized,m}) \quad (7)$$

where $S_{overall,normalized,m}$ is the overall normalized score of GCM m; $S_{P,normalized,m}$, $S_{r,normalized,m}$, $S_{RMSE,normalized,m}$ are normalized scores of probabilistic uncertainty test, correlation coefficient test and

RMSE test of GCM m, respectively. It is noted that, for each test of a given GCM, the normalized score ranges from 0 to 1. Thus, the overall normalized score of a GCM ranges from 0 to 2.

2.3.3 Change factor method

To evaluate future climate change impact at regional scale, it is difficult to use GCM output directly due to the coarser resolution of GCMs. The resolution of GCMs is generally more than 100 km (IPCC, 2007). The downscaling technique is required to utilize the GCM output for regional features. Some studies used change factor method to analyze regional features (Hay et al., 2000; Reason et al., 2004). Figure 2.24 shows the change factor concept between observation and GCM output.

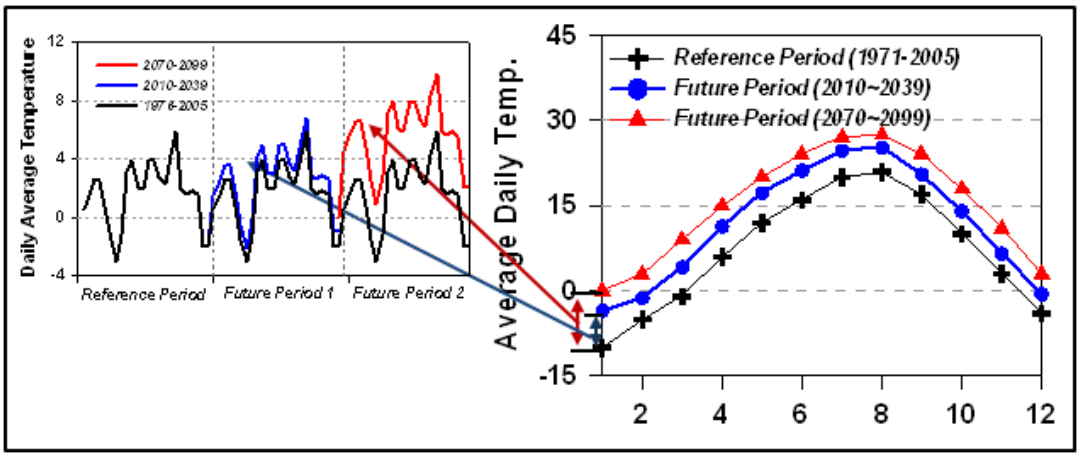

Figure 2.24: Concept of the change factor method between observation and GCM output.

The GCM grid-box output is used to calculate the change factor for delta method. The change in climate for the delta-change experiments is calculated by adding the difference between the GCM current and future monthly means for the grid-box closest to each basin, to the precipitation and temperature observed time series. The changes in precipitation (in percent) and temperature (in °C) at each month are used for the delta change scenario generation. The future scenario of temperature using the change factor is given by:

$$T_{fut,i} = T_{obs,i} + (\sum_{i=1}^{m} T_{s.fut,i} - \sum_{i=1}^{m} T_{s.ref,i}) \quad (8)$$

where T_{fut} is the future scenario of the temperature; $T_{obs,i}$ denotes the observed temperature at grid point i; $T_{s.fut,i}$ and $T_{s.ref,i}$ represent the future scenario and the reference scenario of temperature at grid point i, respectively. Similarly, the future scenario of precipitation using the change factor method is given by:

$$P_{fut,i} = P_{obs,i} \times \frac{\sum_{i=1}^{m} P_{s.fut,i}}{\sum_{i=1}^{m} P_{s.ref,i}} \quad (9)$$

2.4 Hydrologic model

2.4.1 VIC model

In this study, the VIC model was used to analyze water resources over Asia monsoon region. The VIC model was developed for incorporation in GCMs, aiming to improve the representation of horizontal resolution and subgrid heterogeneity in a simple way. Employing the infiltration and surface runoff scheme in Xianjiang model (Zhao, 1980), VIC was first described as a single soil layer model by Wood et al. (1992) and implemented in the GFDL and Max-Planck-Institute (MPI) GCMs (Stamm et al., 1994). The single soil layer model requires three parameters: an infiltration parameter, an evaporation parameter, and a base flow recession coefficient. In 1994, Liang et al. (1994) generalized the two-layer VIC model (VIC-2L) to include the multiple soil layers and spatially varying vegetation and evaporation within a grid cell. In VIC-2L, infiltration, drainage from the upper soil layer into the lower soil layer, surface and subsurface runoff are calculated for each vegetation cover tile (in addition to the statistical parameterization of heterogeneity of infiltration and runoff generation within a vegetation cover tile present in the original VIC model). Therefore, the sub-grid scale heterogeneity is represented in soil moisture storage, evaporation, and runoff production. As a semi-distributed land surface model, VIC calculates the sensible and latent heat fluxes according to physical formulations, but it uses conceptual schemes to represent the surface runoff and base flow. In 1996, Liang et al. (1996) found that the VIC-2L tends to underestimate the evaporation due to the low soil moisture in its upper soil layer, and the main cause of this error is the lack of a mechanism for moving moisture from the lower to the upper soil layer. VIC-2L was then modified to allow diffusion of moisture between soil layers, and to have an additional 10cm thin soil layer on top of the previous upper soil layer. In this way the three-layer VIC model (VIC-3L) was generated, and the VIC-3L framework has been used ever since. The model currently allows for more than three soil layers if desired.

A number of modifications to VIC have been made to improve the model such that it can deal with complicated hydrological processes. Since the VIC model does not represent the geometry of the sub-grid variations, a separate routing model has been developed to simulate the streamflow (Lohmann et al., 1996, 1998a, 1998b). To represent the cold land processes, the VIC model was upgraded to include a two-layer energy balance snow model (Andreadis et al., 2009; Wigmosta et al., 1994; Storck et al., 1998), frozen soil and permafrost algorithm (Cherkauer et al., 1999, 2003; Cherkauer and Lettenmaier, 2003), and blowing snow algorithm (Bowling et al., 2004). To improve the simulations of elevation-dependent components within a grid cell, elevation bands representing topography were introduced (Nijssen et al., 2001b). With the evapotranspiration algorithm, canopy responses to wind profile and surface radiation budget have been incorporated (Wigmosta et al., 1994), and the leaf area index (LAI) and the vegetation fraction were allowed to vary at each time step (Liang et al., 1996). The effects of lake and wetlands on moisture storage and evaporation

which are particularly important for runoff at high latitude have been included (Bowling et al., 2003c; Bowling and Lettenmaier, 2009; Cherkauer et al., 2003). To simulate water management impacts, a reservoir module has been implemented to the routing model and a sprinkle irrigation scheme has been added to the soil moisture simulation (Haddeland et al., 2006a, 2006b, 2007).

Over view of VIC model process

The VIC model framework has been described in detail in literature (Liang et al. 1994; Liang et al., 1996; Nijssen et al., 1997). The key characteristics of the grid-based VIC are the representation of vegetation heterogeneity, multiple soil layers with variable infiltration, and non-linear base flow. Figure 2.25 (A) shows the schematic of the VIC model with a mosaic representation of vegetation coverage and three soil layers. The surface of each grid cell is described by N+1 land cover tiles, where n = 1, 2, … , N represents N different tiles of vegetation, and n = N+1 represents bare soil. For each vegetation tile, the vegetation characteristics, such as LAI, albedo, minimum stomatal resistance, architectural resistance, roughness length, relative fraction of roots in each soil layer, and displacement length (in the case of LAI) are assigned. Evapotranspiration is calculated according to the Penman-Monteith equation, in which the evapotranspiration is a function of net radiation and vapor pressure deficit. Total actual evapotranspiration is the sum of canopy evaporation and transpiration from each vegetation tile and bare soil evaporation from the bare soil tile, weighted by the coverage fraction for each surface cover class. Associated with each land cover type are a single canopy layer, and multiple soil layers (three layers are used for description in this ATBD). The canopy layer intercepts rainfall according to a Biosphere-atmosphere transfer scheme (BATS) parameterization (Dickinson et al., 1986) as a function of LAI. The top two soil layers are designed to represent the dynamic response of soil to the infiltrated rainfall, with diffusion allowed from the middle layer to the upper layer when the middle layer is wetter. The bottom soil layer receives moisture from the middle layer through gravity drainage, which is regulated by a Brooks-Corey relationship (Brooks and Corey, 1988) for the unsaturated hydraulic conductivity. The bottom soil layer characterizes seasonal soil moisture behavior and it only responses to short-term rainfall when the top soil layers are saturated. The runoff from the bottom soil layer is according to the drainage described by the Arno model (Franchini and Pacciani, 1991). Moisture can also be transported upward from the roots through evapotranspiration. Although vegetation subgrid-scale variability is a critical feature for the VIC model, the soil characteristics (such as soil texture, hydraulic conductivity, etc.) are held constant for each grid cell. In the model, soil moisture distribution, infiltration, drainage between soil layers, surface runoff, and subsurface runoff are all calculated for each land cover tile at each time step. Then for each grid cell, the total heat fluxes (latent heat, sensible heat, and ground heat), effective surface temperature, and the total surface and subsurface runoff are obtained by summing over all the land cover tiles weighted by fractional coverage.

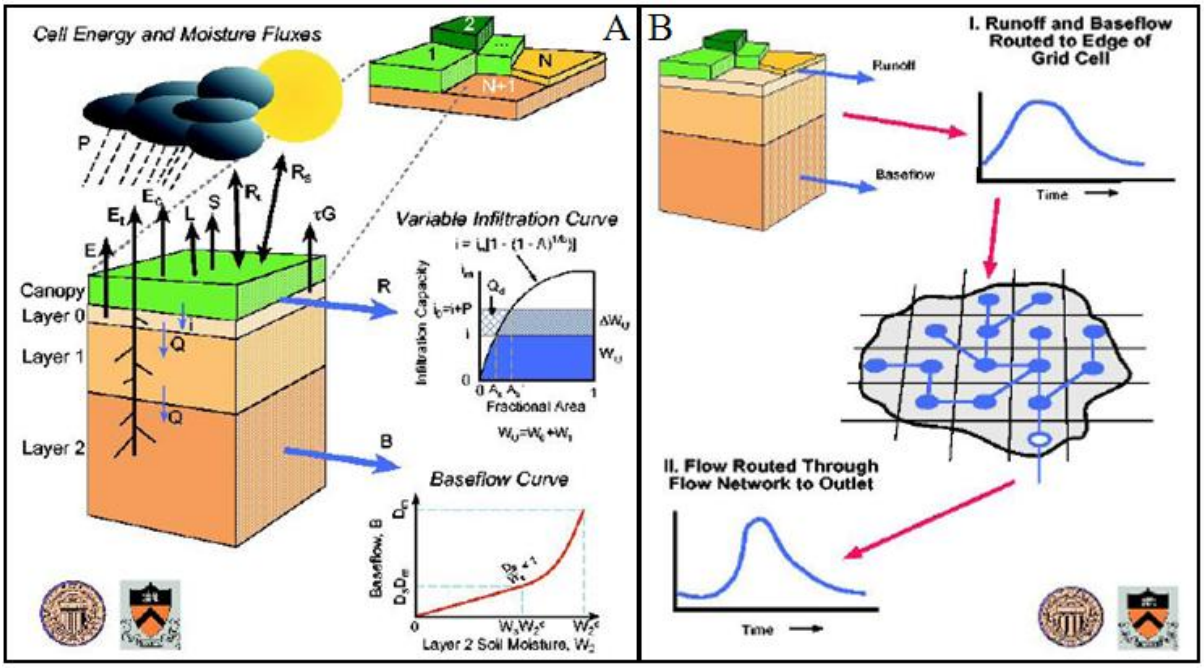

Figure 2.25: Schematic of the VIC model with mosaic representation of vegetation coverage (A) and VIC network routing models (B).

Each grid cell in the VIC model is modeled independently without horizontal water flow. The grid-bas ed VIC model simulates the time series of runoff only for each grid cell, which is non-uniformly distri buted within the cell. Therefore, a stand-alone routing model (Lohmann., et al., 1996, 1998a) is empl oyed to transport grid cell surface runoff and base flow to the outlet of that grid cell then into the riv er system. In the routing model, water is never allowed to flow from the channel back into the grid c ell. Once it reaches the channel, it is no longer part of the water budget. Figure 2.24 (B) shows the sc hematic of the routing model. A linear transfer function model characterized by its internal impulse r esponse function is used to calculate the within-cell routing. Then by assuming all runoff exits a cell i n a single flow direction, a channel routing based on the linearized Saint-Venant equation is used to s imulate the discharge at the basin outlet.

2.4.2 Parameter regionalization method

In this study, a regionalization method was used for parameter estimation of VIC model at ungauged basins. The regionalization method assumes that the basins with similar topography and climate exhibit similar hydrological response.

There are some studies about regionalization method. Bae et al. (2007) and Jung et al. (2007) applied regionalization method for parameters estimation of PRMS model by using regression equation. Lee et al. (2009) conducted runoff modeling at 109 basin of South Korea using seven parameters calculated from multivariate statistics analysis. Also, Son et al. (2010) conducted runoff analysis at overall South Korea using VIC parameters. However, these studies focused on regional basins and there was no study of runoff analysis at large-scale area like as Asia monsoon region.

On the other hand, Nijssen et al. (2001a) conducted the global runoff analysis using parameters separated by same temperature and precipitation regions. Xie et al., (2007) conducted runoff analysis using same method of Nijssen et al. (2001a) and evaluated its applicability over China. In this study, parameter regionalization method was used based on climate zone classification to localize model parameters at Asia region. The Köppen climate classification method was used to obtain climate zones over Asia. Table 2.5 shows the climate zone classification method of Köppen using temperature and precipitation (Kottek et al. 2006). Köppen classification criteria for the climatic types are based on annual and monthly sums of precipitation (cm) and annual and monthly temperature means (degrees Celsius). Boundaries of the categories represent some vegetation based threshold values. The fundamental scheme of the climate classification consists of five major climate types A, B, C, D, E, (Köppen, 1931). In the following text the terms, used by Peel et al. (2007), are employed.

Climate zone

Tropical rain climates A correspond to the climate in which the mean temperature of the coldest month exceeds +18°C, and the annual precipitation amount is higher than the aridity threshold defined for type B. A few subtypes are defined according to the annual cycles of precipitation:

- **Af Tropical rainforest climate -** driest month has on average ≥ 6 cm rain
- **Am Tropical monsoon climate -** driest month has < 6 cm**,** rainfall in rainy season compensates this enough to allow for forest growth:
  · Driest month precipitation (in cm)
  · Required annual sums of precipitation
- **Aw Savanna climate -** driest month < 6 cm**,** annual rainfall insufficient compensate the shortage of precipitation

Arid Climates B is defined in the following way (R denotes the average annual sum of precipitation in cm, and T is the annual mean temperature in °C):

- **R < 2T + 28** where summer is a dominating rain season
- **R < 2T + 14** a well pronounced dry season does not exist
- **R < 2T** winters are the seasons with most rain

Within type B two subtypes are distinguished with respect to the value of the aridity threshold: BS (the steppe grassland climate) and BW (desert climate).

- **BS Steppe climate (bush to grassland)**
  · T + 14 ≤ R < 2T + 28 for summer rain areas
  · T + 7 ≤ R < 2T + 14 no marked dry season
  · T ≤ R < 2T for winter rain areas
- **BW Desert**
  · R < T + 14 for summer rain areas
  · R < T + 7 no marked dry season
  · R < T for winter rain areas

Warm temperature climates C is defined according to a value of the mean temperature of the coldest month which should be between –3°C and +18°C. The precipitation amounts must be higher

than the aridity threshold. Further subdivision is related to the annual cycles of both the temperature and precipitation:

- **Cs** wettest (winter) month of the year has ≥ 3 times the average rainfall of the driest (summer) month, i.e. s means a summer dry season
- **Cf** f is linked with the humid climate without a marked dry season
- **Cfa** hot summers - mean temperature of the warmest month > +22°C
- **Cfb** warm summers - mean temperature of the warmest month below +22°C, at least 4 months > +10°C
- **Cfc** cool summers - only 1−4 months > +10°C, the coldest month temperature is higher than −38°C
- **Cw** wettest (summer) month of the year has ≥ 10 times the average rainfall of the driest winter month, i.e. w denotes a winter dry season.

Cold climates D meets the following requirements: the mean temperature of the warmest month must be higher than 10°C, and the coldest month temperature should be below −3°C, precipitation amounts exceed the aridity threshold. Subtypes are again related to the annual cycles:

- **Dw** Same as under C
- **Df** Same as under C
- **Dfa** and **Dwa -** mean temperature of the warmest month > +22°C
- **Dfb** and **Dwb -** at least 4 months > +10°C, the warmest one is of temperature below 22°C
- **Dfc** and **Dwc -** only 1−4 months > +10°C, the coldest month temperature is above −38°C.

Polar climates E is defined according to the mean temperature of the warmest month that must be lower than 10°C. This type is subdivided into two subtypes: ET (tundra climate) and EF (polar desert - frost climate):

- **ET** mean temperature of the warmest month moves in the range 0 − 10°C
- **EF** mean temperature of the warmest month < 0°C.

Table 2.5 The climate zone classification method of Köppen using temperature and precipitation

Type	Description	Criterion
A	**Tropical climates**	**T_{min} ≥ +18℃**
Af	Rainforest	$P_{min} \geq 60$ ㎜
Am	Monsoon	Not(Af) & $P_{min} \geq 100\text{-}P_{ann}/25$
Aw	Savannah	Not(Af) & $P_{min} < 100\text{-}P_{ann}/25$
B	**Arid climates**	**$P_{ann} < 10P_{th}$**
BS	Steppe climate	$P_{ann} > 5P_{th}$
BW	Desert climate	$P_{ann} \leq 5P_{th}$
C	**Warm temperate climates**	**-3℃ < T_{min} < +18℃**
Cs	Warm temperate climate with dry summer	$P_{smin} < P_{wmin}$ & $P_{wmax} > 3P_{smin}$ & $P_{smin} < 40$ ㎜
Cw	Warm temperate climate with dry winter	$P_{wmin} < P_{smin}$ & $P_{smax} > 10P_{wmin}$

Cf	Warm temperate climate without dry season	Neither Cs nor Cw
D	**Cold climates**	**$T_{min} \leq -3℃$**
Ds	Cold climate with dry summer	$P_{smin} < P_{wmin}$ & $P_{wmax} > 3P_{smin}$ & $P_{smin} < 40$ ㎜
Dw	Cold climate with dry winter	$P_{wmin} < P_{smin}$ & $P_{smax} > 10P_{wmin}$
Df	Cold climate without dry season	Neither Ds nor Dw
E	**Polar climates**	**$T_{max} < +10℃$**
ET	Tundra climate	$0℃ \leq T_{max} < +10℃$
EF	Frost climate	$T_{max} < 0℃$

T_{ann} : annual mean temperature(℃), T_{max} : mean temperature of the warmest months (℃), T_{min} : mean temperature of the coldest months (℃), T_{mon} : monthly mean temperature(℃), P_{ann} : annual precipitation(㎜/year), P_{min} : precipitation of most dry months (㎜/month), P_{smin} : precipitation of the most dry months in summer (㎜/month), P_{smax} : precipitation of the most humid months in summer (㎜/month), Pwmin : precipitation of the most dry months in winter (㎜/month), Pwmax : precipitation of the most humid months in winter (㎜/month), P_{th} : i) $2\{T_{ann}\}$ (when 70% of the annual precipitation falls in the coldest 6 months, ㎜), ii) $2\{T_{ann}\}+28$ (when 70% of the annual precipitation falls in the warmest 6 months, ㎜), iii) $2\{T_{ann}\}+14$ (when less than 70% of the annual precipitation falls in the warmest and coldest 6 months, ㎜)

2.5 Data analysis for detecting trends

Trend analysis is an aspect of technical analysis that tries to predict the future movement of an event based on past data. Trend analysis is based on the idea that what has happened in the past gives traders an idea of what will happen in the future. For the analysis of past historical and future scenario data of climate models, the Mann-Kendall and linear regression statistical tests were used in this study to determine the significance of trends in precipitation and temperature of Asian countries. The Mann–Kendall test is a non-parametric test for detecting trends in time series data. The test is widely used for analyzing environmental data, including precipitation (Partal and Kahya, 2007), streamflow (Liu and Zheng, 2004), and water quality data (Donohue *et al*., 2001). The Mann–Kendall test is simple and robust, and it can cope with missing values and values below a detection limit. The test was first created by Mann (1945) and Kendall (1975) and covariances between Mann–Kendall statistics were developed by Dietz and Kileen (1981). The test was further extended in order to include seasonality (Hirsch *et al*., 1982), multiple monitoring sites (Lettenmaier, 1988) and covariates representing natural fluctuations (Libiseller and Grimvall, 2002).

Calculation of the Mann-Kendall test

The Mann-Kendall test is a non-parametric test for identifying trends in time series data. The test compares the relative magnitudes of sample data rather than the data values themselves (Gilbert, 1987). The advantage of this test is that the data need not to conform to any particular distribution. Moreover, data reported as missing can be included by assigning them a common value that is

smaller than the minimum measured value in the dataset. The procedure described in the subsequent paragraphs assumes that there exists only one data value per time period. When multiple data points exist for a single time period, the median value is used.

The data values are evaluated as an ordered time series. Each data value is compared to all subsequent data values. The initial value of the Mann-Kendall statistic, S, is assumed to be 0 (e.g., no trend). If a data value from a later time period is higher than a data value from an earlier time period, S is incremented by 1. On the other hand, if the data value from a later time period is lower than a data value sampled earlier, S is decremented by 1. The net result of all such increments and decrements yields the final value of S.

Let x_1, x_2,… x_n represent n data points where x_j represents the data point at time j. Then the Mann-Kendall statistic (S) is given by:

$$S = \sum_{k=1}^{n-1} \sum_{j=k+1}^{n} sign(x_j - x_k) \tag{10}$$

where:

sign $(x_j - x_k) = 1$ if $x_j - x_k > 0$

$= 0$ if $x_j - x_k = 0$

$= -1$ if $x_j - x_k < 0$

The higher positive value of S is an indicator of an increasing trend, and the higher negative value indicates a decreasing trend. However, it is necessary to compute the probability associated with S and the sample size n, to statistically quantify the significance of the trend. The procedure to compute this probability is described in the following section.

Computation of probability associated with M-K statistic S

Kendall (1975) described a normal-approximation test that could be used for datasets with ***more than 10 values,*** provided there are not many tied values within the dataset. The test procedure is as follows:

- Calculate S as described in eq. 10.
- Calculate the variance (var) of S, as:

$$\mathrm{var}(S) = \frac{1}{18}[n(n-1)(2n+5) - \sum_{p=1}^{g} t_p(t_p-1)(2t_p+5)] \tag{11}$$

where n is the number of data points, g is the number of tied groups (a tied group is a set of sample data having the same value), and t_p is the number of data points in the p^{th} group. For example, in the sequence {2, 3, 4, 3, 4, 3}, we have n=6, g =2, t_1 =2 for the tied value 4, and t_2 =3 for the tied value 3.

- Compute the Mann–Kendall normalized test statistic Z_c as:

$$Z_c = \frac{S-1}{\sqrt{\text{var}(S)}} \text{ if S>0} \quad (12)$$

$$Z_c = 0 \text{ if S=0}$$

$$Z_c = \frac{S+1}{\sqrt{\text{var}(S)}} \text{ if S<0} \quad (13)$$

- Compute the probability associated with normalized test statistic (Z_c). The probability density function for a normal distribution with a mean of 0 and a standard deviation of 1 (standard normal distribution) is given by the following equations:

$$f(x) = \frac{1}{\sqrt{2\pi}} e^{-\frac{x^2}{2}} \quad (14)$$

$$P = \frac{1}{\sqrt{2\pi}} \int_{-\infty}^{z_c} e^{-\frac{x^2}{2}} dx \quad (15)$$

- Decide on a probability level of significance (95% typically).
- The trend is said to be decreasing if S is negative and the computed probability is greater than the level of significance. The trend is said to be increasing if the S is positive and the computed probability is greater than the level of significance. If the computed probability is less than the level of significance, there is no trend.

3.0 Results & Discussion

3.1 Verification of Gridded Climate and Hydrological Datasets

In this study, the global observed runoff data was collected from Global Runoff Data Centre (GRDC) to estimate parameters of hydrology model. Also, the gridded climate data was collected from APHRODITE at 0.5° grid resolution. To verify the data quality of APHRODITE and GRDC, we compared these datasets with regional observed station data. The details of climate and hydrological data verification are given in the following sections.

Verification of climate data

To verify the quality of gridded climate dataset (APHRODITE) the comparison test of both rainfall and temperature was conducted for selected stations in South Korea. The grid point rainfall data was compared with corresponding observed station data obtained from four Automated Surface Observing System (ASOS) stations i.e. Busan, Seoul, Daejeon and Mokpo. Figure 3.1 shows the comparison of APHRODITE grid points and their corresponding ASOS stations data. The comparison shows that overall both datasets have same tendency for all selected stations. The APHRODITE slightly underestimated rainfall especially for heavy precipitation events in Busan and Seoul. That is probably because of smoothing effect in gridded dataset. The Correlation Coefficient (CC) and Volume Error (VE) computed between APHRODITE and ASOS stations is given in Table 3.1. The VE was -27.20%, -25.68%, -12.07% and -19.55% for Busan, Seoul, Daejeon and Mokpo respectively. The CC was 0.98 for Busan and Seoul, and 0.99 for Daejeon and Mokpo. It showed that the gridded APHRODITE precipitation data was useful to analyze climate and hydrology trend and change impact assessment over Asia region because the tendency between ASOS and APHRODITE was almost same.

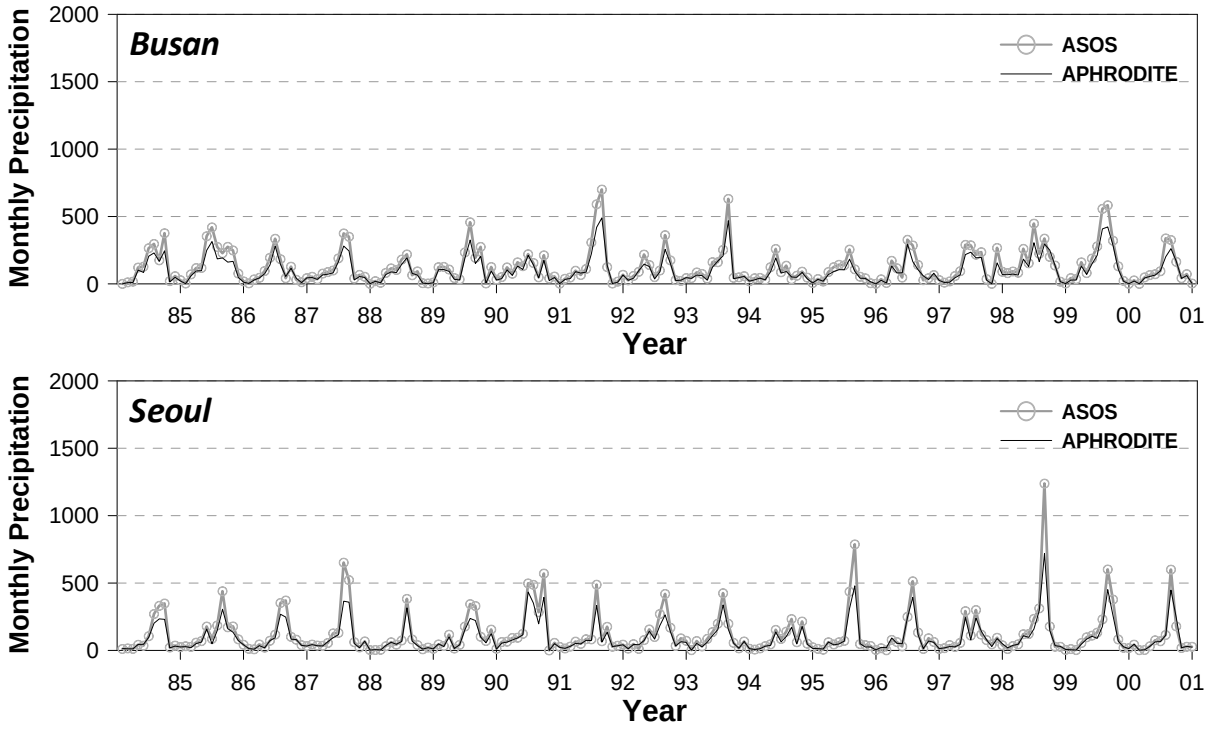

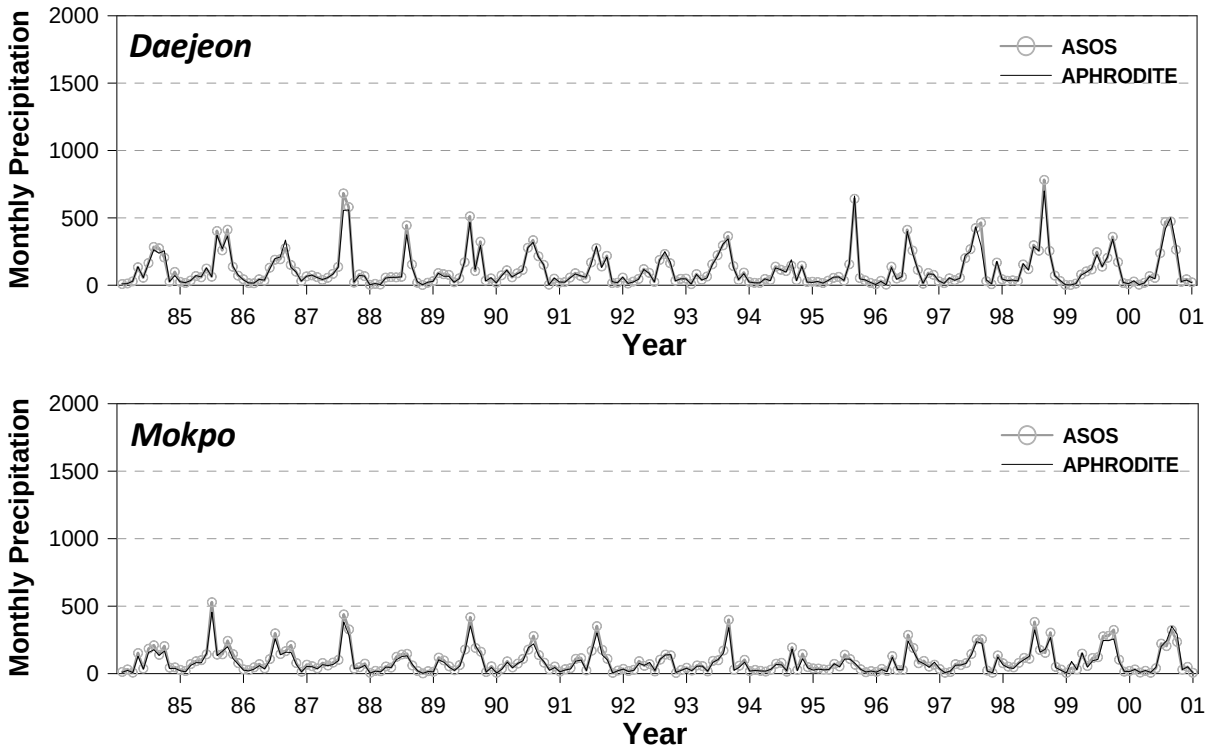

Figure 3.1: APHRODITE Vs. ASOS monthly precipitation data for Busan, Seoul, Daejeon and Mokpo from 1984 to 2001

Table 3.1: CC and VE for selected four stations over South Korea.

	Busan	Seoul	Daejeon	Mokpo
CC	0.98	0.98	0.99	0.99
VE(%)	-27.20	-25.68	-12.07	-19.55

The gridded temperature data was also compared with station data for selected four ASOS stations. Figure 3.2 shows the comparison of ASOS and APHRODITE monthly temperature data at Busan, Seoul, Daejeon, and Mokpo. Both datasets followed same trend for all four stations. The average temperature (ASOS and APHRODITE) was 14.67°C and 13.92 °C for Busan, 12.44 °C and 11.78 °C for Seoul, 12.65 °C and 12.16 °C for Daejeon, and 13.92 °C and 14.11 °C for Mokpo. The average monthly temperature from ASOS data was higher than APHRODITE data for all the stations except Mokpo.
Table 3.2 shows the CC and VE for selected four stations. The CC was above 0.99 for all the stations. The highest VE was -5.11% for Seoul station and lowest VE was 1.32% for Mokpo station. The average VE for all four stations was -3.24%. These statistics show that the gridded APHRODITE temperature data is reliable to use for analysis of climate and hydrology over Asia region.

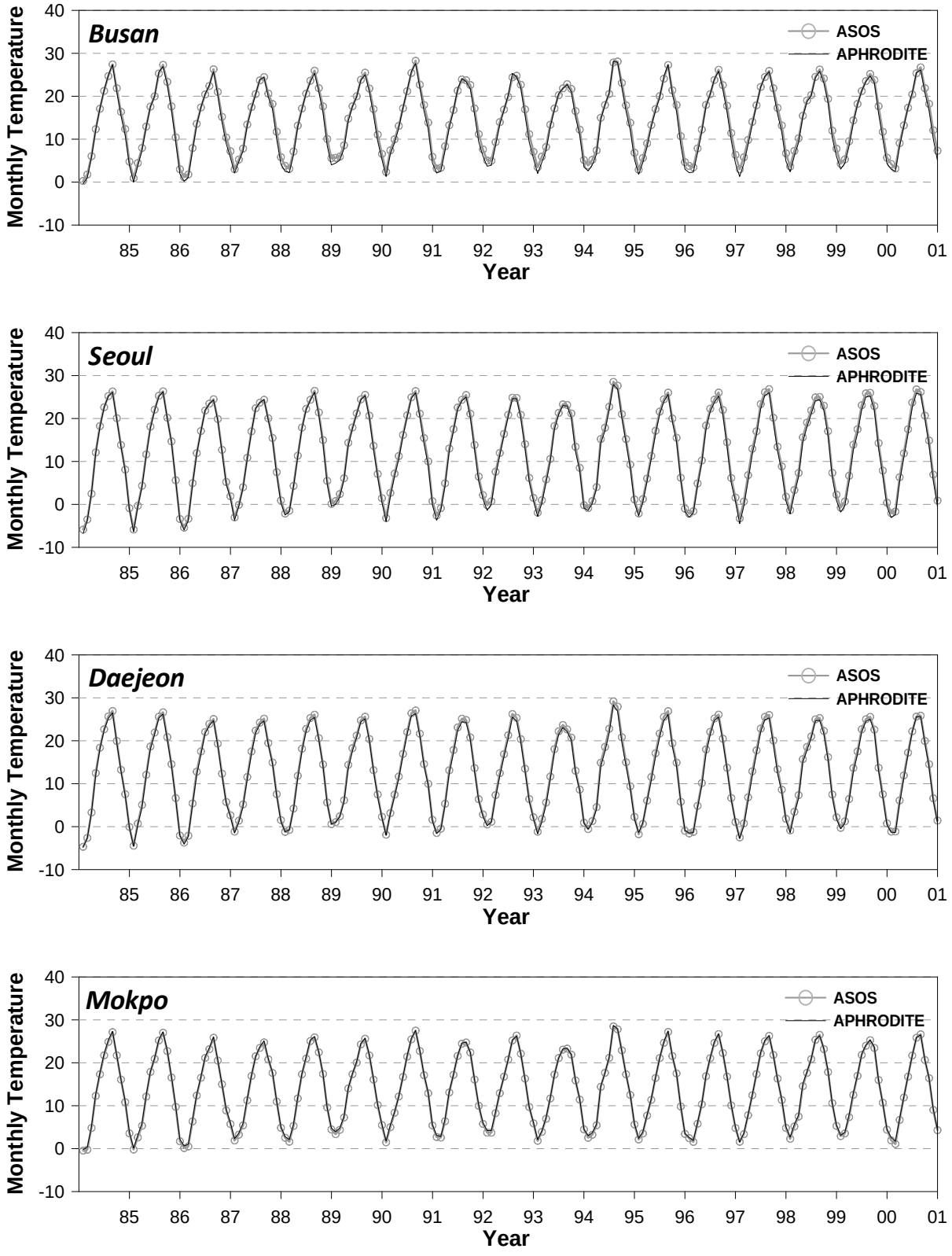

Figure 3.2: APHRODITE Vs. ASOS monthly temperature data for Busan, Seoul, Daejeon and Mokpo from 1984 to 2001

Table 3.2: Results of Correlation coefficient and volume error main four stations between station data and gridded APHRODITE data over South Korea.

	Busan	Seoul	Daejeon	Mokpo
CC	0.99	0.99	0.99	0.99
VE(%)	-5.11	-5.32	-3.83	1.32

Verification of hydrology data

In this study, the global observed runoff data was collected from Global Runoff Data Centre (GRDC) to estimate parameter of hydrology model. Figure 3.3 shows the location of runoff observatories and river basins used in the study. The observatories were selected considering that the selected observatory take effect from hydraulic structures as dam and have availability of observational data. As a result twenty observatories were identified, among these seven were located in Japan, five in China, two in each country Russia and Malaysia, and one in each country Mongolia, India and Cambodia. For South Korea the Chungju dam was selected as target basin and runoff data was obtained from Ministry of Land, Transport and Maritime Affairs (MLTM). Table 3.3 shows the selected observatories, available data period and area of target basin for each country.

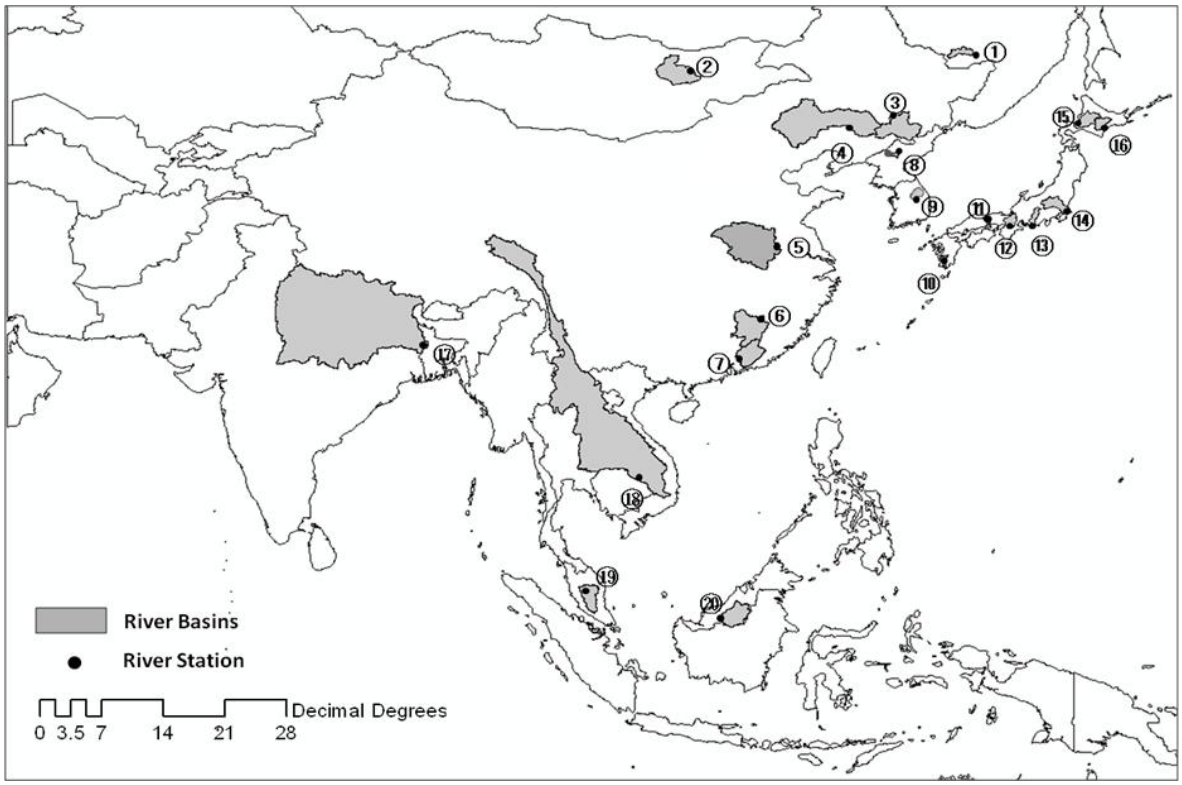

Figure 3.3: Location of selected station and river basins on East Asia

Table 3.3: Characteristics of the selected study basins and available data period

Country	No.	Sation Name	Study Basins	Characteristics	
				Area (km^2)	Data Period (year)
Russia	①	Birobidzhan	Bolshaya Bira	5,910	1978 - 1986

Mongolia	②	Undurkham	Kerulen	39,400	1978 - 1984
China	③	Jilin	Songhua Jiang	44,100	1978 - 1986
	④	Chiling	Liao He	120,764	1978 - 1985
	⑤	Bengbu	Huai He	121,330	1978 - 1989
	⑥	Jian	Gan Jiang	56,200	1978 - 1984
	⑦	Boluo	Dong Jiang	25,325	1978 - 1987
North Korea	⑧	Jong Chon	Sangwan	2,192	1982 - 1984
South Korea	⑨	ChungJu Dam	Chung Ju	6,648	1986 - 2013
Japan	⑩	Onobuchi	Sendai	1,348	1995 - 2000
	⑪	Miyasu	Yoshino	1,996	1993 - 2000
	⑫	Hirakata	Yodo	7,281	1995 - 2005
	⑬	Kashima	Tenruy	4,880	1993 - 2003
	⑭	Fukawa	Tone	12,458	1995 - 2005
	⑮	Ishikari-Ohashi	Ishikari	12,697	1995 - 2002
	⑯	Moiwa	Tokachi	8,277	1993 - 2001
India	⑰	Hardinge bridge	Ganges	846,300	1985 - 1992
Thailand	⑱	Stung Treng	Mekong	635,000	1991 - 1994
Malaysia	⑲	Buluh Kasap	Muar	3,130	1982 - 2000
	⑳	Kapit Wharf	Rajang	34,053	1982 - 1994

To analyze and check the quality of GRDC runoff data the Yeoju observatory in South Korea was selected because the observed runoff data for this observatory was also available from MLTM Korea. For comparison the daily data was used for the period of 1997 to 2007. Figure 3.4 shows the comparison result between observation data from MLTM and GRDC data at Yeoju. As a result, runoff movement was almost same. However, there was difference at movement of low-flow. These differences are believed to be occurred due to transmission problem. The comparison showed that the reliability of GRDC runoff data is high to evaluate results of runoff analysis.

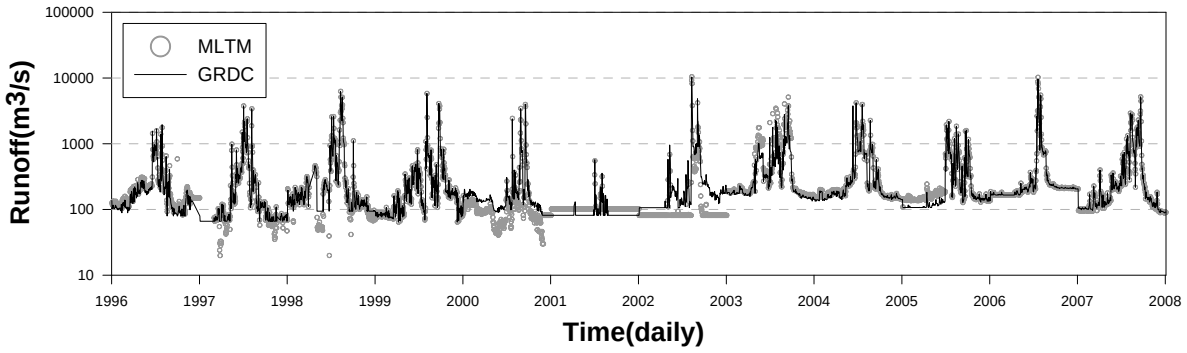

Figure 3.4 : Comparison of local (MLTM) and Global (GRDC) runoff data at Yeoju station

3.2 Hydrological analysis

3.2.1 Classification of climate zone

The climate classification over Asia was obtained using Köppen climate classification method to regionalize parameters of VIC model for ungauged area (Fig. 3.5). Looking into climate zones according to latitude we can see that the tropical rainforest climate zone (Af) spreads over Indonesia, Malaysia, and Philippines below 10°N. The tropical monsoon climate zone (Am) covers Greater Sunda Islands in northern part of Indonesia, Cambodia and Vietnam between equatorial and 20°N. The Tropical savannah climate zone is located over India, Thailand, Myanmar, Laos, Cambodia, and Sri Lanka between 23°N and 40°N. The climate zone of warm temperature with dry summer (Cs) is distributed over some parts of the Hindustan plains in India. The climate zone of warm temperature with dry winter spreads over eastern part of Pakistan, Hindustan of India, southern and eastern part of China, and South Korea. The climate zone of warm temperature without dry season (Cf) appeared over all area except the Southeastern part of China, and coastal area of South Korea. The Arid and Cold climate zone is distributed over most region above 38°N. The arid clime zone covers region from Iranian plateau to Gobi desert including Taklamakan desert. The desert climate zone (Bw) and Steppe climate zone are located around Arid climate zone. The cold climate zone appeared over northeastern part of China, North Korea, East of Russia, and Hokkaido Island of Japan. The Tundra climate zone in Polar climate zone is distributed over Himalaya mountain range. For South Korea, the climate zone of cold with dry winter (Dw) lies in northern part, the climate zone of warm temperature without dry season lies in coastal area, and the climate zone of warm temperature with dry winter lies in inland area. These climate zones reflect current climate of South Korea well that shows the reliability of classified climate zones.

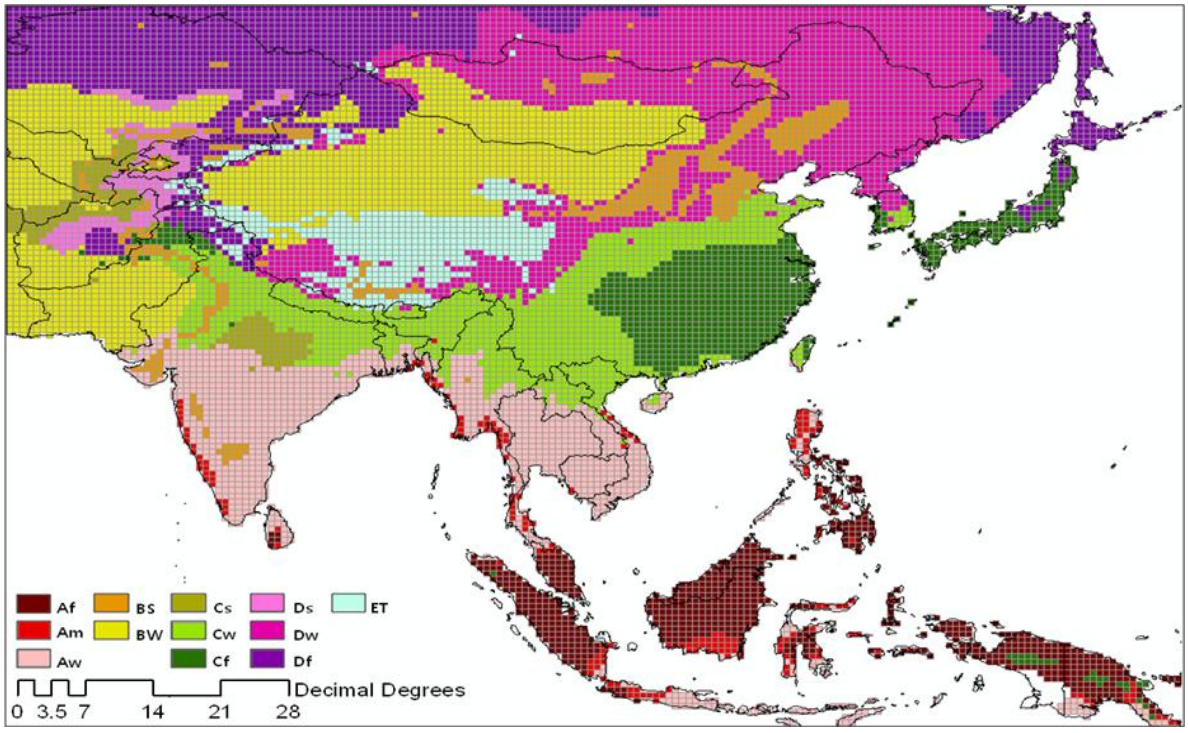

Figure 3.5: Climate zones in Asia according to Köppen climate zone

3.2.2 Parameter estimation and regionalization

To conduct runoff analysis, it is important to identify the characteristics of model parameters. However estimation of model parameters is difficult task because model parameters are sensitive to runoff results. The parameters for VIC hydrological model were estimated from measurable basin characteristics using geographical information system (GIS) database that includes DEM, river network, soils, vegetation type, and land cover. Appropriate parameter estimation method is also needed at ungauged basin. The regionalization method was used for parameter estimation of VIC model at ungauged basins. The regionalization method assumes that the basins with similar topography and climate exhibit similar hydrological response. Table 3.4 shows the list of VIC model parameters used in regionalization. The b_infilt parameter is to determine infiltration from precipitation. The surface runoff increases with increasing value of b_infilt. The D_{smax}, D_s, and W_s determine movement and amount of baseflow. Specifically the D_{smax} and D_s determine movement of baseflow recession segment, and the W_s determine capacity of base flow. The d1, d2, and d3 represent depth of soil layer. The soil layer thickness determines the quantity of soil moisture, evaporation and runoff.

Table 3.4: VIC model parameters

Parameters	Description	Realistic range
b_infilt	Exponent of variable infiltration capacity curve	0.0-10.0
D_s	Fraction of maximum base flow	0.0-1.0
D_{smax}	Maximum velocity of baseflow (m/day)	0.0-40.0
W_s	Fraction of maximum soil moisture content of the lower layer	0.0-1.0
d_1, d_2, d_3	Three soil layer thickness(m)	0.05-2.0

To verify the results of parameter estimation and regionalization methods in Asia region ten gauged basins were used for calibration and remaining ten gauged basins were assumed to be ungauged and used for verification purpose. The model parameters were estimated for calibration basins and that for verification basins were regionalized based on similar basin characteristics. The monthly runoff data was computed from daily GRDC runoff data for the analysis. The statistical measures i.e. correlation coefficient (CC), model efficiency coefficient (ME), root mean square error (RMSE), and volume error (VE) for calibration (Cal.) and verification (Ver.) basins are presented in Table 3.5. For calibration basins the CC, ME, RMSE, and VE were 0.67～0.96, 0.36～0.91, 1.10～63.29mm/month, and -25.72～9.66%, respectively. For verification basins the same were 0.58～0.96, 0.33～0.92, 1.61～63.29mm/month, and less than 17.89%, respectively.

Table 3.5: Statistics results and estimated parameter at gauged (Cal) and ungauged (Ver) each climate zone.

-	Climate Zone	No.	Basin	Statistics			
				CC	ME	RMSE	VE

Cal.	A	⑳	Rajang	0.67	0.36	51.55	-4.84
		⑱	Mekong	0.95	0.91	16.05	-2.25
	B	②	Kerulen	0.79	0.59	1.10	-6.83
	C	⑤	Huai He	0.81	0.63	17.19	-11.50
		⑦	Dong Jiang	0.87	0.66	27.29	-10.79
		⑨	ChungJu Dam	0.96	0.88	31.05	-3.54
		⑬	Tenryu	0.95	0.88	23.97	9.66
	D	⑧	Sangwan	0.88	0.68	31.59	-25.72
	E	⑯	Tokachi	0.73	0.45	32.25	19.01
Ver.	A	⑲	Buluh Kasap	0.58	0.33	63.29	0.46
		⑰	Gangis	0.90	0.76	21.87	17.39
	B	④	Liao He	0.77	0.58	1.61	0.59
	C	⑥	Gan Jian	0.89	0.79	27.79	1.32
		⑩	Sendai	0.96	0.92	41.49	-2.68
		⑪	Yoshino	0.93	0.85	28.10	5.54
		⑫	Yodo	0.86	0.71	30.76	10.60
		⑭	Tone	0.88	0.75	21.58	14.83
	D	③	Songhua Jiang	0.79	0.35	16.31	12.66
	E	⑮	Ishikari	0.64	0.35	46.38	-8.52

Figure 3.6 shows the simulated and observed runoff for ungauged basins. The simulated runoff did not reflect observed runoff well at Songhua Jiang, and Ishikari basins. For Gangis and Gan Jiang basins, the simulated runoff captured the trend of observed runoff very well although the area of basin was more than 100,000km^2. Similarly, the simulated runoff at Sendai and Tone was in good agreement with observed runoff for six and eleven years respectively. Considering the data resolution of 0.5^o, the reliability of runoff result is high. Furthermore, application of built VIC model is useful.

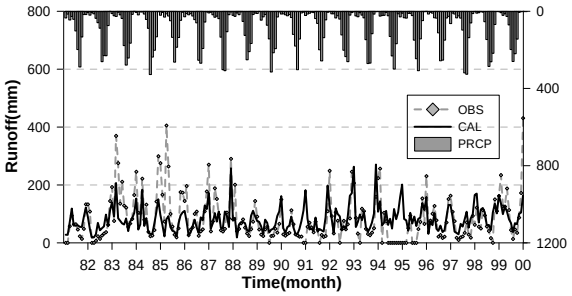

a) Buluh Kasap

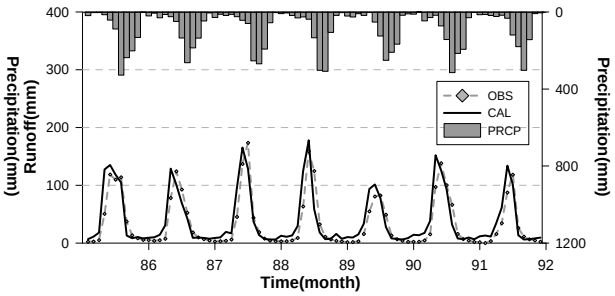

a) Gangis

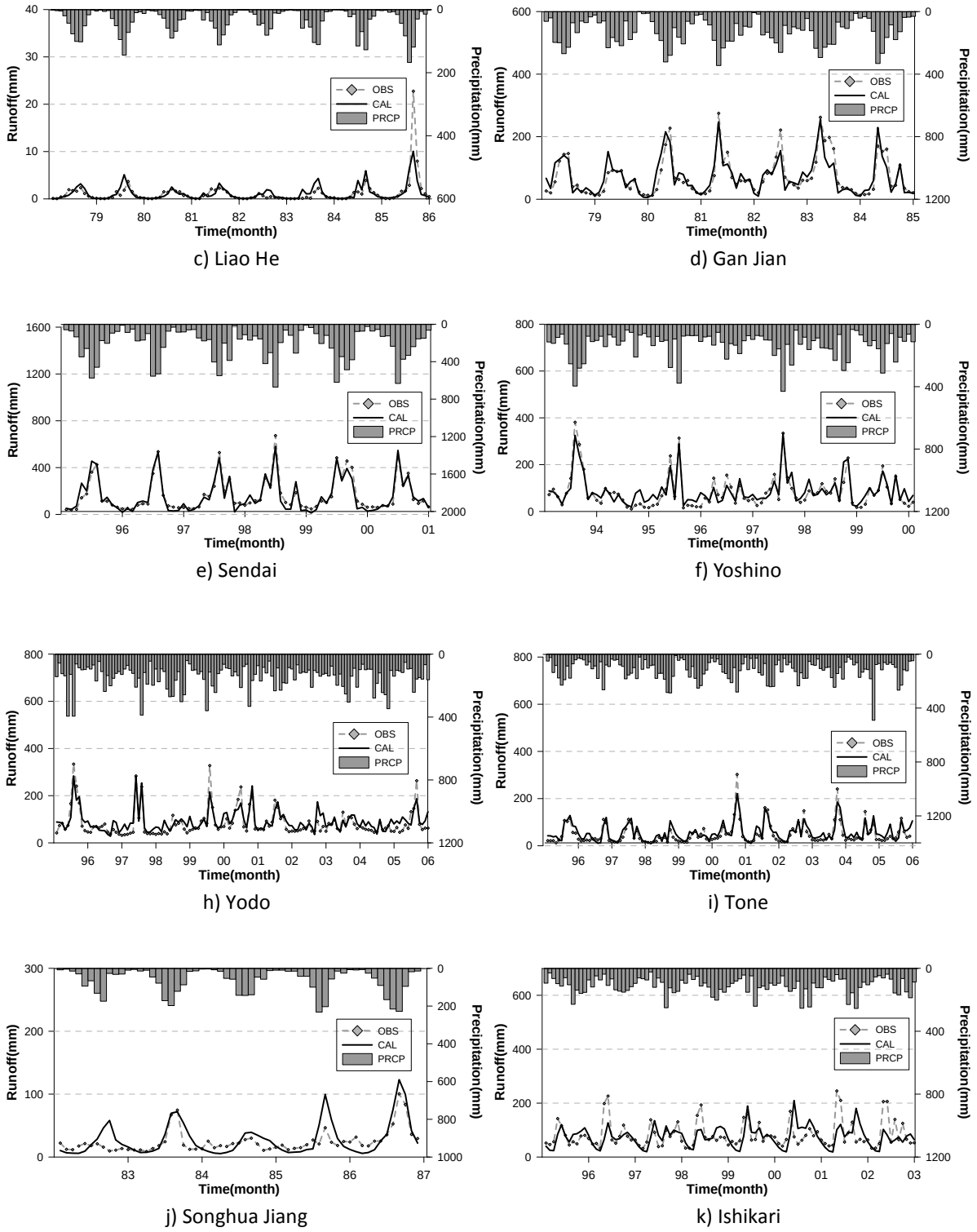

c) Liao He d) Gan Jian

e) Sendai f) Yoshino

h) Yodo i) Tone

j) Songhua Jiang k) Ishikari

Figure 3.6: Simulated runoff at ungauged basin and observed runoff.

3.3 Analysis of historical climate and hydrology

3.3.1 Historical features

Asia region

To analyze the historical features of Asia region the 30-year (1977–2006) averages of climatological variables i.e. temperature and precipitation, and hydrological variable i.e. runoff were computed as shown in Figure 3.7. The temperature decrease with increasing latitude is evident in the figure. As per quantitative analysis the temperature range was 17～32°C in Southeast Asia, 5～32°C in South Asia, -3～20°C in Central Asia , -6～20°C in East Asia, and -6～0°C in North Asia region. Especially for South Korea, average temperature was 12.9°C which was similar to average temperature of South Korea. The analysis of precipitation showed low rainfall over continental regions as compared to coastal regions. The average precipitation over tropical region was approximately 1,500～3,200mm. For South Asia, Southeast Asia, and East Asia regions which are influenced by sea winds the average precipitation was 1,250～3,000mm. The average precipitation over Central Asia and desert region of East Asia was 110～250mm. In South Korea, the average precipitation was 1,566mm. The spatial distribution of runoff was similar to precipitation. The western East Asia including Taklamakan desert, Pakistan, south Afghanistan, and part of western Central Asia were the most low runoff regions. The runoff in South Korea, Japan and Southern China was in range of 600~1600mm, and it was above 2000mm in tropical regions including Indonesia, Thailand and Southern Vietnam.

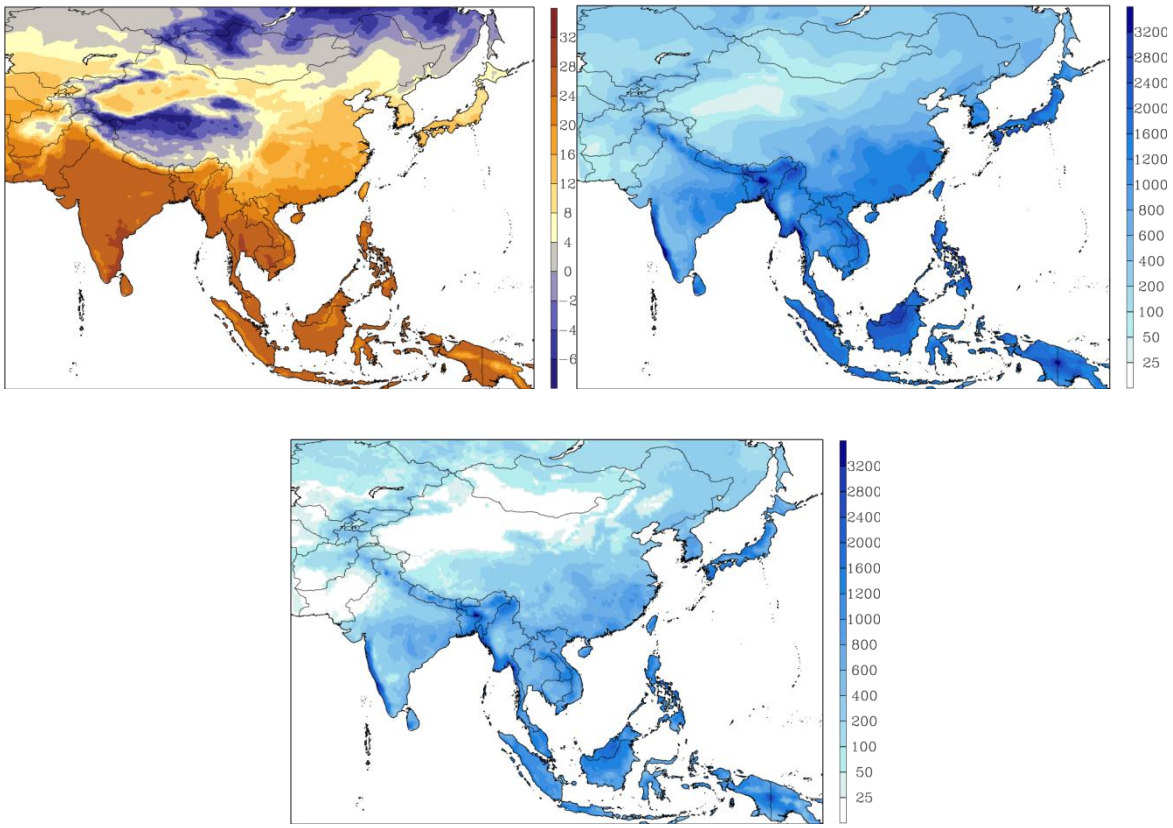

Figure 3.7: 30-year (1977-2006) averages of temperature (left of top), precipitation (right of top), and runoff (bottom) over Asian region.

The seasonal analysis of historical 30-year averages for temperature, precipitation, and runoff was conducted for Asia region (Fig. 3.8). The seasonal features of spring and autumn were almost same for temperature, precipitation, and runoff. Temperature in spring and autumn decreased with increasing latitude to northward. The most low temperature regions were Himalaya Mountain, northern part of Mongolia and China. The summer temperature was high over all regions except

Himalaya Mountain. The most high temperature regions were north India, Pakistan, and south Afghanistan. Regarding the autumn temperature, north part of East Asia and central Asia including Himalaya Mountain were colder regions with below freezing temperature. The most high temperature was observed over tropical regions including south India, Cambodia, Indonesia, and Malaysia.

The seasonal analysis of precipitation showed that the precipitation in spring and autumn was high near tropical regions, and it was very low around Himalaya Mountain and western East Asia. In summer the high precipitation region was between 10°N and 20°N including northern Southeast Asia, India, and Nepal regions. In winter season, precipitation was low over all regions, as compared to other seasons. The most high precipitation region was southern Tropical region, and the lowest precipitation was observed in Himalaya Mountain, China, and Mongolia regions.

The spatial features of runoff were similar to features of precipitation. However, the intensity of runoff was small compared to the precipitation. In spring season the most high runoff regions were almost same with spring precipitation, but the lowest runoff region existed over East Asia, Himalaya Mountain, northwest India, and Pakistan. The summer runoff was increased in most regions compared to spring season, especially the northwestern India region which showed significant increase. The autumn runoff was almost same with spring except for western Central Asia that was clearly increased. The winter runoff showed same distribution compared to the winter precipitation. The winter runoff was very low at Central Asia and Northern Asia. The most high runoff was observed near tropical regions.

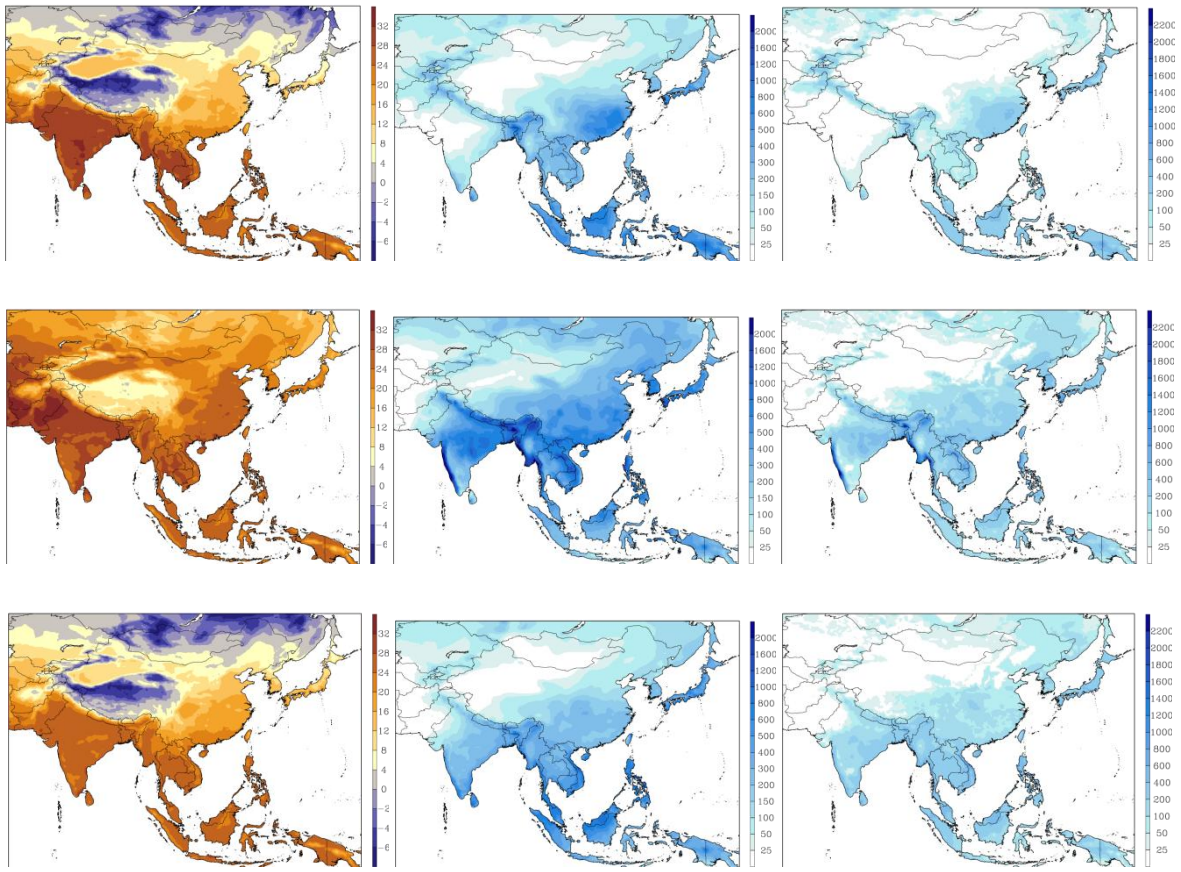

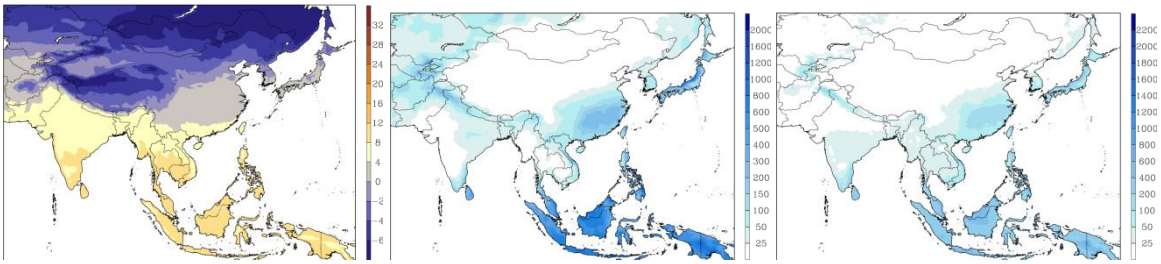

Figure 3.8: Features of seasonal temperature (left), precipitation (middle), and runoff (right) over Asian region. Figure from top to bottom mean spring to winter.

AWCI 18 basins

In this study, the hydrological components were calculated over Asia regions using the VIC model. Figure 3.9 shows the monthly average of calculated hydrological components i.e. precipitation, runoff, evapotranspiration, and soil moisture from 1977 to 2006 for AWCI 18 basins. Most of the basins had high precipitation between June and September and low precipitation between December and February. In Meghna basin, Bangladesh, the peaks of precipitation, runoff, evapotranspiration, and soil moisture were observed between June and July. The peaks of hydrological components in Punatsanghhu basin, Bhutan, and Sanker basin, Cambodia were observed in July and September respectively. In Seonath basin, India, the peak of precipitation was in August with almost no precipitation between November and May. Other components in Seonath basin had similar features. For Manberamo basin, Indonesia, the hydrological components did not show any distinct feature around the year. In Tone basin, Japan, the peak of precipitation was in September, but runoff had one more peak in April because of snow melt. In Upper Chungju basin of South Korea, the peaks of all hydrological components were in July. In case of Sebangfai basin, Laos, the peaks of all hydrological components were in August. In Langat basin, Malaysia, there were two peaks in April and November for all hydrological components. For Selbe basin, Mongolia, the peaks of all hydrological components were in August except evapotranspiration which showed peak in July. In Shwegyin basin, Myanmar, the features of hydrological components were similar to Selbe basin, Mongolia. The hydrological components at Bagmati basin in Nepal were similar to Upper Chungju-basin in South Korea. In case of Gilit basin, Pakistan, the peaks of precipitation and runoff were observed in April and that of soil moisture in May. On the other hand, the evapotranspiration remained almost same during January to August and it decreased from September to December. All hydrological components in Pampanga of Philippines had peaks in July. In case of Kalu Ganga basin, Sri Lanka, all hydrological components had distinct two peaks in May and October. In Mae Wang basin of Thailand, the precipitation had two peaks in May and September. Other hydrological components were almost same in Mae Wang basin. In case of Chirchik Okhangaran basin, Uzbekistan, the precipitation had two peaks in April and December, but other hydrological components had only one peak in April. Lastly, in Huong basin, Vietnam, the precipitation had one peak in October, and all other components showed similar features. The analysis of calculated hydrological components for 18 basins showed that most of the basins have special distinct features.

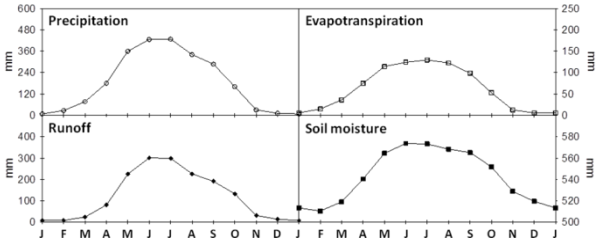

a) Meghna

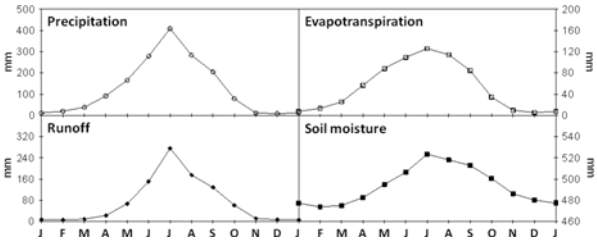

b) Punatsangchhu

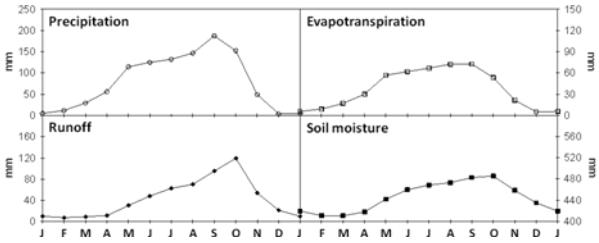

c) Sanker

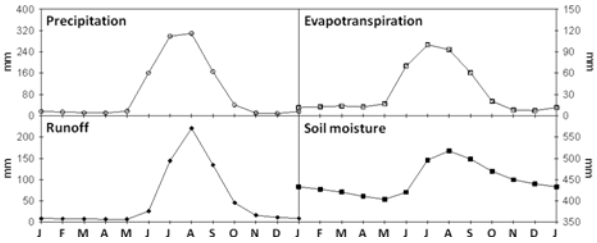

d) Seonath

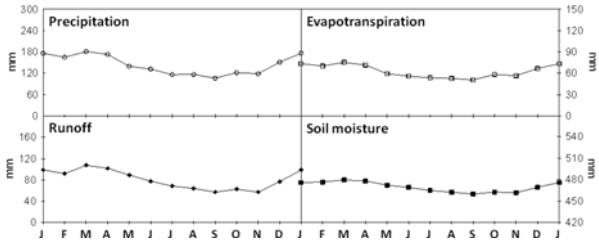

e) Mamberamo

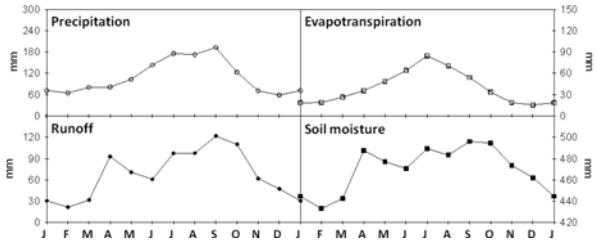

f) Tone

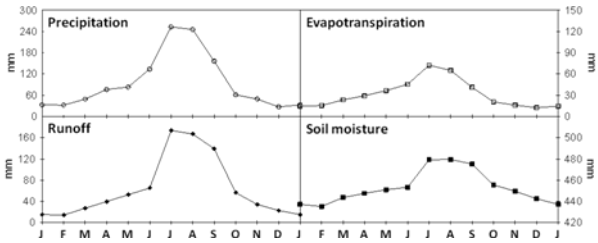

g) ChungJu-Dam

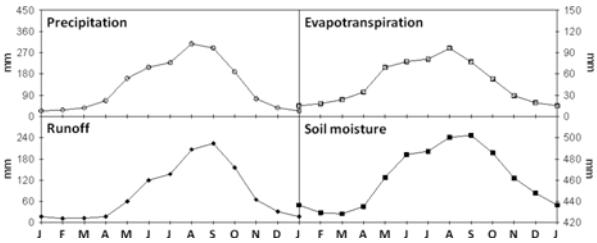

h) Sebanfai

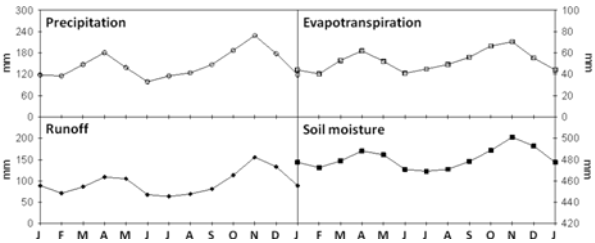

i) Langat

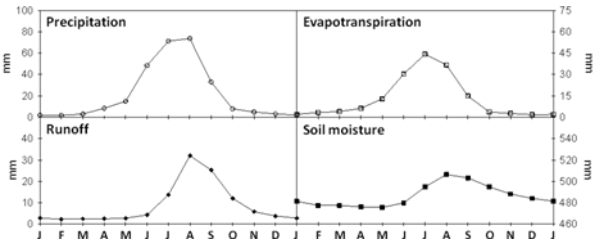

j) Selbe

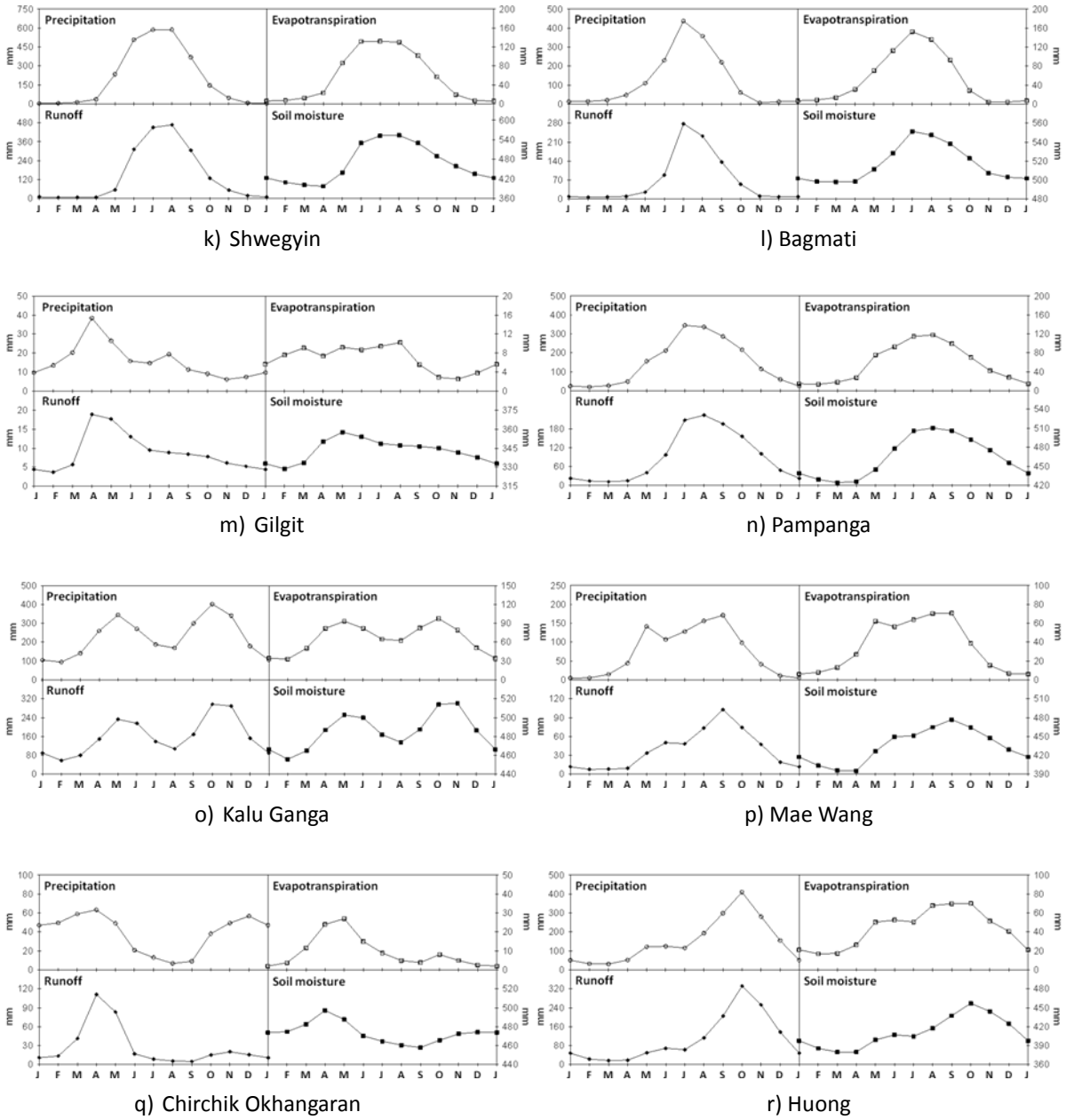

k) Shwegyin l) Bagmati

m) Gilgit n) Pampanga

o) Kalu Ganga p) Mae Wang

q) Chirchik Okhangaran r) Huong

Figure 3.9: Monthly average of calculated hydrological components from 1977 to 2006 at AWCI 18 countries.

3.3.2 Trend analysis

Asia region

To analyze the historical trend over Asia region the Mann-Kendall test was employed on 30-years (1977-2006) averages of temperature, precipitation and runoff. The Mann-Kendall test is nonparametric verification method to analyze trend of long term time series data. Other verification methods are influenced by the sample size, dispersion, and distortion. However, the Mann-Kendall test is not sensitive to the sample size and can analyze trend easily (Gibsons, 1990). The Mann-Kendall test is being widely used for analysis of hydrological variables because it can be applied to data having missing values (Hirsch et al, 1984; Bae et al., 2008a; Jung et al., 2011).

Figures 3.10 to 3.12 show the Mann-Kendall test results of historical temperature, precipitation, and runoff for period of 1977 to 2006 over Asia region. The left panels in figures indicate distribution of annual temperature, precipitation, and runoff, and right panels in figures show statistical results of Mann-Kendall test. The distribution results in figures show the 95% and 90% mean significance level. The arrows (↑) and (↓) denote the increase and decrease tendency respectively. During the past 30 years average temperature increased approximately 1～1.5°C with R^2=0.60 in the study area. Most regions showed increasing trend except Thailand and Bangladesh. Especially, there were distinct increasing trends (95% confidence level) over Indonesia, Malaysia, Tibetan Plateau, Mongolia, china, North Korea, and Japan. Other regions also had increase tendency although confidence level was not significant.

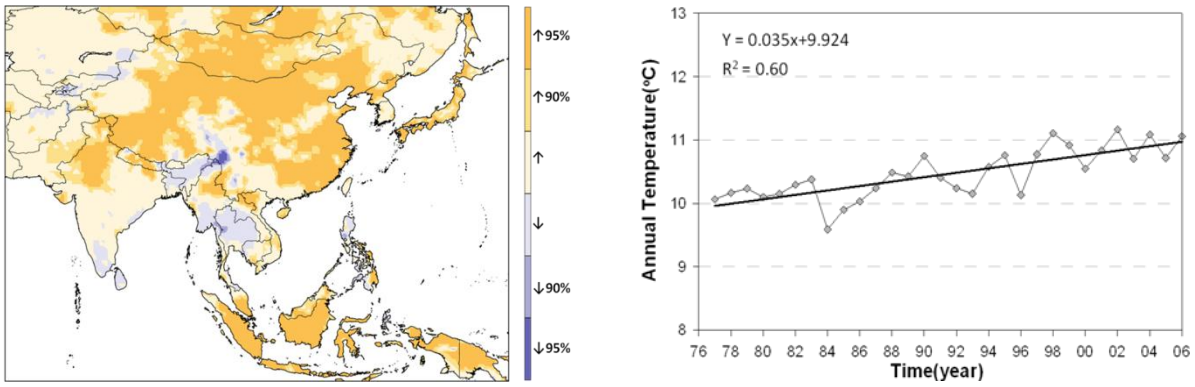

Figure 3.10: Mann-Kendall test results of annual historical temperature over Asian region. Graph means average of Asian region.

The Mann-Kendall test results for precipitation showed 100~200mm decrease in precipitation with slope coefficient -1.477 (R^2=0.22) during 30 years over Asia region (Fig. 3.11) The decreasing trend of precipitation appeared over Indonesia, Malaysia, inland of India, and east of North Asia. The increasing trend was also observed (95% confidence level) over bordering regions between Southern Asia and Central Asia, and southward of Tibetan Plateau. There was increasing tendency of precipitation over Mongolia, west China, South Korea, Myanmar, Thailand, Vietnam, and Japan although it was not significant statistically. On the other hand, the decreasing trend of precipitation was observed over China, India, Afghanistan, and Uzbekistan. The change in precipitation was higher than change in temperature over Asia region.

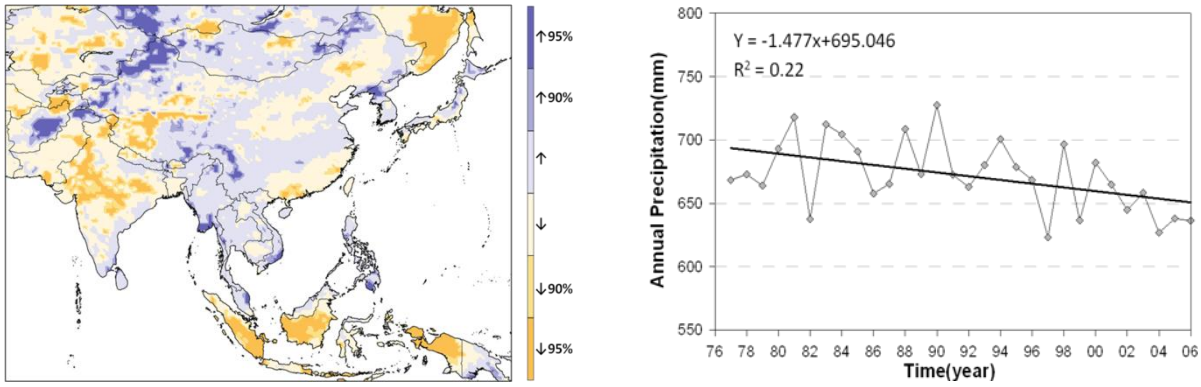

Figure 3.11: Mann-Kendall test results of annual historical precipitation over Asian region. Graph means average of Asian region.

Figure 3.12 shows the Mann-Kendall test results of annual historical runoff over Asia. The runoff over Asian region decreased approximately 70～80mm during past 30 years (1977-2006). The distribution of runoff change was similar to precipitation. The runoff decrease over Central Asia and east part of Southeast Asia was statistically significant with 95% confidence level. The increasing trend of runoff was observed over bordering regions between Southern Asia and Central Asia, and southward of Tibetan Plateau. Generally, the decreasing trend of runoff was sharp compared to precipitation.

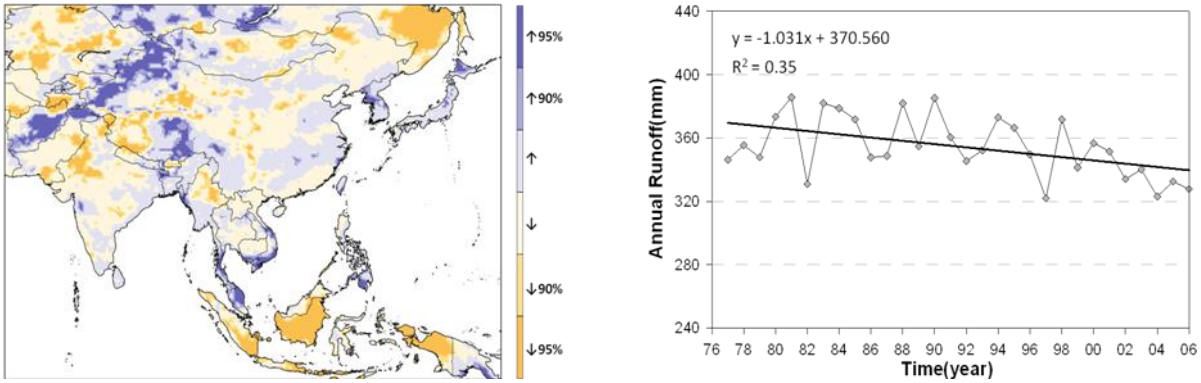

Figure 3.12: Mann-Kendall test results of annual historical runoff over Asian region. Graph means average of Asian region.

The seasonal trend analysis (spring, summer, autumn, winter) using Mann-Kendall test for 30-years (1977-2006) averages of temperature, precipitation and runoff are depicted in Figure 3.13 to 3.15. In spring season, the increasing temperature trend appeared over most regions of Asia except Thailand and Myanmar (Fig. 3.13). Especially, distinct increasing trend was observed over Malaysia, China, Japan and Mongolia. For precipitation, strong decreasing trend was shown over Indonesia, Malaysia, and west and south part of China. The decreasing trend of precipitation was also observed over Southern Asia and Central Asia although it was not statistically significant. In case of spring runoff, the regional pattern was almost similar to precipitation, however the strong decreasing trend appeared over China, India, and east part of Northern Asia. The increasing trend of runoff was observed over bordering regions between Central Asia and East Asia because of the snow melting from Jengish Chokusu, K2, Nanga Parbat, Himalaya, and Everest.

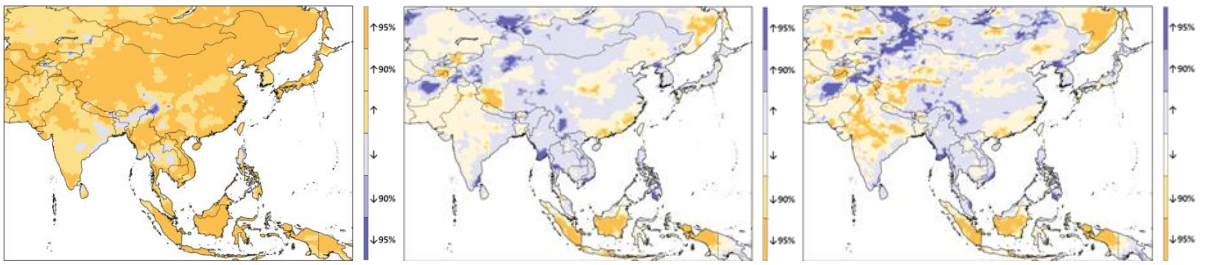

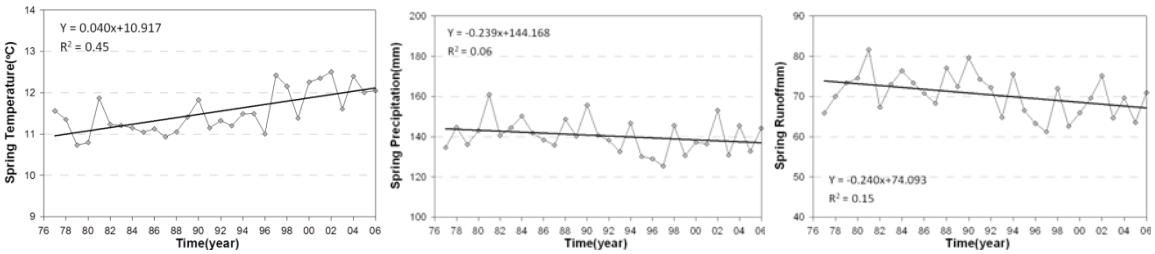

Figure 3.13: Mann-Kendall test results of spring historical temperature (left), precipitation (middle), and runoff (right) over Asian region. Graphs mean average of all Asian regions.

In summer season, distinct increasing trend of temperature was observed over China, Mongolia, south part of Japan, Indonesia, and Malaysia (Fig. 3.14). The decreasing temperature trend existed over some regions although it was not statistically significant. The trend analysis results for precipitation showed increasing trend over Central Asia, northwest and southeast part of China, North Korea, South Korea, and Japan. The decreasing precipitation trend was observed over Mongolia, inland of China, and India, although it was not statistically significant. In summer the trend of runoff was similar to annual trend of runoff.

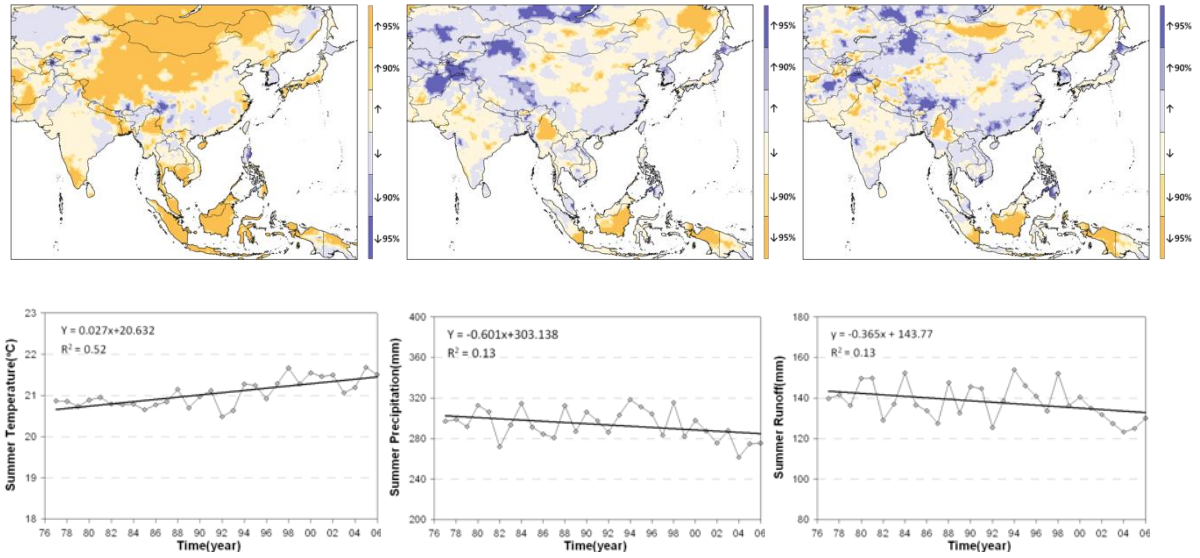

Figure 3.14: Mann-Kendall test results of summer historical temperature (left), precipitation (middle), and runoff (right) over Asian region. Graphs mean average of all Asian regions.

Figure 3.15 shows the Mann-Kendall test results of autumn for historical temperature, precipitation, and runoff over Asia region. Autumn temperature showed increasing trend over most regions of Asia except west part of Northern Asia. The distinct increasing trend of temperature appeared over eastern part of Northern Asia, Tibetan Plateau of China, North Korea, some parts of Japan, Afghanistan, Vietnam, Indonesia, and Malaysia. In autumn the increasing precipitation trend existed over some regions although it was not statistically significant. The features of runoff in autumn season were similar to precipitation.

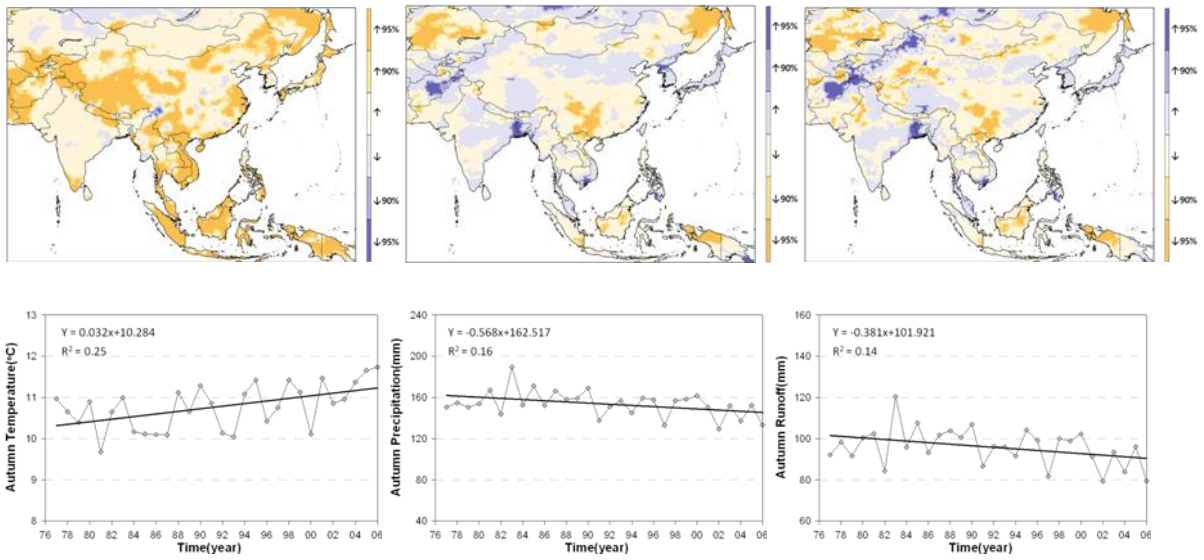

Figure 3.15: Mann-Kendall test results of autumn historical temperature (left), precipitation (middle), and runoff (right) over Asian region. Graphs mean average of all Asian regions.

The Mann-Kendall test results of winter for historical temperature, precipitation, and runoff over Asia regions are shown in Figure 3.16. The winter temperature increased over most regions except India and east part of Kazakhstan. The increasing trend was strong over China, Tibetan Plateau, Myanmar, Vietnam, Malaysia, and Indonesia. The trend analysis of precipitation in winter showed that the increasing trend was high over northwest, northeast, and southeast parts of China, and south part of Vietnam compared to other regions. The average precipitation over Asia region did not show any statistically significant increasing or decreasing trend. The increasing trend of winter runoff appeared over south part of Mongolia, west part of china, and India, however the trend was not statistically significant. Furthermore the increasing trend of runoff was weaker as compared to precipitation.

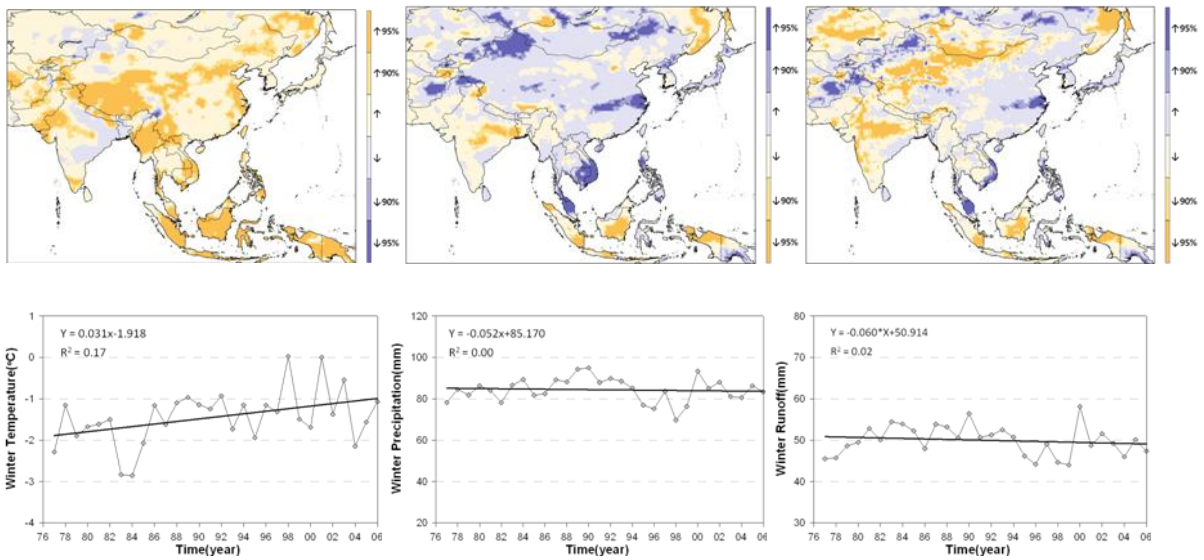

Figure 3.16: Mann-Kendall test results of winter historical temperature (left), precipitation (middle), and runoff (right) over Asian region. Graphs mean average of all Asian regions.

AWCI 18 basins

To evaluate the annual trend of temperature, precipitation, and runoff at basins scale the analysis was conducted at AWCI 18 basins. Figure 3.17 shows the annual mean change of temperature, precipitation, and runoff from 1977 to 2006 at each basin. In Meghna basin, Bangladesh, the increasing trend was observed for temperature, precipitation, and runoff while R square was low. The Punatsangchhu, Sangker, and Seonath basins located in Bhutan, Cambodia, and India, respectively showed similar features. The temperature was observed to increase with slight decrease in precipitation and runoff, although it was not statistically significant. In Mamberamo basin, Indonesia, the temperature (R^2=0.407) showed increasing trend, while precipitation (R^2=0.456) and runoff (R^2=0.408) were observed to decrease. The value of R square in Mamberamo basin was high compared to other basins. For Tone basin, Japan, and Chungju-Dam basin, Korea, the temperature, precipitation, and runoff showed increasing trend, although R square was statistically low. In case of Sebanfai basin, Laos, the temperature was observed to increase with slight increase in precipitation and decrease in runoff. The decrease in runoff was possibly because of increased temperature. In Langat basin, Malaysia, temperature, precipitation, and runoff showed increasing trend. Especially, the R square of temperature (0.62) and precipitation (0.32) was comparatively high. In Selbe basin, Mongolia, the temperature showed increasing trend, but precipitation and runoff were observed to decrease. In case of Shwegyin and Bagmati basins in Myanmar and Nepal, respectively, all variables had increasing tendency. Especially, Bagmati basin showed distinct increasing trend with R square value of 0.69. In Gilgit basin, Pakistan, the increasing trend was observed for temperature (R^2=0.31), precipitation (R^2=0.34), and runoff. In case of Pampanga, Kalu Ganga, and Mae Wang basins in Philippines, Sri Lanka, and Thailand, respectively, there was no distinct change in temperature, precipitation and runoff. In Chirchik-Okhangaran basin, Uzbekistan, the temperature was observed to increase, but precipitation and runoff had no significance change. In Huong basin, Vietnam, all variables showed increasing tendency although it was not statistically significant. Overall, the temperature showed increasing trend in most of the regions. Although the precipitation was observed to increase in most regions, the decreasing tendency was also observed in some regions. The trend of runoff was similar to that of precipitation. Furthermore, there was no significant impact of temperature on runoff features.

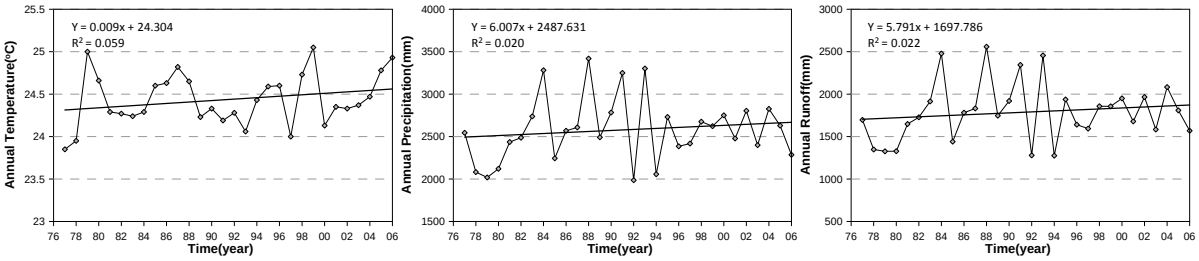

a) Meghna

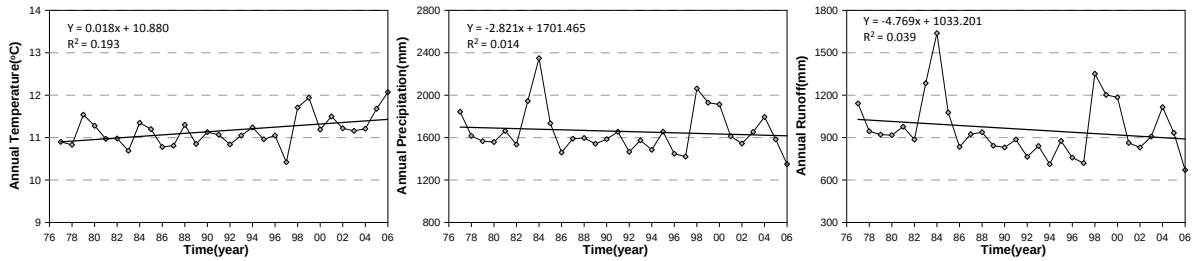

b) Punatsangchhu

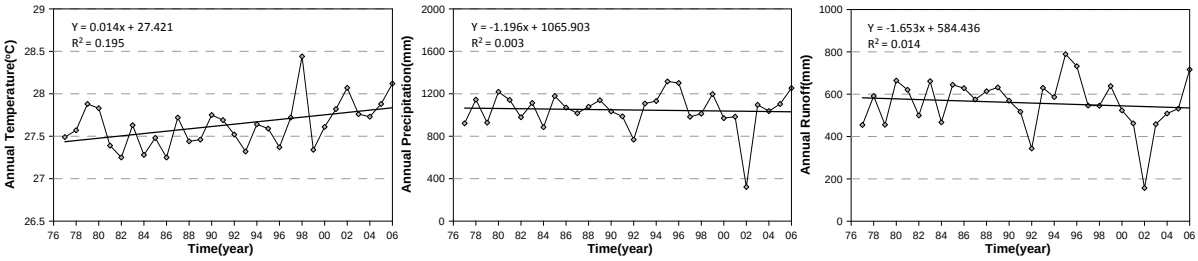

c) Sangker

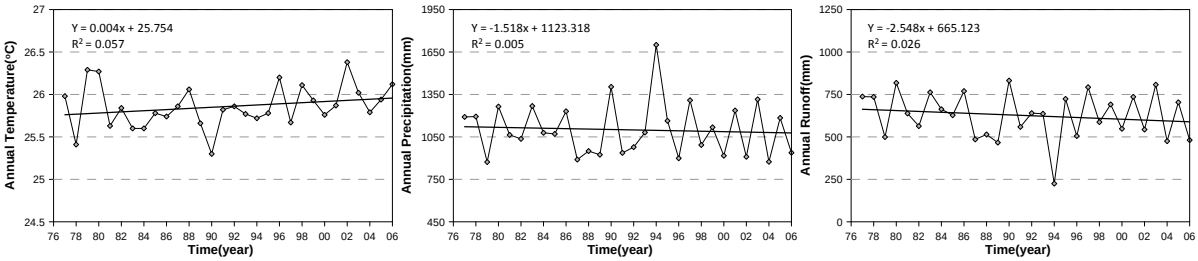

d) Seonath

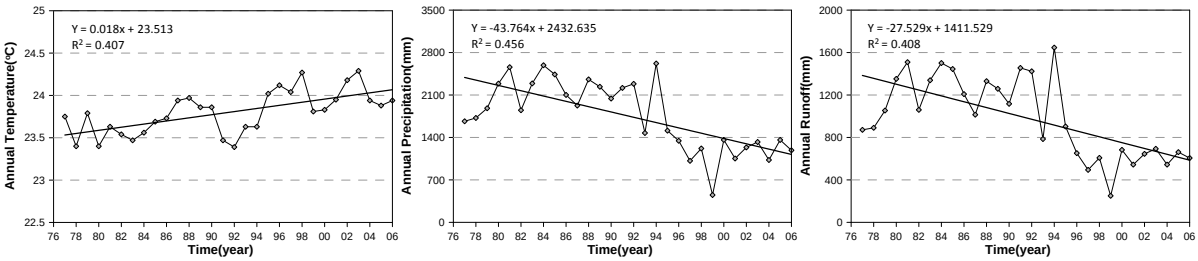

e) Mamberamo

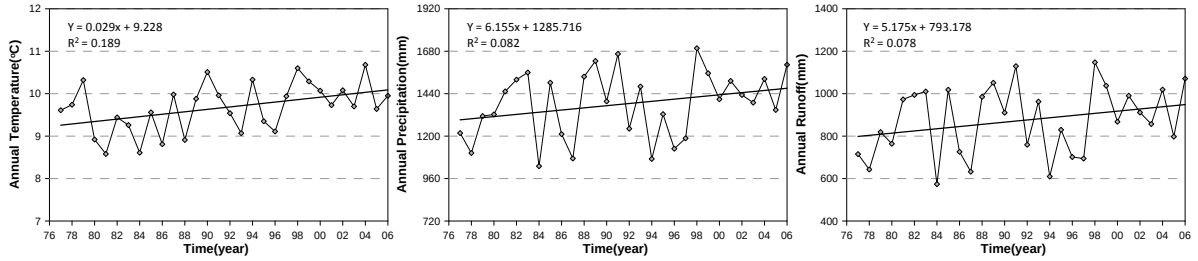

f) Tone

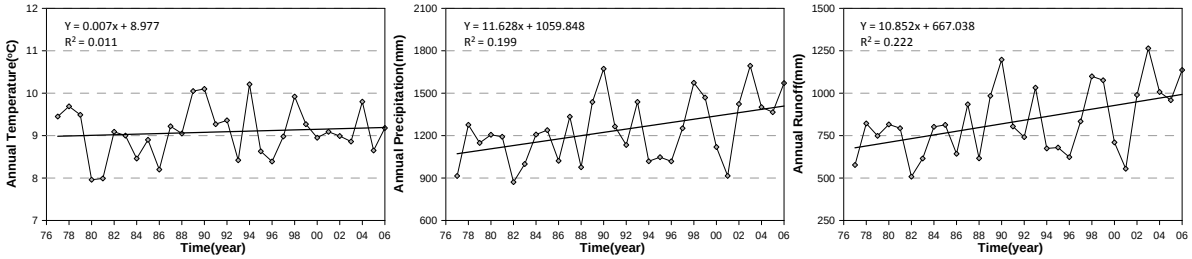

g) ChungJu-Dam

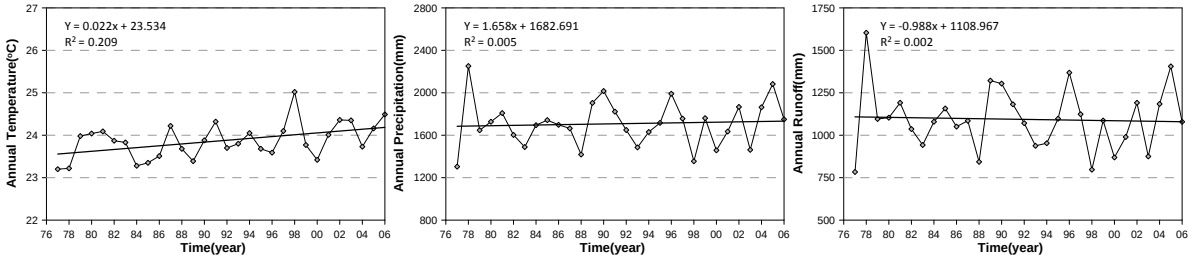

h) Sebanfai

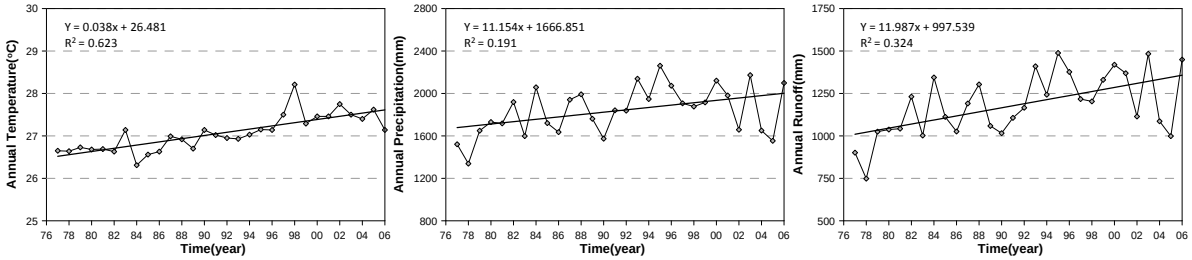

i) Langat

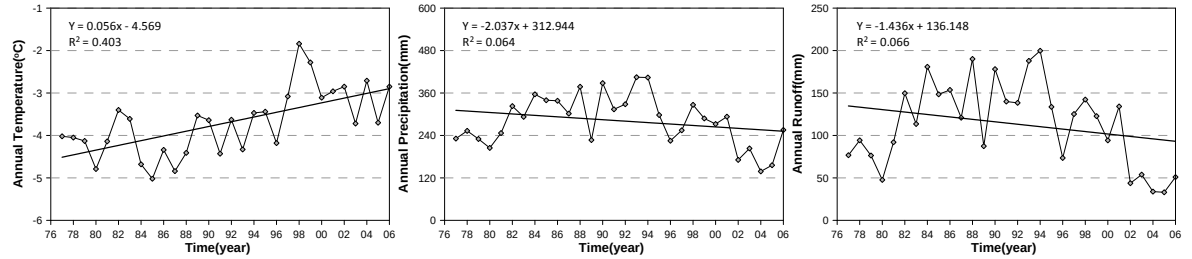

j) Selbe

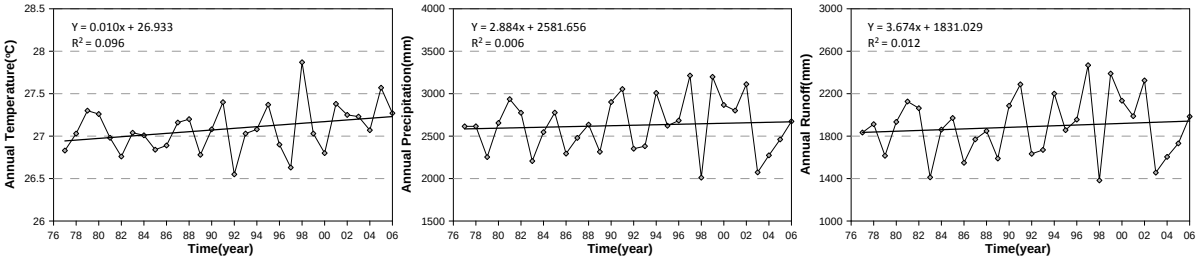

k) Shwegyin

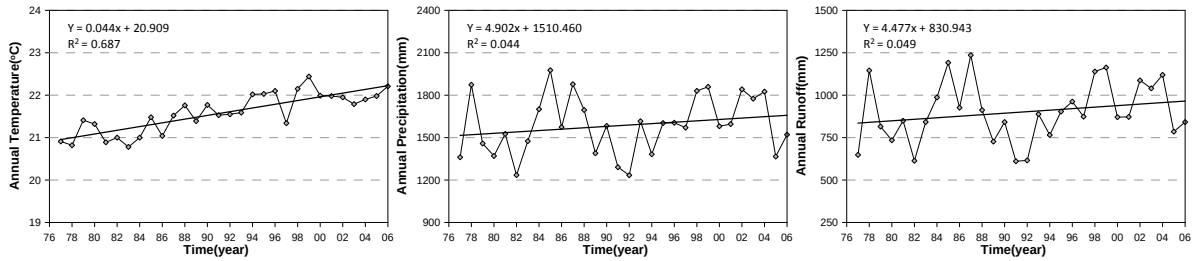

l) Bagmati

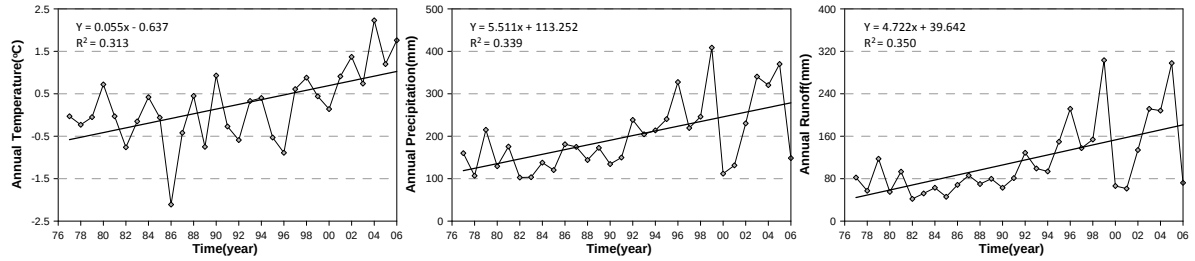

m) Gilgit

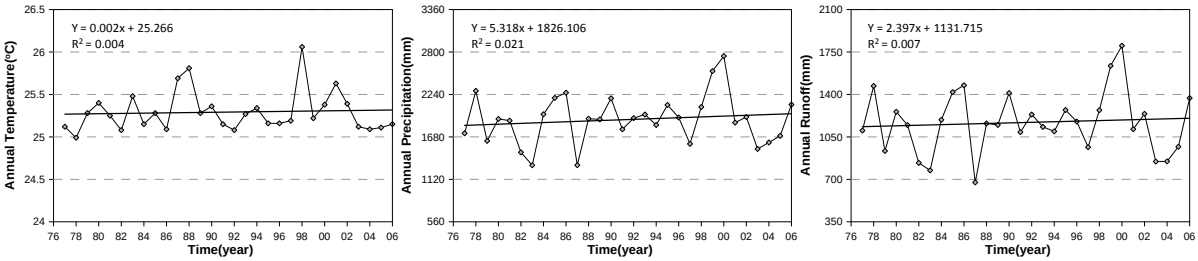

n) Pampanga

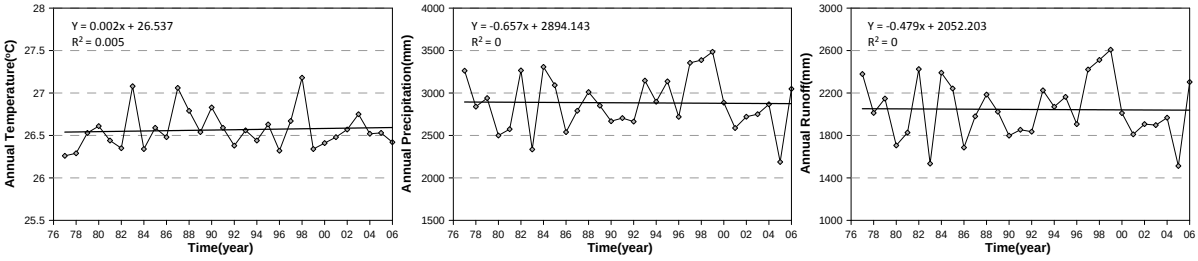

o) Kalu Ganga

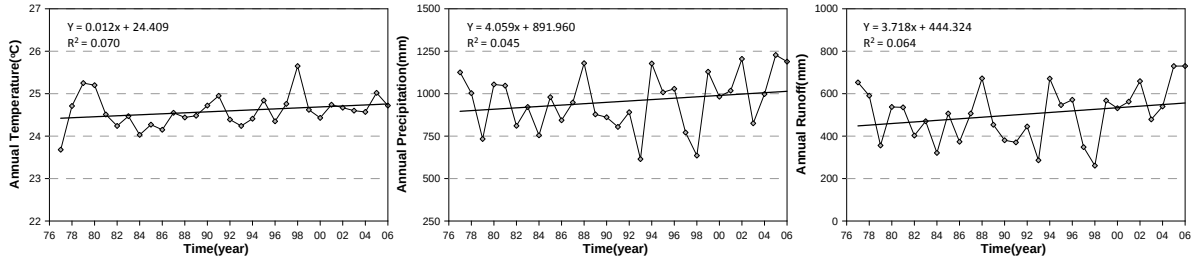

p) Mae Wang

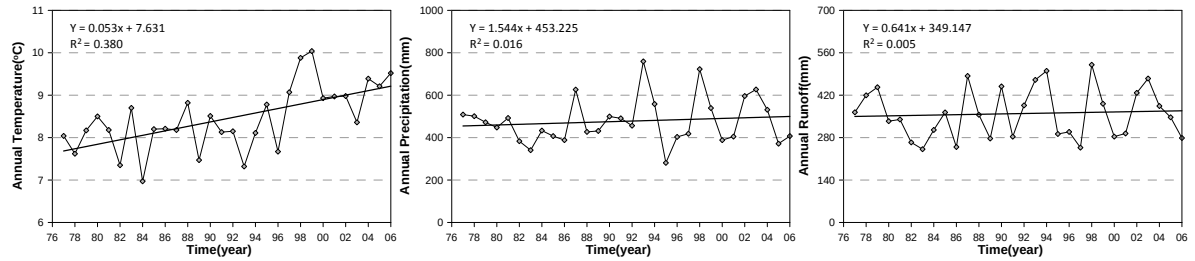

q) Chirchik-Okhangaran

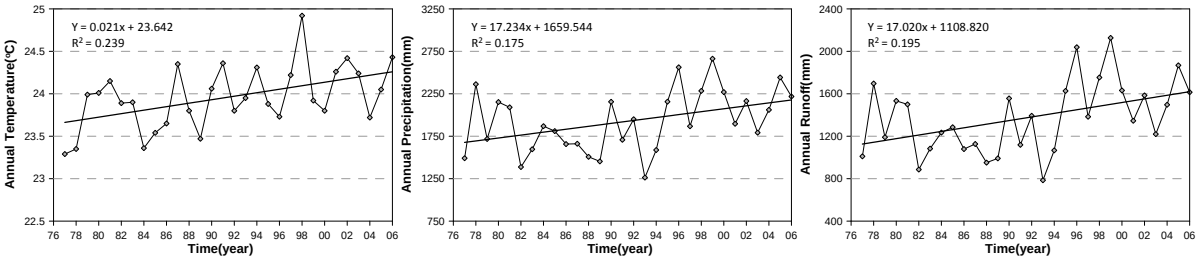

r) Huong

Figure 3.17: Annual mean change of temperature, precipitation, and runoff at AWCI 18 basins.

The annual and seasonal trend was also evaluated at AWCI 18 basins. The results of Mann-Kendall test for temperature, precipitation and runoff are shown in Tables 3.6～3.8. The trend analysis of annual temperature showed increasing trend for all the basins. Particularly, the temperature increase at ten basins was statistically significant at 95% confidence level. The seasonal trend analysis of temperature showed statistically significant increasing trend at four, five, six, and five basins for spring, summer, autumn, and winter respectively. In particular, the increasing trend at Mamberamo basin, Indonesia and Bagmati basin, Nepal was estimated high for all four seasons. The increasing trend of temperature was estimated in spring and summer for Selbe basin, Mongolia, and in autumn and winter for both Gilgit basin, Pakistan and Chirchik Okhangaran, Uzbekistan basin. The increasing temperature trend was also estimated at some other basins, however it was not statistically significant.

The Mann-Kendall test results of precipitation revealed decreasing trend for annual precipitation at Mamberamo basin, and increasing trend at Gilgit, Langat, and Huong basins with statistical significance at 95% confidence level. All basins showed increasing trend for annual precipitation except three basins. The seasonal precipitation increased at Gilgit basin and decreased at Mamberamo basin for all four seasons. The precipitation at Shwegylin basin highly increased in spring and decreased at Sebangfai basin in summer and autumn season, The increase in precipitation was observed at Langat and Huong basins in winter season.

The trend analysis of runoff showed decrease in the annual runoff at Mamberamo basin and increase at both Langat and Gilgit basins. All basins had increasing trend for annual runoff except five basins. The Mann-Kendall test results for seasonal runoff estimated decrease at Mamberamo basin and increase at Gilgit basin for all four seasons. The runoff in spring season increased at Shwegylin basin and decreased at Seonath and Selbe basins. The runoff increased at Bagmati basin in summer, at Huong basin in winter and at Langat basin in both summer and winter season. Overall the decreasing

trend of runoff was high as compared to the precipitation decrease at selected basins.

Table 3.6: Trend analysis of temperature using the Mann-Kendall test at AWCI 18 countries. The filled triangle indicate statistical significant at 95% confidence level.

No.	Country	Basin	Trend analysis of temperature				
			Spring	Summer	Autumn	Winter	Year
1	Bangladesh	Meghna	▽	△	▽	▽	△
2	Bhutan	Punatsangchhu	△	▽	△	△	△
3	Cambodia	Sangker	▽	▲	△	△	▲
4	India	Seonath	△	△	△	△	△
5	Indonesia	Mamberamo	▲	▲	▲	▲	▲
6	Japan	Tone	△	△	△	△	▲
7	Korea	Chungju-dam	△	▽	△	△	△
8	Lao PDR	Sebangfai	△	△	▲	△	▲
9	Malaysia	Langat	▲	▲	▲	▲	▲
10	Mongolia	Selbe	▲	▲	△	△	▲
11	Myanmar	Shwegylin	▽	△	△	△	△
12	Nepal	Bagmati	▲	▲	▲	▲	▲
13	Pakistan	Gilgit	△	△	▲	▲	▲
14	Philippines	Pampanga	▽	▽	△	△	△
15	Sri Lanka	Kalu Ganga	▽	△	△	△	△
16	Thailand	Mae Wang	▽	▽	▽	△	△
17	Uzbekistan	Chirchik-Okhangaran	△	△	▲	▲	▲
18	Vietnam	Huong	△	△	△	△	▲

Table 3.7: Trend analysis of precipitation using the Mann-Kendall test at AWCI 18 countries. The filled triangle indicate statistical significant at 95% confidence level.

No.	Country	Basin	Trend analysis of precipitation				
			Spring	Summer	Autumn	Winter	Year
1	Bangladesh	Meghna	▽	△	△	▽	△
2	Bhutan	Punatsangchhu	△	▽	▽	△	△
3	Cambodia	Sangker	▽	▽	▽	△	▽
4	India	Seonath	▽	△	△	△	▽
5	Indonesia	Mamberamo	▼	▼	▼	▼	▼
6	Japan	Tone	△	▽	△	△	△

7	Korea	Chungju-dam	△	△	△	△	△
8	Lao PDR	Sebangfai	△	▲	▼	▽	▽
9	Malaysia	Langat	▽	△	△	▲	▲
10	Mongolia	Selbe	▽	▽	▽	△	▽
11	Myanmar	Shwegylin	▲	▽	▽	△	△
12	Nepal	Bagmati	△	▲	▽	△	△
13	Pakistan	Gilgit	▲	▲	▲	▲	▲
14	Philippines	Pampanga	△	△	▽	▲	△
15	Sri Lanka	Kalu Ganga	△	△	△	△	△
16	Thailand	Mae Wang	△	△	△	△	△
17	Uzbekistan	Chirchik-Okhangaran	▽	△	△	△	△
18	Vietnam	Huong	△	△	▽	▲	▲

Table 3.8: Trend analysis of runoff using the Mann-Kendall test at AWCI 18 countries. The filled triangle indicate statistical significant at 95% confidence level.

No.	Country	Basin	Trend analysis of runoff				
			Spring	Summer	Autumn	Winter	Year
1	Bangladesh	Meghna	▽	△	△	△	△
2	Bhutan	Punatsangchhu	△	▽	▽	△	▽
3	Cambodia	Sangker	▽	▽	▽	▽	▽
4	India	Seonath	▼	▽	△	▼	▽
5	Indonesia	Mamberamo	▼	▼	▼	▼	▼
6	Japan	Tone	△	▽	△	△	△
7	Korea	Chungju-dam	△	△	△	△	▲
8	Lao PDR	Sebangfai	△	△	▼	△	▽
9	Malaysia	Langat	△	▲	△	▲	▲
10	Mongolia	Selbe	▼	▽	▽	△	▽
11	Myanmar	Shwegylin	▲	▽	▽	△	△
12	Nepal	Bagmati	△	▲	▽	△	△
13	Pakistan	Gilgit	▲	▲	▲	▲	▲
14	Philippines	Pampanga	△	△	▽	△	△
15	Sri Lanka	Kalu Ganga	△	△	△	△	△
16	Thailand	Mae Wang	△	△	△	▽	△
17	Uzbekistan	Chirchik-Okhangaran	△	△	△	△	△

18	Vietnam	Huong	△	△	△	▲	▲

3.4 Analysis of future climate and hydrology

3.4.1 GCMs selection

The selection of appropriate GCM is a primary step for projection of future climate and hydrology. In this study nine GCMs were compared for their future application in Asian region. The comparison was made on several statistical measures i.e. the probabilistic uncertainty analysis, correlation coefficient, and RMSE. The overall ranking of each GCM was computed based on the scores of all three statistical tests. The target GCMs for comparison include MPIM: ECHAM5, CSIRO: MK3.0, GFDL: CM2_1, CNRM: CM3, MRI: CGCM2_3_2, UKMO: HADCM3, IPSL: CM4, CCCMA: CGCM3_T47, and CONS: ECHO-G. The results of statistical test are explained in the following sections.

Probabilistic uncertainty analysis

The results of probabilistic uncertainty test for selected nine GCMs are shown in Table 3.9. From results it is evident that the best GCM was CGCM_T47 with highest total score of 131. It was followed by CM4 and ECHO-G both with score of 109. The CGCM2_3_2 was ranked as 4th for probabilistic uncertainty analysis test with score of 104. The other GCMs had the score ranging from 83 to 104.

Table 3.9: Score index of GCMs based on the results of probabilistic uncertainty test

No.	Model (agency: version)	Total score ($S_{P,total}$)	Normalized score ($S_{P,normalized}$)	Remarks
1	MPIM: ECHAM5	94	0.23	-
2	CSIRO: MK3.0	83	0.00	-
3	GFDL: CM2_1	89	0.13	-
4	**CNRM: CM3**	**103**	**0.42**	**5th**
5	**MRI: CGCM2_3_2**	**104**	**0.44**	**4th**
6	UKMO: HADCM3	93	0.21	-
7	**IPSL: CM4**	**109**	**0.54**	**2rd**
8	**CCCMA: CGCM3_T47**	**131**	**1.00**	**1st**
9	**CONS: ECHO-G**	**109**	**0.54**	**2rd**

Correlation coefficient test

Table 3.10 shows the results of correlation coefficient test for nine GCMs. As can be seen from the results, the best GCM was CGCM3_T47 with the score of 172 which was followed by CGCM2_3_2 and HADCM3 with the score of 157 and 156, respectively. It is noted that, CGCM3_T47 ranked best among all GCMs for correlation coefficient test like the probabilistic uncertainty test. The GCMs showing good result in this test can be assumed to provide the predicted data having high correlation with the observed data.

Table 3.10: Score index of GCMs based on the results of correlation coefficient test

No.	Model (agency: version)	Total score ($S_{r,total}$)	Normalized score ($S_{r,normalized}$)	Remarks
1	**MPIM: ECHAM5**	**152**	**0.59**	**5th**
2	CSIRO: MK3.0	147	0.49	-
3	GFDL: CM2_1	123	0.00	-
4	**CNRM: CM3**	**153**	**0.61**	**4th**
5	**MRI: CGCM2_3_2**	**157**	**0.69**	**2nd**
6	**UKMO: HADCM3**	**156**	**0.67**	**3rd**
7	IPSL: CM4	151	0.57	-
8	**CCCMA: CGCM3_T47**	**172**	**1.00**	**1st**
9	CONS: ECHO-G	142	0.39	-

RMSE test

The results of RMSE test for nine GCMs are shown in Table 3.11. The results indicate that the CGCM2_3_2 was best GCM with highest score of 245. Unlike probability uncertainty analysis and correlation coefficient test the CGCM3_T47 was ranked 4th for RMSE test. On the other hand ECHAM5 and MK3.0 showed good performance for RMSE test with scores of 212 and 202 respectively. The RMSE test considers the quantity of each projected value. Thus, the GCM with good performance in this test can be applied to most of the future events.

Table 3.11: Score index of GCMs based on the results of RMSE.

No.	Model (agency: version)	Total score ($S_{RMSE,total}$)	Normalized score ($S_{RMSE,normalized}$)	Remarks
1	**MPIM: ECHAM5**	**212**	**0.58**	**2nd**
2	**CSIRO: MK3.0**	**202**	**0.46**	**3rd**
3	GFDL: CM2_1	188	0.28	-
4	CNRM: CM3	167	0.01	-
5	**MRI: CGCM2_3_2**	**245**	**1.00**	**1st**
6	UKMO: HADCM3	166	0.00	-
7	IPSL: CM4	189	0.29	-
8	**CCCMA: CGCM3_T47**	**198**	**0.41**	**4th**
9	**CONS: ECHO-G**	**198**	**0.41**	**5th**

Quantifying the overall effectiveness of 9 GCMs

To obtain most appropriate GCMs we combined the scores of all three tests and computed overall effectiveness score. Table 3.12 shows the result of 9 GCMs with their overall normalized scores. It is noted that the range of overall normalized score for all GCMs was from 0 to 2. As can be seen from the table, CGCM3_T47 model showed the best results in all 3 tests with the score of 1.70, while the GCM having lowest score was CM2_1 with score of 0.26. Based on overall effectiveness score the GCMs CGCM3_T47, CGCM2_3_2 and CM4 with 1st, 2nd and 3rd ranking, respectively were selected for future climate change and hydrology impact assessment over Asia.

Table 3.12: Overall effectiveness of 9 GCMs.

No.	Model (agency: version)	Overall normalized score	Remarks
1	MPIM: ECHAM5	0.82	-
2	CSIRO: MK3.0	0.47	-
3	GFDL: CM2_1	0.26	-
4	CNRM: CM3	0.73	-
5	**MRI: CGCM2_3_2**	**1.28**	**2nd**
6	UKMO: HADCM3	0.55	-
7	**IPSL: CM4**	**0.97**	**3rd**
8	**CCCMA: CGCM3_T47**	**1.70**	**1st**
9	CONS: ECHO-G	0.94	-

3.4.2 Future climate and hydrology analysis

GCMs uncertainty

To evaluate uncertainty of selected GCMs for future scenarios the projection results of each GCM were analyzed. Figure 3.18 shows the annual and seasonal change of temperature and precipitation in future periods (10 years mean) compared to the reference period (1977-2006). The simulations projected annual temperature increase of about 3.6℃ in future. The CM4 showed high increase in temperature of 4.1℃ and CGCM3_T47 projected comparatively low increase of about 3.0℃. The seasonal analysis showed temperature increase of 3.7℃, 3.6℃, 3.5℃ and 3.4℃ in winter, summer, autumn and spring respectively by 2090s. To evaluate uncertainty of selected GCMs, the difference between maximum and minimum projected values was used. The high uncertainty appeared in summer (1.4℃) and spring (1.3℃) season by 2090s. The uncertainty was comparatively low in winter season with value of 0.8℃.

The GCMs simulations projected about 13.4% increase of annual mean precipitation by 2090s. On seasonal scale, the precipitation was expected to increase by 13.0%, 12.6%, 18.8% and 14.3% in spring, summer, autumn, and winter respectively. The projection results of summer precipitation were similar to that of annual precipitation with very low uncertainty. On the other hand, there were large differences between spring and autumn projection results. The CGCM3_T47 showed decreasing tendency of precipitation in spring season while other GCMs showed increasing trend. In autumn season, CM4 projected quite high increase in precipitation as compared to other GCMs. The uncertainty in spring and winter season was 15.0% and 14.5%, respectively.

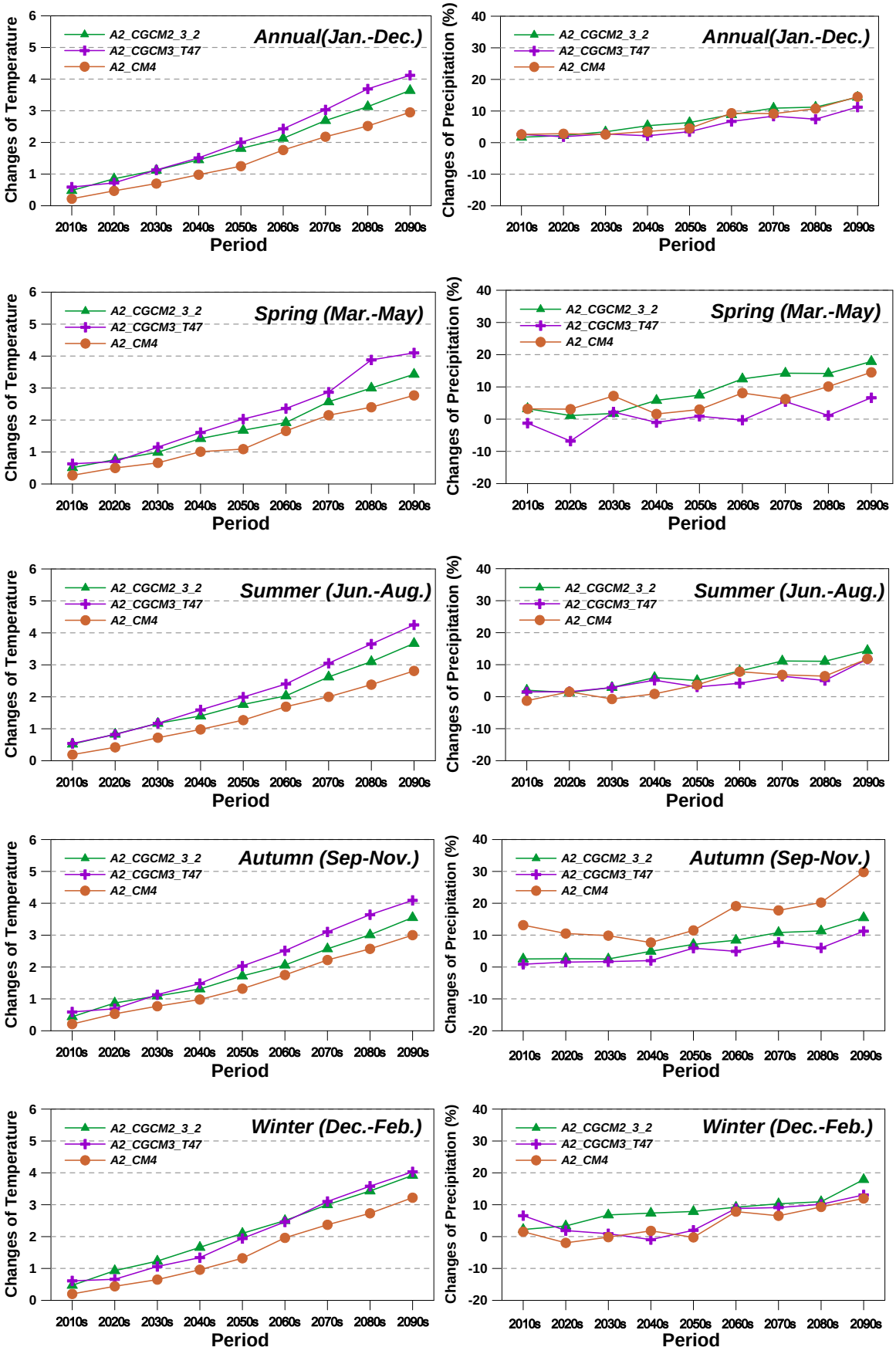

Figure 3.18: Annual and seasonal temperature and precipitation in future periods (10 years mean)

compared to reference period (1977-2006).

Annual average change

To investigate the features of future climate scenarios (0.5° **x** 0.5°) the spatial analysis of change in annual temperature, precipitation, and runoff relative to the reference period was conducted over Asia region. Figure 3.19 shows the relative change of temperature, precipitation, and runoff at future periods (2020s:2011-2040; 2050s:2041-70; 2080s:2071-2100). The projections showed consistent increase of average temperature in future periods i.e. 2020s, 2050s and 2080s. In 2020s the average temperature over Asia was expected to rise by 0.71℃. The high increase in temperature (1.33~1.82℃) was projected over Russia, Mongolia, and Pakistan. In East Asia, the temperatures were expected to increase by 0.64℃, 0.76℃, 0.53℃ and 0.91℃ in China, North Korea, South Korea and Japan respectively by 2020s. In 2050s, average temperature over Asia will increase by 1.78℃, with high increase of 2.5℃ in Mongolia. The average temperature over Asia was projected to increase by 3.27℃ in 2080s. The expected increase in annual temperature may further intensify the regional bias in future.

The projection results for annual precipitation showed 3.1% increase in 2020s compared to the reference period over Asia. However, the precipitation at west China, southeast China, Kazakhstan, Tajikistan, Kyrgyzstan, east India, south India, Myanmar, Vietnam, and Thailand was expected to decrease about 4.0~15.0%. In South Korea, precipitation was projected to increase by 12.0% and 17.0% in southern and central part, respectively. In 2050s, the decreasing rate was more prominent over Thailand, Vietnam, and Southeast Asia. Over west China and northeast of India precipitation change rate was expected to be -13.0%. On the other hand the precipitation was projected to increase by 10.0~80.0% over west India and Pakistan in 2050s. In 2080s, the annual precipitation was expected to increase by 11% over Asia except west China and Afghanistan.

Future scenarios projected increase in annual runoff over Asia region like precipitation. However, regional bias was expected to be intensified. In 2020s, the runoff over Asia region was expected to increase by 5.9%. The decrease of 3.0~25.0% in annual runoff was projected over Russia, west China, southeast China, south India, west India, Myanmar, Thailand, Cambodia, and Vietnam. In 2050s, the runoff rate over west China and northeast India was expected to be intensified with range -15.0%~61.0%. The simulations projected large increase in annual runoff over west India and Pakistan with rate of 105.0~353.0%. In 2080s, runoff over most regions in Asia was appeared to increase. However, the runoff at west China and Afghanistan was expected to decrease. Overall the change rate of runoff was larger than the precipitation change.

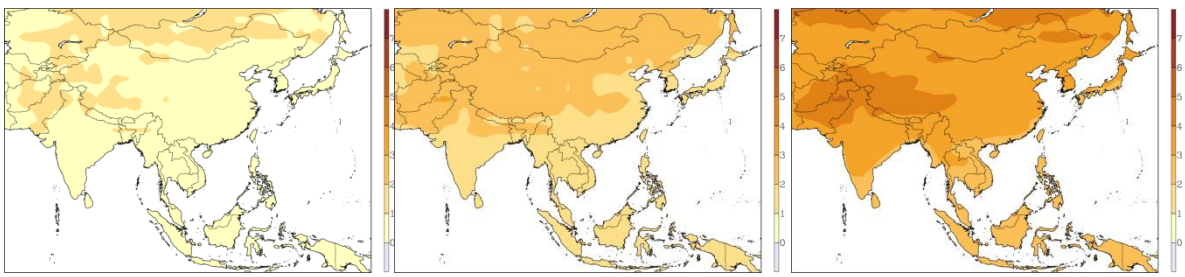

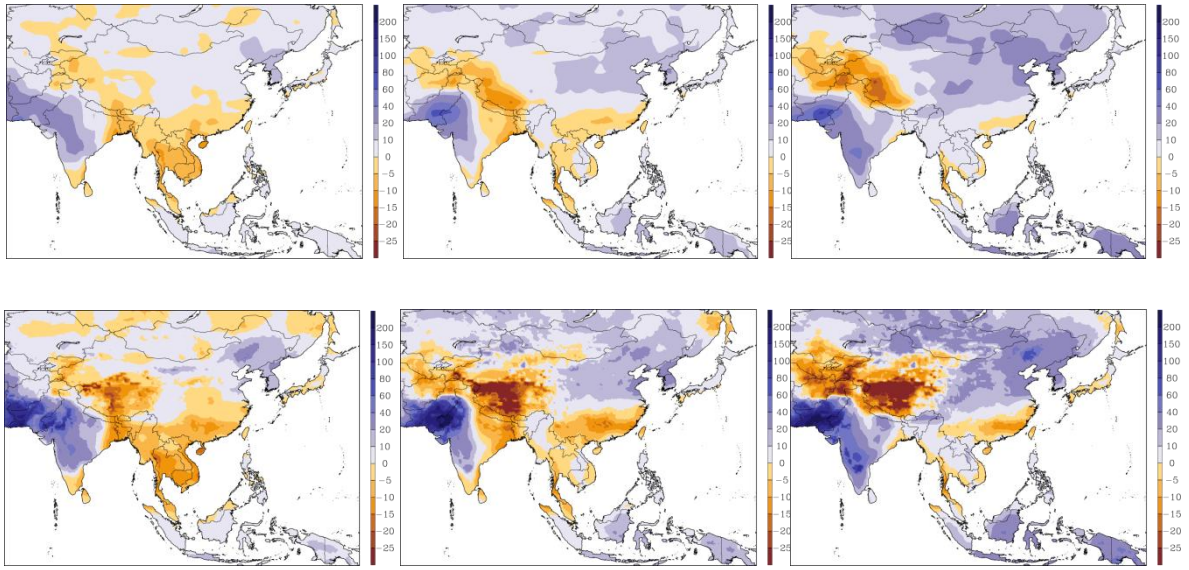

Figure 3.19: Relative change of temperature (top), precipitation (middle), and runoff (bottom) at future at 2020s (left), 2050s (center), 2080s (right).

Seasonal change

The projected change of seasonal temperature, precipitation, and runoff in 2080s relative to the reference period is portrayed in Figure 3.20. The seasonal analysis showed increase of 0.5℃ temperature in spring season over Asia region. The high increase in temperature (4.1~5.6℃) was expected over Kazakhstan, north India, Pakistan, and Afghanistan. The spring precipitation and runoff was projected to increase by 11.6% and 15.0%, respectively. The precipitation and runoff at west China, central China, and India was expected to increase by 45.0~68.1% and 52.0~390.0%, respectively. On the other hand, the precipitation and runoff at Afghanistan, Uzbekistan, Vietnam, Thailand, and Japan was expected to decrease with rate of -5.0~-21.0% and -13.0~-64.0%, respectively. In summer season the temperature was expected to increase by 3.6℃ over Asia, with high increase of 3.5~5.1℃ over west China, Pakistan, and Afghanistan. The average precipitation and runoff over Asia during summer season was expected to increase by 9.2% and 14.1%, respectively. The high increase in precipitation and runoff was projected over west China, central China, and India with rate of 45.0~68.0% and 45.0~348.0%, respectively. On the other hand, the precipitation over Afghanistan and Uzbekistan was expected to decrease about -2.0~-46.0%. The decrease of runoff (-5.0~-85.0%) was projected over west China, east Russia, Vietnam, and Thailand. The autumn temperature was expected to increase about 3.5℃ over Asia. Particularly, the increase of 4.1~4.6℃ temperature was projected over east Russia, west China, and Pakistan. The average precipitation and runoff during autumn season was appeared to increase about 10.0% and 8.6%, respectively. The high increase in precipitation (45.0~68.0%) and runoff (15~191%) was projected over China, east Mongolia, central Mongolia, Malaysia, India, and south Pakistan during autumn season. The precipitation and runoff was appeared to decrease about -2.0~-15.0% and -3.0~-63.0% respectively over Afghanistan, west China, east Russia, and Japan. The winter temperature was expected to increase about 4.1℃ over Asia with high increase of 5.6℃ over southwest China and Tibetan Plateau. The average precipitation and runoff over Asia was expected to increase about 14.0% and 11.2%, respectively. Especially, the high increase (45.0~97.0%) of precipitation was estimated over north

China, Mongolia, east Kazakhstan, east Russia, and south Pakistan. The runoff was appeared to increase by 60.0~368.0% over Pakistan, Uzbekistan, Turkmenistan, and Afghanistan. However, the increasing rate of runoff during winter season over China, Mongolia, and Russia was low compared to the precipitation. The decrease in runoff (-6.0~-65.0%) and precipitation (-4.0~-35.0%) was projected during winter season over China, South Korea, south Japan, Thailand, Myanmar, and Vietnam.

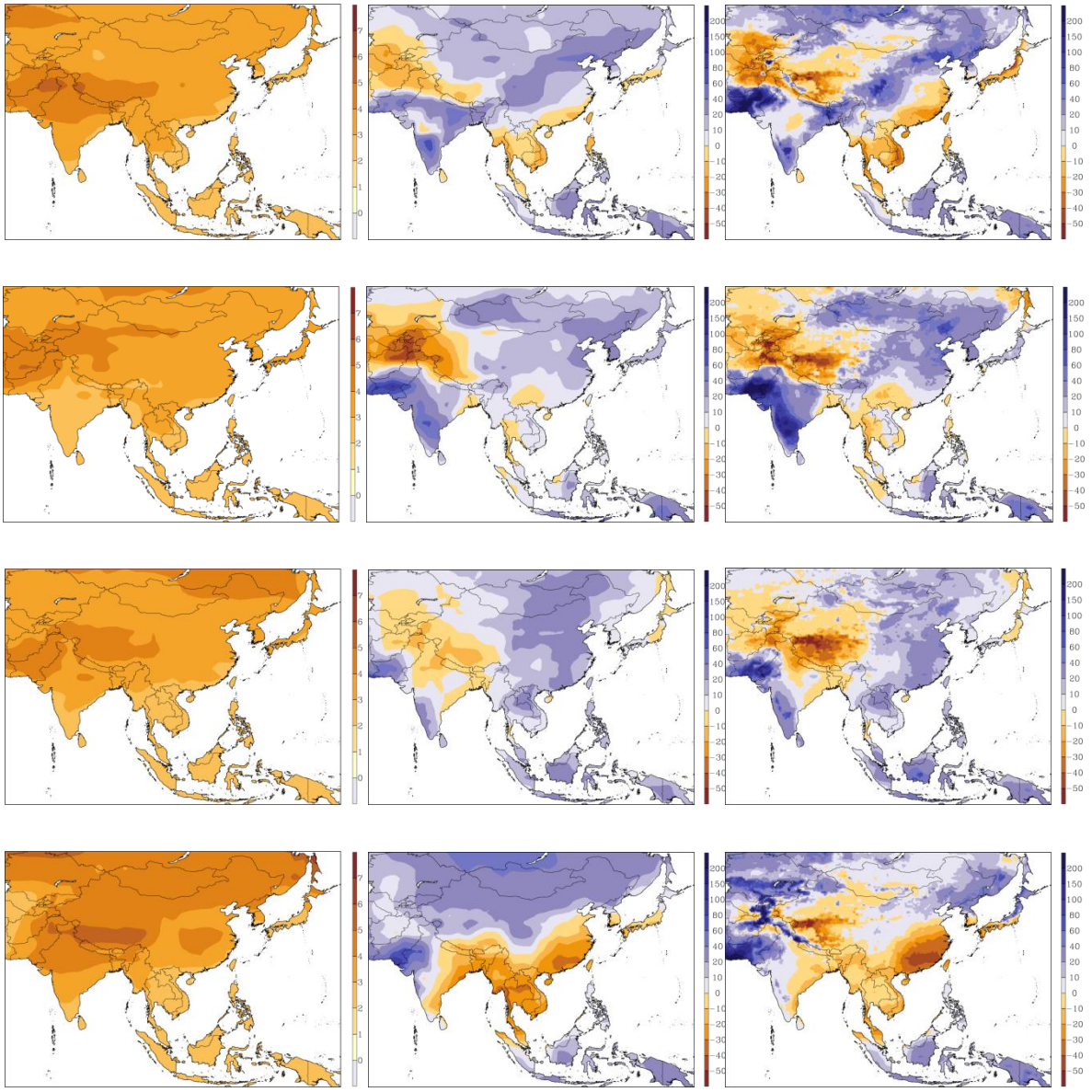

Figure 3.20: future change of spring (top), summer (second), autumn (third), and winter (bottom) temperature (left), precipitation (center), and runoff (right) at 2080s.

Latitudinal Analysis

Generally, temperatures decrease with increasing latitudes. Several climate zones exist according to varying latitudes. Therefore, it is important to analyze hydrological components at different latitudes. Figure 3.21 shows the latitudinal temperature change at each season. The temperature was projected to increase consistently during future periods i.e. 2020s, 2050s and 2080s. The increasing

rate was also observed to increase with increasing latitudes. The high change in temperature was projected at latitudes ranges 30°~35°N, 30°~50°N, 25°~55°N, and 25°~55°N for spring, summer, autumn, and winter, respectively. Especially, in 2080s, the temperature increase of 4.35~4.91℃ was expected in spring and winter season at 30°~35°N.

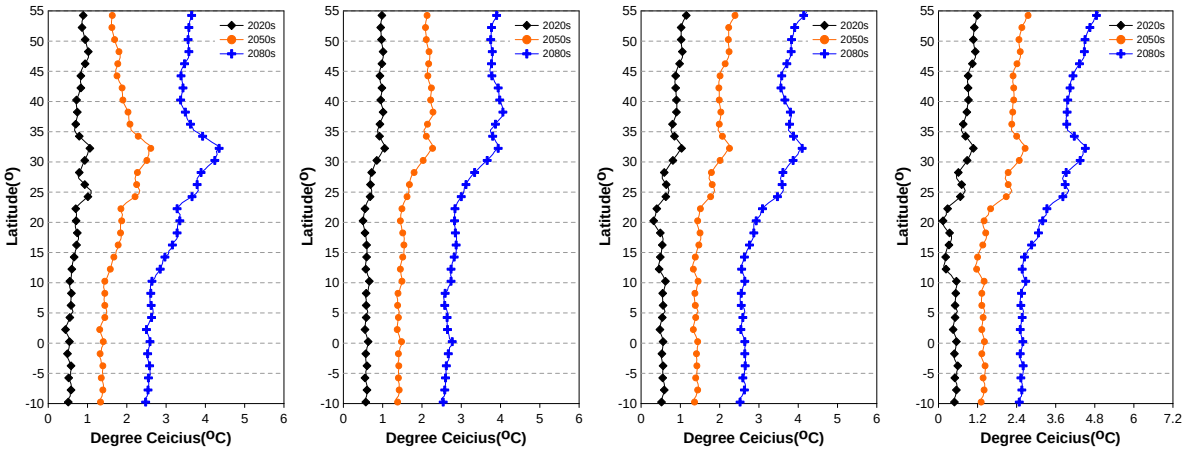

Figure 3.21: Latitudinal temperature change in spring (left), summer (second), autumn (third), and winter (right).

Figure 3.22 shows the latitudinal precipitation change rate for each season. In spring season, the distinct increase and decrease in precipitation was projected for future periods at different latitudes. The high increase rate of precipitation was expected at 40°~55°N, 25°~30°N, and 10°S~5°N. In summer season, the change rate was low compared to spring. However, there was increasing tendency at 25°~30°N and 10°S~5°N. In autumn season, the precipitation increase was low compared to spring and summer. Also, there was no distinct latitudinal change rate. In winter season, the difference of precipitation increase was appeared at high latitudes (40°~55°N) and low latitudes (0°~10°S). The winter precipitation during 2080s at high latitude region and low latitude region was expected to increase by 37.0% and 29.0%, respectively. On the other hand, the precipitation at 5°~25°N was expected to decrease compared to the reference period. The difference of future three periods was almost same.

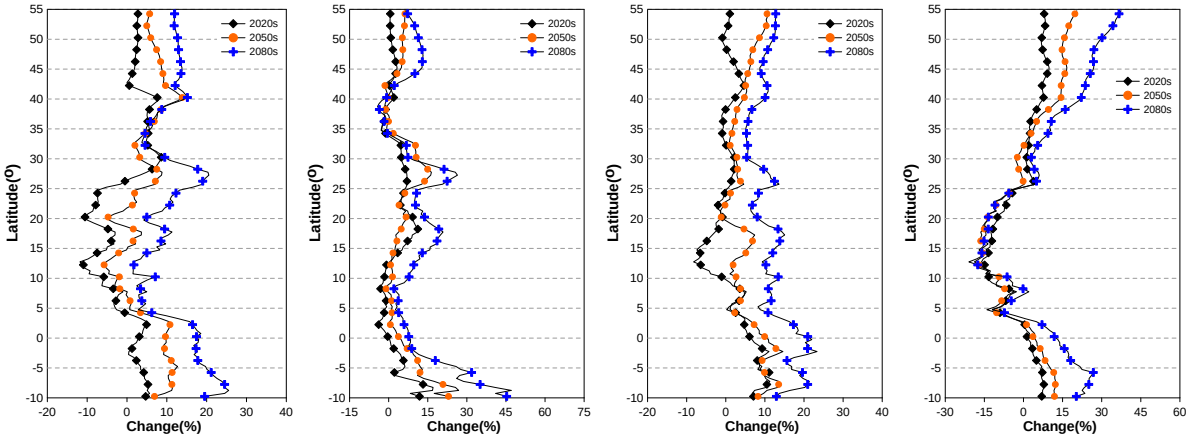

Figure 3.22: Latitudinal precipitation change in spring (left), summer (second), autumn (third), and winter (right).

Figure 3.23 shows the latitudinal runoff change for future periods in spring, summer, autumn, and winter seasons. During spring season, the high increase in runoff was projected at 45°~55°N, 25°~30°N, and 0°~10°S. Particularly, the runoff increase of about 43.0% was estimated at 25°~30°N that was due to high increase in precipitation at same latitudes. In summer season, the features of runoff change were similar to summer precipitation. However, the increasing rate of runoff was almost two times compared to that of precipitation. The increasing rate of autumn runoff was lower as compared to other seasons. In winter season, the runoff at high latitudes (40°~50°N) and low latitudes (0°~10°S) was expected to highly increase. The runoff increase of about 34% and 41% was projected by 2080s at high and low latitudes respectively. On the other hand, the runoff at 5°~25°N was expected to decrease up to -15%. The difference of change rate was not much at three future periods.

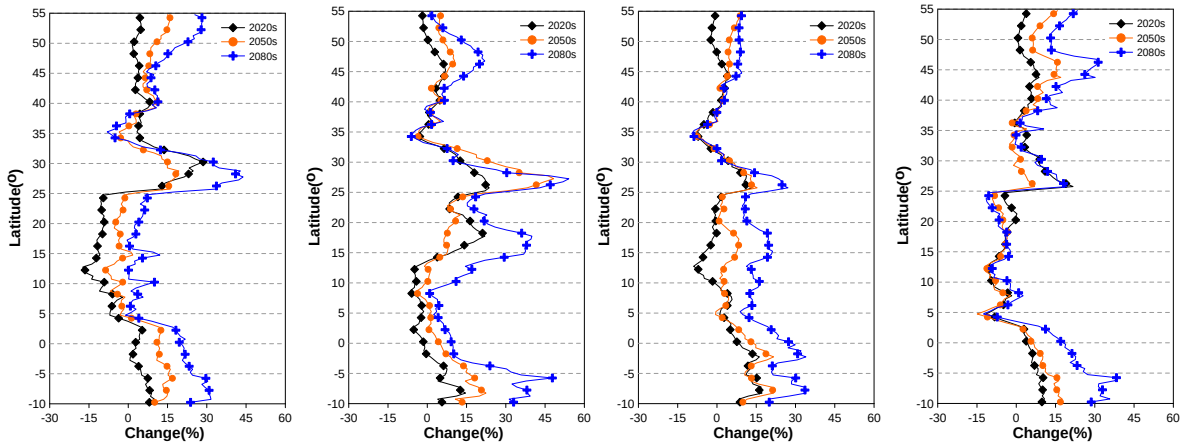

Figure 3.23: Latitudinal runoff change in spring (left), summer (second), autumn (third), and winter (right).

Analysis of water balance

The evaluation of hydrological components was conducted over AWCI 18 basins. Figure 3.24 shows the change of water balance for precipitation, runoff, evapotranspiration, and soil moisture at each selected basin. All variables indicated high change rate in future compared to reference period. Several distinct features were observed at each basin. In Meghna basin, Bangladesh, the precipitation, runoff and soil moisture in 2020s were expected to decrease, but precipitation and runoff appeared to increase by 28.0~50.0% during April and May, and soil moisture by 28.0% during May in 2050s and 2080s. The Punatsangchhu basin, Bhutan, showed similar features to Meghna basins with increase of May precipitation and runoff in 2050s and 2080s. In Sangker basin, Cambodia, there was no significant increasing tendency. However, the evapotranspiration in March was expected to decrease upto -68%. In Seonath basin, India, both precipitation and runoff was expected to increase in May, June, and July. However, evapotranspiration in January, February, and March was expected to decrease upto -50% at all future periods. In Mamberamo basin, Indonesia, the water balance at all future periods was expected to increase, but there was no distinct seasonal change. In Tone basin, Japan, there was no clear precipitation change except small increase in August. However, the runoff in April and May was expected to decrease upto -30.0%. These results

were influenced by impact of evapotranspiration according to increasing temperature. In Upper Chungju-dam basin, South Korea, water balance at future periods was expected to increase. Especially, evapotranspiration in warm season was appeared to increase due to increase of temperature by global warming. In Sebangfai basin, Laos, the water balance was expected to increase upto 35% in July, August, September, and October, however during other months the decreasing tendency was expected at all future periods. Regarding the Langat basin in Malaysia, the water balance had two peaks in April and November. On the other hand, the decreasing tendency was projected in January, February, March, and December. In Selbe basin, Mongolia, the precipitation and evapotranspiration was expected to increase in all months, however the increase in runoff was expected in between July and October. For Shwegyin basin, Myanmar, the precipitation and runoff was expected to increase during August and September in 2050s and 2080s. In Bagmati basin, Nepal, the precipitation and runoff was projected to increase only in 2080s. In Gilgit basin Pakistan, the precipitation, runoff, and soil moisture had almost same features. However, the evapotranspiration appeared to change dynamically with increasing tendency in April, May, and October, and decrease in other months. In case of Pampanga basin, Philippines, the small increase was expected in water balance for all months except May and June. For Kalu Ganga basin, Sri Lanka, the water balance had small increasing tendency at future periods around the year except for the months of January to April. In Mae Wang basin, Thailand, the decreasing trend was projected for all months except August, September, and October. In Chirchik-Okhangaran basin, Uzbekistan, the water balance was expected to increase from May to September, and that was expected to increase during other months. The Huong basin, Vietnam, had almost similar features to Mae Wang basin. Overall, the water balance was expected to increase over Asian region with increasing future periods.

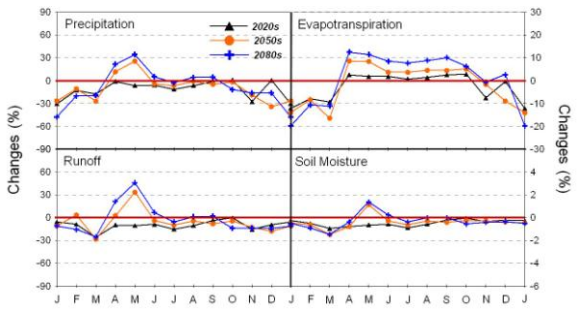

a) Meghna

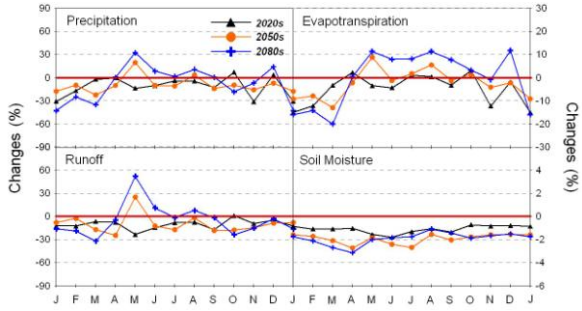

b) Punatsangchhu

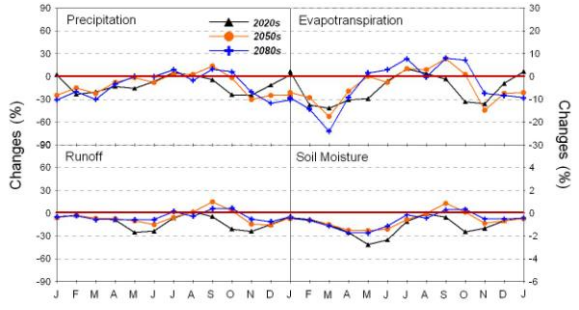

c) Sangker

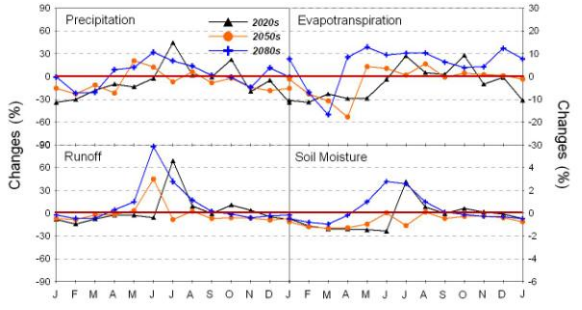

d) Seonath

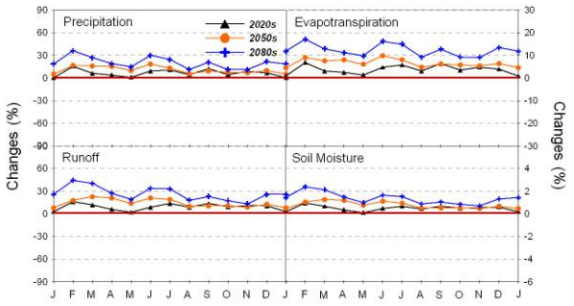

e) Mamberamo

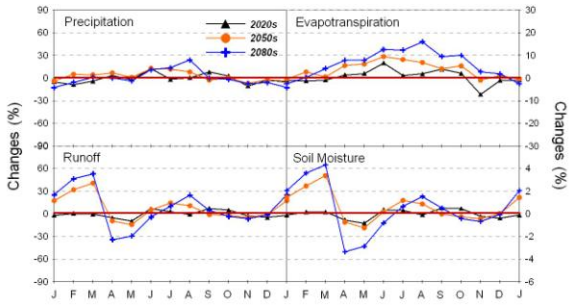

f) Tone

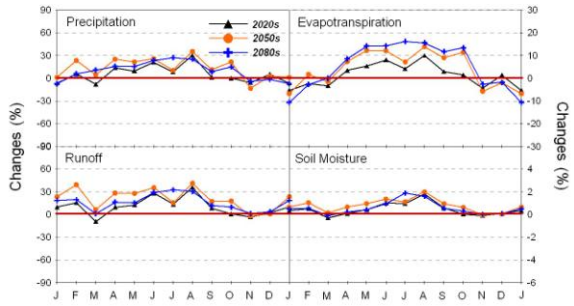

g) Chungju-dam

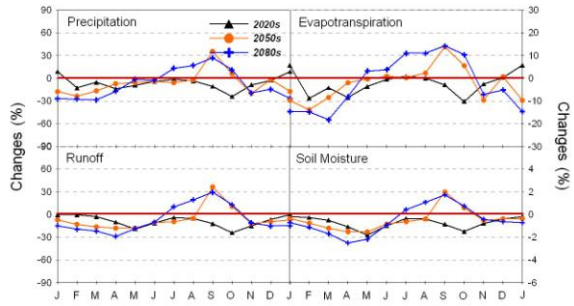

h) Sebangfai

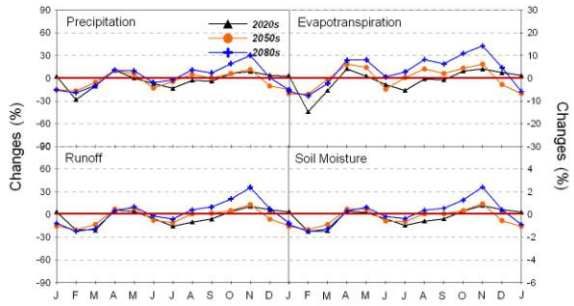

i) Langat

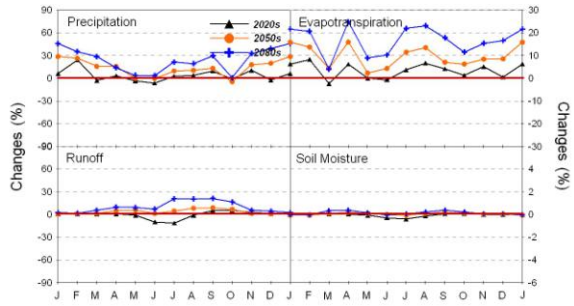

j) Selbe

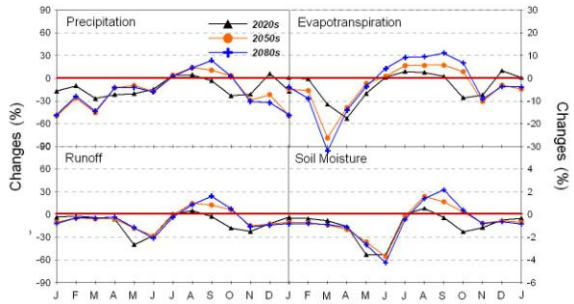

k) Shwegylin

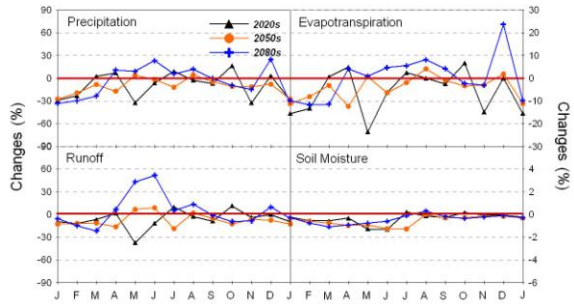

l) Bagmati

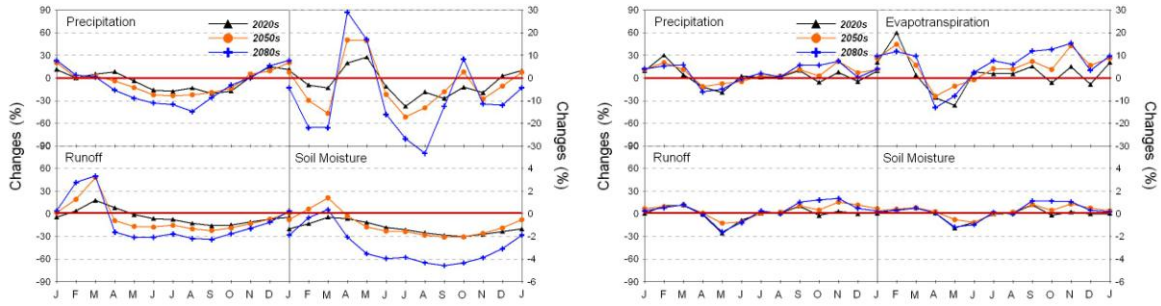

m) Gilgit n) Pampanga

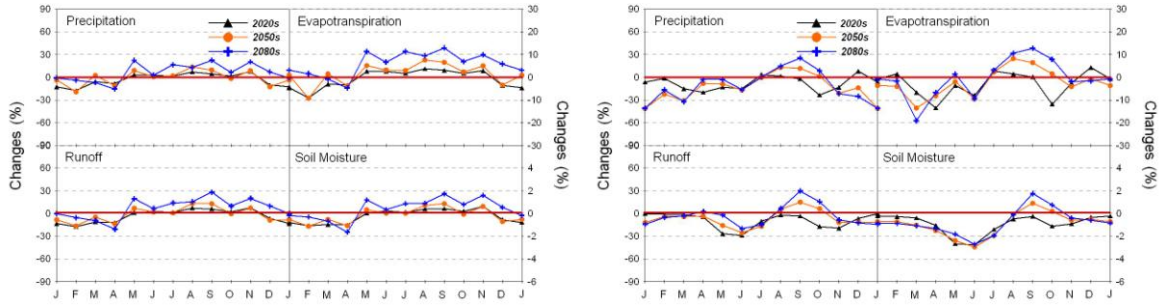

o) Kalu Ganga p) Mae Wang

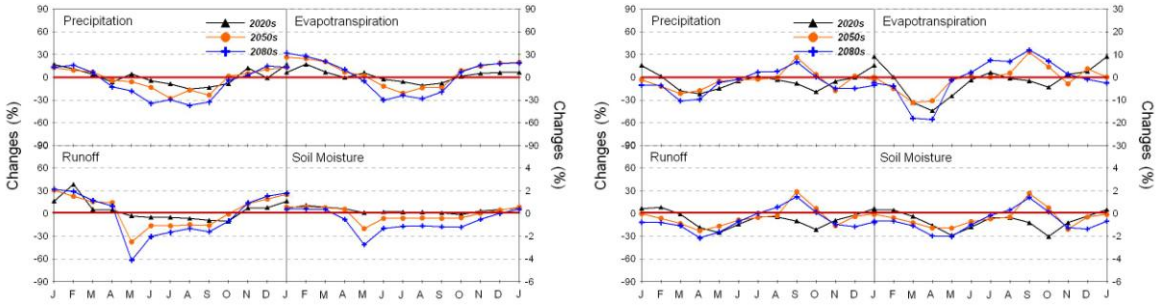

r) Chirchik Okhangaran s) Huong

Figure 3.24: Change of water balance for precipitation, runoff, evapotranspiration and soil moisture over AWCI 18 basins.

Table 3.13 shows the change rate of seasonal and annual precipitation at 2020s and 2080s over AWCI 18 basins. In 2020s, spring was most expected to decrease until -7.1%, and winter also was appeared to decrease until -4.1%. The annual precipitation was also expected to decrease about -1.2%. In 2080s, the precipitation in spring, summer, and autumn was expected to increase except winter season (-5.6%). Especially, the precipitation in autumn was appeared to increase until 6.5%. As a result, the precipitation over 18 basins has increasing tendency toward the future period.

Table 3.13: Change rate of seasonal and annual precipitation over AWCI 18 basins.

Demonstration basins		Spring		Summer		Autumn		Winter		Annual	
		2020s	2080s	2020s	2080s	2020s	2080s	2020s	2080s	2020s	2080s
1	Meghna	-6.2	24.5	-8.1	2.1	-1.9	-2.2	-12.6	-23.9	-6.4	6.6

2	Punatsangchhu	-8.1	13.6	-6.0	6.2	-8.3	-4.9	-16.4	-21.4	-7.1	4.8
3	Sanker	-15.6	-6.9	0.5	1.2	-14.5	4.5	-14.9	-25.3	-8.7	0.4
4	Seonath	-13.9	30.2	17.6	19.2	2.9	0.4	-26.3	-5.6	11.8	14.9
5	Mamberamo	3.9	20.8	8.3	22.3	8.5	14.1	7.5	25.5	6.8	21.1
6	Tone	-1.1	-1.1	3.1	16.4	3.0	-1.9	-5.7	-8.3	1.0	4.1
7	ChungJu-Dam	7.0	14.5	19.6	25.7	-0.2	7.7	1.4	-0.8	11.6	17.7
8	Sebanfai	-9.9	-9.2	-3.1	10.4	-15.1	15.3	-2.7	-21.8	-8.2	7.2
9	Langat	0.9	4.1	-7.7	1.8	4.8	20.5	-5.3	-9.4	-0.9	5.7
10	Selbe	-1.3	10.0	0.8	16.1	7.9	25.1	6.7	40.3	1.9	17.6
11	Shwegyin	-20.7	-13.4	-1.4	0.4	-9.9	13.6	-3.5	-32.7	-5.4	1.6
12	Bagmati	-17.6	5.9	1.6	12.0	-2.4	-2.5	-16.7	-13.3	-1.9	7.9
13	Gilgit	3.9	-15.1	-15.3	-38.0	-14.3	-14.2	7.4	13.1	-3.0	-16.4
14	Pampanga	-14.8	-11.7	1.4	2.7	4.3	18.0	5.4	6.3	0.6	6.2
15	Kalu Ganga	-2.5	3.7	3.7	9.7	4.5	15.7	-12.6	2.2	0.1	9.3
16	Mae Wang	-14.6	-5.1	-2.3	1.6	-10.4	13.9	2.5	-26.7	-7.6	3.6
17	Chirchik Okhangaran	0.4	-7.6	-7.6	-33.3	1.7	-3.2	8.5	14.7	2.7	-1.5
18	Huong	-17.0	-16.2	-2.5	4.5	-11.9	2.1	3.4	-13.2	-8.3	-1.3
Max.		7.0	30.2	19.6	25.7	8.5	25.1	8.5	40.3	11.8	21.1
Min		-20.7	-16.2	-15.3	-38.0	-15.1	-14.2	-26.3	-32.7	-8.7	-16.4
Ave.		-7.1	2.3	0.1	4.5	-2.8	6.8	-4.1	-5.6	-1.2	6.1

The seasonal and annual change in runoff was also evaluated over AWCI 18 basins as shown in Table 3.14. The change rate of runoff was almost similar to that of precipitation. The average spring runoff over 18 basins was expected to decrease upto -9.2%. Specifically, -22.4% runoff change was projected at Bagmati basin during spring season in 2020s. The annual mean runoff in 2020s was appeared to decrease about -1.8%. However, the annual mean runoff in 2080s was expected to increase upto 6.5% within increasing tendency in all four seasons.

Table 3.14: Change rate of seasonal and annual runoff over AWCI 18 basins.

Demonstration basins		Spring		Summer		Autumn		Winter		Annual	
		2020s	2080s	2020s	2080s	2020s	2080s	2020s	2080s	2020s	2080s
1	Meghna	-11.4	35.0	-11.7	0.7	-3.4	-5.4	-8.2	-13.8	-9.7	6.1
2	Punatsangchhu	-18.3	31.1	-9.8	4.3	-11.2	-9.3	-10.0	-12.5	-11.0	3.8
3	Sanker	-18.1	-8.5	-7.6	-2.9	-15.6	3.5	-10.0	-7.9	-12.8	-0.6
4	Seonath	-4.3	3.9	30.3	31.5	2.5	0.8	-8.4	-3.9	18.8	19.5
5	Mamberamo	6.9	29.5	10.2	28.8	11.2	17.9	9.5	32.1	9.2	28.0
6	Tone	-6.1	-18.4	2.5	12.3	4.3	-0.9	-2.9	17.2	0.5	1.2
7	ChungJu-Dam	6.6	12.5	25.0	31.3	4.7	9.8	8.1	12.4	15.4	21.2
8	Sebanfai	-15.2	-20.9	-6.4	9.1	-16.7	17.9	-3.7	-15.9	-11.3	8.8
9	Langat	-2.4	0.0	-10.1	-0.4	4.8	24.9	-1.1	-5.4	-1.2	6.2
10	Selbe	0.0	8.3	-4.6	19.5	5.0	17.9	0.9	3.1	-0.1	16.7
11	Shwegyin	-31.6	-14.2	-4.9	-4.3	-8.9	15.5	-7.4	-11.5	-7.1	0.4
12	Bagmati	-22.4	22.8	1.8	15.3	-3.0	-3.7	-6.9	-2.5	-0.8	10.8
13	Gilgit	5.6	-17.3	-8.3	-30.2	-14.0	-27.4	-3.2	8.6	-3.5	-19.9
14	Pampanga	-13.8	-12.3	-1.1	-0.6	4.4	17.5	1.9	6.3	0.6	6.5

15	Kalu Ganga	-5.3	1.6	3.6	10.8	5.2	17.9	-10.7	4.0	0.0	10.3
16	Mae Wang	-18.6	-1.2	-12.1	-7.2	-11.3	17.1	-3.4	-11.4	-11.7	4.3
17	Chirchik Okhangaran	1.9	-14.1	-5.3	-26.9	-1.4	5.0	20.5	64.3	3.1	-3.9
18	Huong	-18.8	-24.4	-7.0	1.0	-14.4	1.8	0.9	-15.4	-10.9	-2.7
Max.		6.9	35.0	30.3	31.5	11.2	24.9	20.5	64.3	18.8	28.0
Min		-31.6	-24.4	-12.1	-30.2	-16.7	-27.4	-10.7	-15.9	-12.8	-19.9
Ave.		-9.2	0.7	-0.9	5.1	-3.2	6.7	-1.9	2.7	-1.8	6.5

Table 3.15 shows the change rate of seasonal and annual evapotranspiration over AWCI 18 basins. The features of evapotranspiration were slightly different compared to that of precipitation and runoff because evapotranspiration was influenced by temperature increase. The projected change rate of evapotranspiration was low as compared to that of runoff. In 2020s, the high decrease of evapotranspiration (-3.4%) was estimated in spring season. Annual evapotranspiration averaged over AWCI 18 basins was also expected to decrease about -0.2% in 2020s. However, the evapotranspiration in 2080s was expected to increase with average rate of 5.7%. The autumn evapotranspiration was projected to increase upto 8.0% in 2080s

Table 3.15: Change rate of seasonal and annual evapotranspiration over AWCI 18 countries.

Demonstration basins		Spring		Summer		Autumn		Winter		Annual	
		2020s	2080s	2020s	2080s	2020s	2080s	2020s	2080s	2020s	2080s
1	Meghna	0.3	8.3	1.3	8.4	1.9	8.1	-7.3	-9.9	0.8	7.7
2	Punatsangchhu	-1.6	3.0	-0.8	9.1	-2.3	5.9	-10.8	-9.2	-1.7	6.2
3	Sanker	-10.5	-5.7	1.0	3.4	-6.3	5.5	-5.8	-11.3	-4.1	1.4
4	Seonath	-8.9	2.1	3.7	10.1	2.5	5.6	-8.4	2.9	1.3	7.8
5	Mamberamo	2.4	11.5	4.6	13.5	4.8	10.3	3.9	14.1	3.8	12.4
6	Tone	1.1	7.0	3.0	13.6	1.3	8.5	-1.1	-0.2	1.8	9.5
7	ChungJu-Dam	2.5	8.6	7.2	15.5	1.1	9.2	-2.3	-5.2	3.9	10.5
8	Sebanfai	-5.1	-3.9	0.2	8.8	-5.3	9.1	-1.3	-11.2	-2.5	4.4
9	Langat	0.2	4.8	-2.7	4.1	2.4	10.8	-2.9	-2.2	-0.5	5.0
10	Selbe	1.3	12.4	3.5	19.2	3.8	16.5	5.8	19.9	3.3	17.9
11	Shwegyin	-9.3	-8.5	2.0	7.7	-3.1	7.5	1.1	-5.6	-1.2	4.5
12	Bagmati	-13.0	0.3	-0.8	6.2	-0.8	2.5	-11.1	-3.1	-3.2	4.2
13	Gilgit	3.7	6.7	-7.5	-25.8	-7.1	-6.8	-0.1	-13.8	-2.4	-10.6
14	Pampanga	-9.3	-6.4	2.1	5.6	2.8	12.9	5.1	7.1	0.6	5.8
15	Kalu Ganga	-0.8	2.8	2.7	8.9	2.5	9.7	-5.4	3.9	0.5	6.8
16	Mae Wang	-6.6	-3.3	-0.9	2.2	-3.9	9.5	1.8	-1.4	-3.0	2.8
17	Chirchik Okhangaran	3.7	8.8	-5.0	-27.8	0.3	12.7	11.4	67.7	1.6	4.3
18	Huong	-10.6	-9.1	0.1	5.6	-1.8	7.4	3.8	-1.9	-1.9	2.6
Max.		3.7	12.4	7.2	19.2	4.8	16.5	11.4	67.7	3.9	17.9
Min		-13.0	-9.1	-7.5	-27.8	-7.1	-6.8	-11.1	-13.8	-4.1	-10.6
Ave.		-3.4	2.2	0.8	4.9	-0.4	8.0	-1.3	2.3	-0.2	5.7

The features of change in soil moisture over AWCI 18 basins are presented in Table 3.16. The features of soil moisture were different compared to that of other hydrological components. The

seasonal and annual soil moisture was expected to decrease for all future periods. The annual mean soil moisture averaged over 18 basins was projected to decreased upto -0.4% and -0.3% in 2020s and 2080s, respectively. The high decrease of upto -0.8% was projected during spring season in 2080s. The highest annual decrease in soil moisture was projected at Gilgit basin with change rate of upto -1.3% and -3.0 in 2020s and 2080s, respectively.

Table 3.16: Change rate of seasonal and annual soil moisture over AWCI 18 countries.

Demonstration basins		Spring		Summer		Autumn		Winter		Annual	
		2020s	2080s	2020s	2080s	2020s	2080s	2020s	2080s	2020s	2080s
1	Meghna	-0.8	-0.1	-0.7	-0.1	-0.2	-0.3	-0.3	-0.6	-0.5	-0.3
2	Punatsangchhu	-1.2	-2.6	-1.4	-1.6	-1.0	-1.7	-0.9	-1.8	-1.1	-1.9
3	Sanker	-1.8	-1.5	-1.0	-0.6	-1.1	0.1	-0.5	-0.5	-1.1	-0.6
4	Seonath	-1.4	-0.1	0.7	2.1	0.2	-0.1	-0.6	-0.5	-0.2	0.4
5	Mamberamo	0.4	1.6	0.5	1.4	0.6	0.9	0.6	1.7	0.5	1.4
6	Tone	-0.4	-0.8	0.2	0.5	0.3	-0.2	-0.1	1.8	0.0	0.3
7	ChungJu-Dam	0.1	0.2	1.3	1.5	0.2	0.3	0.3	0.4	0.5	0.6
8	Sebanfai	-1.1	-2.1	-0.6	0.2	-1.1	0.7	-0.3	-0.8	-0.8	-0.5
9	Langat	-0.3	-0.1	-0.6	-0.1	0.2	1.4	-0.3	-0.6	-0.2	0.2
10	Selbe	0.0	0.3	-0.3	0.1	0.1	0.2	0.0	0.0	-0.1	0.2
11	Shwegyin	-1.8	-1.6	-1.0	-1.1	-1.0	0.7	-0.4	-0.8	-1.0	-0.7
12	Bagmati	-0.7	-0.9	-0.4	-0.1	-0.1	-0.2	-0.3	-0.4	-0.4	-0.4
13	Gilgit	-0.5	-1.8	-1.4	-4.0	-1.9	-4.3	-1.3	-1.8	-1.3	-3.0
14	Pampanga	-0.2	-0.2	-0.2	-0.3	0.3	1.1	0.1	0.3	0.0	0.2
15	Kalu Ganga	-0.6	-0.4	0.2	0.7	0.4	1.4	-0.8	0.0	-0.2	0.5
16	Mae Wang	-1.4	-1.4	-1.5	-1.6	-0.8	0.7	-0.3	-0.8	-1.0	-0.7
17	Chirchik Okhangaran	0.3	-1.0	0.1	-1.2	0.1	-1.0	0.5	0.3	0.3	-0.7
18	Huong	-1.1	-1.7	-0.6	-0.3	-1.2	0.1	0.1	-0.9	-0.7	-0.7
Max.		0.4	1.6	1.3	2.1	0.6	1.4	0.6	1.8	0.5	1.4
Min		-1.8	-2.6	-1.5	-4.0	-1.9	-4.3	-1.3	-1.8	-1.3	-3.0
Ave.		-0.7	-0.8	-0.4	-0.2	-0.3	0.0	-0.2	-0.3	-0.4	-0.3

4.0 Conclusions

In this study, the analysis of historical climate and hydrology trend with future climate change impact was conducted over Asia region covering 18 designated basins of AWCI. The Mann-Kendall test was employed for historical trend analysis using observed gridded climate data from APHRODITE and hydrology data from VIC model at horizontal grid resolution of 0.5° x 0.5° for period of 1977 to 2006. The trend analysis showed increase in temperature over Asia region except some parts of Southeast Asia. The precipitation was observed to decrease about 100~200mm during past 30 years over Asian region. Similarly, the decreasing trend was observed for runoff. The runoff was observed to decrease approximately 70～80mm over Asia region. The seasonal trend analysis showed increasing trend of temperature for all the seasons. The seasonal precipitation showed decreasing trend over Asia with increase in some parts. The seasonal runoff was also appeared to decrease like precipitation. The spatial features of runoff were similar to that of precipitation. The hydrological components over

AWCI 18 basins were calculated using VIC model which revealed various distinct regional features at each basin.

To analyze future climate change impact, the optimum GCMs were selected using probabilistic uncertainty analysis, correlation coefficient, and RMSE methods. Selected GCMs include CGCM3_T47, CGCM2_3_2, and CM4. The uncertainty of selected GCMs was also evaluated. The results showed increased uncertainty of GCMs toward future periods. For future climate and hydrology impact, the ensemble mean value of selected GCMs was used. The temperature was expected to increase in all regions. The precipitation was projected to increase during all seasons in most regions except central Asia. The future change in runoff was expected similar with that of precipitation. The latitudinal features showed high increase in temperature change with increasing latitudes. The latitudinal precipitation change was estimated high at high latitudes and low at low latitudes. The change rate of latitudinal runoff was high at mid latitude regions. The water balance for precipitation, runoff, evapotranspiration and soil moisture was evaluated over 18 selected basins. The results showed increasing tendency of water balance for the future periods.

The detailed analysis of historical climate and hydrology trend with future climate change impact established better understanding of changing climate and hydrology over Asia region The findings of this study will be useful to establish future climate adaptation measures over Asia.

5.0 Future Directions

In this study, the historical climate and hydrology trend with future climate change impact over Asia was evaluated. The observed gridded data of 0.5° x 0.5° resolution, A2 scenario, and VIC model were used. To conduct detailed analysis of climate and hydrology features, high-resolution observation data will be used. The multi GCM, hydrology model, and climate scenario will be used to evaluate future climate change impact details. Furthermore, in this study we used IPCC AR4 output. We will be able to obtain more useful results using Representative Concentration Pathway of IPCC AR5.

References

Adam, J.C., and Lettenmaier, D.P. (2003). Adjustment of global gridded precipitation for systematic bias, *J. Journal of* Geophysical Research, 108(D9), 1-14.

Adam, J.C., Clark, E.A., Lettenmaier, D.P. and Wood, E.F. (2006). Correction of Global Precipitation Products for Orographic Effects, *Journal of Climate*, 19(1), 15-38.

Andreasson, J., Bergstrom, S., Carlsson, B., Graham, L.P., and Lindstrom, G. (2004). Hydrological change - Climate change impact simulations for Sweden, *AMBIO: A Journal of the Human Environment*, 33(4-5), 228-234.

Andreadis, K., Storck, P. and Lettenmaier, D.P. (2009). Modeling snow accumulation and ablation processes in forested environments, *Water Resources Research*, in review.

Asia Pacific Network (APN) for Global Change Research (2011). River Management System Development in Asia Based on Data Integration and Analysis System under the GEOSS, ARCP2011-02CMY-Koike.

Bae, D.H., Georgakakos, K. P. and Kim, S. (2007). Screening the utility of climate information for watershed applications in Korea, *Journal of Climate*, 336, 38– 47.

Bae, D.H., Jung, I.W. and Chang, H.J. (2008a). Potential changes in Korean water resources estimated by high-resolution climate simulation, *Climate Research,* 35, 213-226.

Bowling, L. C., Kane, D.L., Gieck, R.E., Hinzman, L.D. and Lettenmaier, D.P. (2003c). The role of surface storage in a low-gradient Arctic watershed, *Water Resources Research, 39*(4), -.

Bowling, A. and Gabriel, Z. (2004). An integrated model of quality of life, *Social Indicators Research*, 69, 1–36.

Bowling, L. C. and Lettenmaier, D. P. (2009). Modeling the effects of lakes and wetlands on the water balance of Arctic environments, *Journal of Hydrometeorology*, submitted.

Brooks, R. H. and Corey, A. H. (1988). Hydraulic properties of porous media, *HYDRO PRE-AUTHORIZED PAYMENT , Colorado State University*, *3*.

Cherkauer, K. A. and Lettenmaier, D. P. (1999). Hydrologic effects of frozen soils in the upper Mississippi River basin, *Journal of Geophysical Research: Atmospheres, 104*(D16), 19599-19610.

Cherkauer, K. A., Bowling, L.C. and Lettenmaier, D. P., (2003). Variable infiltration capacity cold land process model updates, *Global Planet Change*, *38*(1-2), 151-159.

Cherkauer, K. A. and Lettenmaier, D. P. (2003). Simulation of spatial variability in snow and frozen soil, *Journal of Geophysical Research: Atmospheres, 108*(D22), 14.

Dietz, E.J. and Killeen, T.J. (1981). A nonparametric multivariate test for monotone trend with pharmaceutical applications, *Journal of the American Statistical Association*, 76, 169-174.

Dickinson, R. E., Henderson-Sellers, A., Kennedy, P. J. and Wilson, M. F. (1986). Biosphere atmospheric transfer scheme (BATS) for the NCAR community climate model, *NCAR, Tech. Note TN-275+STR*.

Donohue, J.J. and Levitt, S.D. (2001). The impact of legalized abortion on crime, The quarterly journal of economics, 2(CXVI), 379-420.

FAO, (1998). FRA 2000 term and definitions. FRA Working Paper No.1 Rome (www.fao.org/forestry/fo/fra/index.jsp)

Franchini, M. and Pacciani, M. (1991). Comparative-analysis of several conceptual rainfall runoff models, *Journal of Hydrology*, *122*(1-4), 161-219.

Georgakakos, K. P. (2003). Probabilistic climate-model diagnostics for hydrologic and water resources impact studies, *Journal of Hydrometeorology*, 4, 92–105.

Gibbons, J.D. (1990). Handbook of tatistical methods for engineers and scientists, *McGrawHill, ed.* Harroson M.W.

Gilbert, R.O. (1987). Statistical Methods for Environmental Pollution Monitoring, *Van Nostrand Reinhold*, New York, 1987.

Haddeland, I., Lettenmaier, D.P. and Skaugen, T. (2006a). Effects of irrigation on the water and energy balances of the Colorado and Mekong river basins, *Journal of Hydrology*, *324*(1-4), 210-223.

Haddeland, I., Skaugen, T. and Lettenmaier, D.P. (2006b). Anthropogenic impacts on continental surface water fluxes, *Geophys Res Lett*, *33*(8), -.

Haddeland, I., Skaugen, T. and Lettenmaier, D.P. (2007). Hydrologic effects of land and water management in North America and Asia: 1700-1992, *Hydrology and Earth System Sciences*, *11*(2), 1035-1045.

Hay, L. E., Wilby, R. L. and Leavesley, G. H. (2000). A comparison of delta change and downscaled GCM scenarios for three mountainous basins in the United States. *Journal of the American Water Resources Association*, 36-2, 387-397.

Hirsch, R.M., Slack, J.R. and Smith, R.A. (1982). Techniques of Trend Analysis for Monthly Water Quality Data. *Water Resources Research*, 18(1), 107-121.

Hirsch, R.M. and Slack, J.R. (1984). A nonparametric trend test for seasonal data with serial dependence, *Water Resources Research,* 20, 727–732.

Intergovernmental Panel on Climate Change (2007). Climate Change 2007: The Scientific Basis, available at www.grida.no/climate/ipcc_tar/wg1/index.htm.

Jung, I.W., Bae, D.H., and Im, E.S. (2007). Generation of High Resolution Scenarios for Climate Change Impacts On Water Resources(2): Runoff Scenarios on Each Sub-basins, *Korea Water Resources Association*, 40(3), 1226-6280.

Jung, I.W., Bae, D.H., and Kim, G. (2011). Recent trends of mean and extreme precipitation in Korea, *International Journal of Climatology*, 31(3), 359-370.

Kalnay, E., Kanamitsu, M., Kistler, R., Collins, W., Deaven, D., Gandin, L., Iredell, M., Saha, S., White, G., Woollen, J., Zhu, Y., Chelliah, M., Ebisuzaki, W., Higgins, W., Janowiak, J., Mo, K. C., Ropelewski, C., Wang, J., Leetmaa, A., Reynolds, R., Jenne, R. and Joseph, D. (1996). The NCEP/NCAR 40-Year Reanalysis Project, *Bulletin of the American Meteorological Society, 77(3), 437–471.*

Kendall, M.G. (1975). Rank correlation methods, 4th ed. Charles Griffin, London

Köppen W. (1931) Grundriss der Kilmakunde. Walter de Gruyter, Berlin

Köppen, W. (1936), Das geographische System der Klimate Handbuch der Klimatologie, Vol. 1, Part C, Gebr. Bornträger Verl., Berlin, p. 388.

Kottek, M., Grieser, J., Beck, C., Rudolf, B. and Rubel, F. (2006). World Map of the Köppen-Geiger climate classification updated, Meteorologische Zeitschrift, 15(3), 259-263.

Lee, B.J., Jung, I.W. and Bae, D.H. (2009). Parameter Regionalization of Semi-Distributed Runoff Model Using Multivariate Statistical Analysis, *Korea Water Resources Association*, 42(2), 149-160.

Lettenmaier, D.P. (1988). Multivariate nonparametric tests for trend in water quality, *Water Resources Research,* 24(3), 503-512.

Liang, X., Lettenmaier, D.P., Wood, E.F. and Burges, S. (1994). A SIMPLE HYDROLOGICALLY BASED MODEL OF LANDSURFACE WATER AND ENERGY FLUXES FOR GENERAL-CIRCULATION MODELS, *Journal of Geophysical Research: Atmospheres*, *99*(D7), 14415-14428.

Liang, X., Wood, E.F. and Lettenmaier, D.P. (1996). Surface soil moisture parameterization of the VIC-2L model: Evaluation and modification, *Global Planet Change*, *13*(1-4), 195-206.

Libiseller, C. and Grimvall, A. (2002). Performance of partial Mann-Kendall tests for trend detection in the presence of covariates*, Environmetrics*, 13, 71-84.

Liu, C.M. and Zheng, H.X. (2004). Changes in components of the hydrological cycle in the Yellow River basin during the second half of the 20th century, *Hydrological Processes*, 18(12), 2337-2345.

Lohmann, D., Holube, N.R. and Raschke, E. (1996). A large scale horizontal routing model to be coupled to land surface parameterization schemes, *Tellus,* (48A), 708-721.

Lohmann, D., Raschke, E., Nijssen, B. and Lettenmaier, D.P. (1998a). Regional scale hydrology: I. Formulation of the VIC-2L model coupled to a routing model, *Hydrol. Sci. J.-J. Sci. Hydrol.*, *43*(1), 131-141.

Lohmann, D., Raschke, E., Nijssen, B. and Lettenmaier, D.P. (1998b). Regional scale hydrology: II. Application of the VIC-2L model to the Weser River, Germany, *Hydrol. Sci. J.-J. Sci. Hydrol.*, *43*(1), 143-158.

Mann, H.B. (1945). Nonparametric Tests Against Trend. Econometrica, Vol. 13, pp. 245-259.

Mitchell, K. E. (2004). The multi-institution North American Land Data Assimilation System (NLDAS): Utilizing multiple GCIP products and partners in a continental distributed hydrological modeling system, *Journal of Geophysical Research*, 109, D07S90, doi:10.1029/2003JD003823.

Nijssen, B., Lettenmaier, D.P., Liang, X., Suzanne, W.W. and Wood, E.F. (1997). Streamflow simulation for continental-scale river basins, *Water Resources Research, 33*(4), 711-724.

Nijssen, B., Lettenmaier, D.P., Lohmann, D. and Wood, E.F. (2001a). Predicting the discharge of global rivers, *Journal of Climate*, *14*(15), 3307-3323.

Nijssen, B., Schnur, R. and Lettenmaier, D.P. (2001b). Global retrospective estimation of soil moisture using the variable infiltration capacity land surface model, 1980-93, *Journal of Climate*, 14(8), 1790-1808.

Partal, T., and Kahya, E. (2007). Is Seaonal Precipitation Decreasing or Increasing in Turkey?, Online Journal of Earth Sciences, 1(1), 43-46.

Peel M.C., Finlayson, B.L. and Mcmahon, T.A. (2007). Upward world map of the Köppen-Geiger climate classification, *Hydrology and Earth System Sciences*, 11, 1633-1644.

Reason, C.J.C. and Keibel, A. (2004). Tropical cyclone Eline and its unusual penetration and impacts over the southern African mainland*, Weather Forecast*, 19, 789-805.

Son, K. H., Lee, J. D. and Bae, D. H. (2010). The Application Assessment of Global Hydrologic Analysis Models on South Korea, *Korea Water Resources Association,* 43(12), 1063-1074.

Stamm, J. F., Wood, E.F. and Lettenmaier, D.P. (1994). SENSITIVITY OF A GCM SIMULATION OF GLOBAL CLIMATE TO THE REPRESENTATION OF LAND-SURFACE HYDROLOGY, *Journal of Climate*, 7(8), 1218-1239.

Storck, P., Bowling, L., Wetherbee, P. and Lettenmaier, D.P. (1998). Application of a GIS-based distributed hydrology model for prediction of forest harvest effects on peak stream flow in the Pacific Northwest, *Hydrological Processes*, 12(6), 889-904.

Variability for General-Circulation Models, *Journal of Geophysical Research: Atmospheres*, *97*(D3), 2717-2728.

Wigmosta, M. S., Vail, L.W. and Lettenmaier, D.P. (1994). A DISTRIBUTED HYDROLOGY-VEGETATION MODEL FOR COMPLEX TERRAIN, *Water Resources Research*, *30*(6), 1665-1679.

Willmott, C.J., and Matsuura, K. (2007). On the use of dimensioned measures of error to evaluate the performance of spatial interpolators, *International Journal of Geographical Information Science*, 20(1), 89-102.

Wood, E. F., Lettenmaier, D.P. and Zartarian, V.G. (1992). A land-surface hydrology parameterization with subgrid variability for general circulation models,

Xie, Z. H., Yuan F., Duan, Q., Zheng, J., Linag, M. and Chen, F. (2007). Regional parameter estimation of the VIC land surface model: methodology and application to river basins in China, *Journal of Hydrometeorology*, *8*(3), 447-468.

Yasutomi, N., Hamada, A. and Yatagai, A. (2011). Development of a long-term daily gridded temperature dataset and its application to rain/snow discrimination of daily precipitation, *Global Environmental Research*, V15N2, pp.165-172.

Yatagai, A., Kamiguchi, K., Arakawa, O., Hamada, A., Yasutomi, N. and Kitoh, A., (2012). APHRODITE: Constructing a Long-term Daily Gridded Precipitation Dataset for Asia based on a Dense Network of Rain Gauges, *Bulletin of American Meteorological Society (in press)*, doi:10.1175/BAMS-D-11-00122.1.

Zhao, R.J. (1980). The Xinanjiang model, *Hydrological Forecasting Proceedings Oxford Symposium, IASH 129*, 351-356.

Appendix

Conferences/Symposia/Workshop

1. The AWCI training course for the Climate Change Assessment and Adaptation Study

- Date: 11th - 12th March 2011

- Venue: University of Tokyo Hongo Campus, Tokyo, Japan

- Meeting Objective

The Training Course was designated for the leaders of the AWCI Climate Change Assessment and Adaptation (CCAA) Study to get familiar with necessary methods for correcting bias of Global Climate Model (GCM) projection outputs, downscaling the GCM output, and use of hydrological models for assessment of possible climate change impact on water resources on a basin scale. The two-day intensive course was organized by collaborative efforts of the University of Tokyo, Japan, Sejong University, Korea, and ICHARM, Japan.

- Main Agenda & Photo

1) Welcome and Introduction
2) Rainfall bias correction and downscaling methods by the University of Tokyo group
3) Hydrological model WEB-DHM (Water and Energy Budget Distributed Hydrological Model) use for the CCAA purposes by Dr. Lei Wang and the University of Tokyo team
4) Flood modeling system IFAS (Integrated Flood Analysis System) applications by Dr. Fukami and the ICHARM team
5) Multi-model Hydrological modeling in use for Climate Change assessment by Prof. Bae – Sejong University

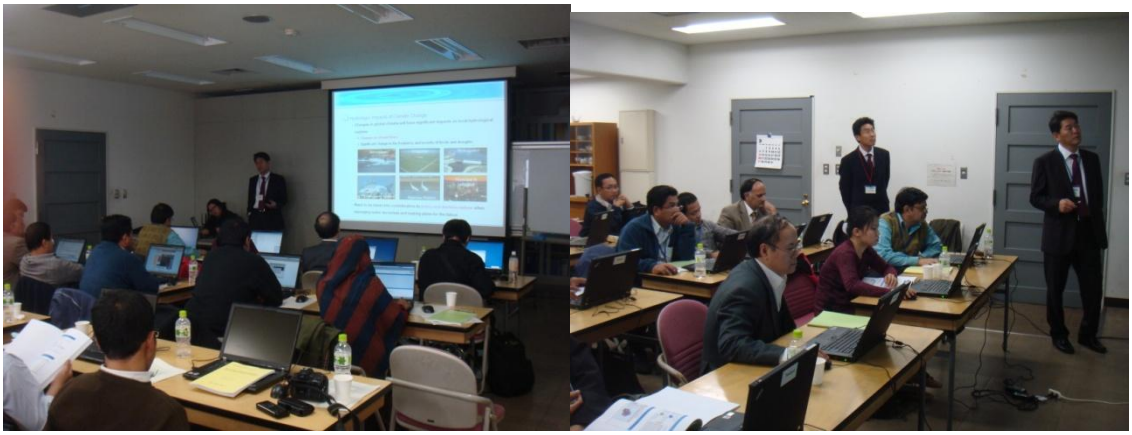

2. The AWCI training course for the Climate Change Assessment and Adaptation Study

- Date: 6th - 8th October 2011

- Venue: COEX, World Trade Center, Seoul, South Korea

- Meeting Objective

Aside from the usual review of the AWCI and its working group activities, the ICG meeting focused on preparation for planning of the next step of the Initiative. With its strong collaborative framework and data integration principles developed, AWCI is now eligible as one of the pillars of the newly proposed GEOSS Water Cycle Integrator (WCI), targeting enhanced coordination in the water cycle arena on the global level.
In addition to the ICG business, the meeting reviewed progress and results of the CCAA study and the outcomes were considered for the planning of the later steps of AWCI. Accordingly, all the CCAA leaders were invited to attend the meeting to share their view on pursuing the study.

- Main Agenda & Photo

1) Opening Session
2) AWCI Working Group Activity Review Session
3) Country Activity Review and Possible Contributions to the AWCI Next Stage Session
4) Capability of Observation, Data Integration and Prediction Session
5) Breakout discussion session 1 – GEOSS WCI: needs and capabilities
6) Breakout discussion session 2 – GEOSS WCI: practical implementation ideas
7) Breakout session summary
8) Implementation planning for a regional coordination project targeting Climate Change Adaptation
9) Summary and Closing session

3. The 9th AWCI International Coordination Group (ICG) Meeting and the Workshop on Climate Change Adaptation organized by APWF

- Date: 29th September – 2nd October 2012

- Venue: University of Tokyo Hongo Campus, Tokyo, Japan

- Meeting Objective

To synthesize the provided country inputs into a complex implementation plan that will be in line with the GEOSS Water Cycle Integrator (WCI) goals.
To kick-off two AWCI projects funded under the Asia Pacific Network for Global Change Research (APN) programmes: (i) Impact of Climate Change on Glacier Melting and Water Cycle Variability in Asian River Basins (led by Dr. G. Rasul, Pakistan Meteorological Department, PMD) and (ii) GEOSS/Asian Water Cycle Initiative/Water Cycle Integrator (led by Dr. O. Ochiai, Japan Aerospace Exploration Agency, JAXA).
To contribute to the Asia Pacific Water Forum (APWF) Workshop on "Meta-Guidelines" for Climate Change Adaptation held subsequently after the AWCI ICG meeting on 1 - 2 October.

- Main Agenda & Photo

1) Opening Session
2) AWCI Working Group Activity Review Session
3) APN activities on Climate Change Adaptation
4) Country Reports on "Climate Change Adaptation and Water Nexus"
5) Inputs form International Cooperative Activities
6) Breakout discussion for Implementation Planning


List of Young Scientists

1. Le Vinh Thanh,
- Thesis title: Detecting the future climate of Asian countries using information from IPCC AR4 GCMs
- Graduation date: Febuary 2012 (Mater degree)
- APN project's Role: selection of GCMs for climate change impact assessment on water resources in Asia
- e-mail: levinhthanh.lvt@gmail.com

2. Shin Sang Hoon

- Thesis title : Future Projections of Climate Shifts in the Asia Regions Using A2 Scenario
- Graduation date : August 2012 (Mater degree)
- APN project's Role : Collection and analysis of the climate and hydrologic observation data
- e-mail: hjhssh@naver.com